Design, Fabrication and Testing of 3D-Printed Spheres for Macro Self-Assembly Experiments

A.P. (Alexander) Dijkshoorn

BSc Report

Committee:
Prof.dr.ir. G.J.M. Krijnen
Dr.ir. A.J. Annema

July 2016

022RAM2016
Robotics and Mechatronics
EE-Math-CS
University of Twente
P.O. Box 217
7500 AE Enschede
The Netherlands

Abstract

This report presents the design, fabrication and testing of spheres with integrated functionality for self-assembly experiments. At the Korean Institute for Science and Technology (KIST) currently experiments are done on self-assembly by means of a macroscopic reactor with magnetic spheres in a turbulent flow. The current set-up does measurements by means of video analysis; however this method poses problems for more than two spheres.

The goal of this work is to design, manufacture and test magnetic spheres that can sense connections with other spheres and provide data on connections for use in the self-assembly experiments. From literature similar research has been studied for useful information. Next a design has been made by applying a systems engineering methodology: the requirements and needed functionality of the system were used to define subsystems. Scenarios for the total system were designed from proposed subsystem options and a best fitting scenario was chosen, including reed switches for sensing and separated magnets as interaction source.

The size and position of the magnets were based on the flow forces in the reactor. It was shown that two smaller separated magnets can be used for the experiments instead of a single large magnet, without affecting the interaction of the spheres. Reed switches were studied as sensing mechanism. There was looked into the magnetic fields inside the spheres and the operation of the switches. This resulted in positioning the reed switches next to the magnets, perpendicular to the magnetic field. A PCB containing a micro-controller and flash memory has been designed and manufactured for providing the needed functionality of the spheres. A micro-controller code based on the needed operations has been written for use in the experiments. The full system has been manufactured and changes have been made for the optimal performance.

With experiments it could be shown that the system works in a controlled, dry environment. The tests in the self-assembly reactor did not yield the desired results due to flaws in the electronics and the sealing of the sphere. With improvements of the sensing subsystem, the batteries and the water tight sealing it is expected to meet all requirements. The combination of all outcomes shows the viability of the system, however extra testing should be done and improvements should be made before the system can be used for the macro self-assembly experiments.

Acknowledgments

This report is written as BSc-thesis for Advanced Technology. The research has been carried out at the Robotics and Mechatronics research group within the NIFTy chair at the University of Twente. Given the multi-disciplinary nature of the study, the advice and assistance of a lot of people was sought. Therefore I would like to take this opportunity to thank everyone who has been involved in the project.

For doing this BSc-thesis, I could rely on the help of some amazing persons. Therefore I would like to thank Gijs Krijnen for supervising the assignment and providing good ideas, Leon Abelmann for his support, hospitality and for the opportunity to do experiments at KIST, Remco Sanders for his help with all kind of parts and equipment and Anne-Johan Annema for serving as an external member of the committee. Next to that I would like to thank the people at KIST for their warm welcome; the help of Per Loethman, Tijmen Hageman and Thomas Janson was essential in doing the experiments with the self-assembly reactor. Furthermore I thank Gerben te Riet from RAM for helping out with 3D printing parts. Finally my thanks goes out to fellow NIFTy students taking part in the group meetings, for their feedback, help and ideas.

A special thanks goes out to Marcel Welleweerd for all his help and advice with the electronics, soldering and the programming, as well as sharing his experiences with 3D printing.

Contents

Abbreviations and Symbols

Symbols

μ_0	Permeability of free space
ρ	Density (ρ_w is density of water)
$\vec{\tau}_{\mathrm{ab}}$	Torque exerted by magnet a on magnet b
A	Normalization term for the Maxwell-Boltzmann distribution
A	Surface area
$\vec{B}_{\mathrm{ab}}$	Magnetic field of magnet a experienced by magnet b
$\vec{B}_{\mathrm{r}}$	Remanence (residual magnetization)
C_{D}	Drag coefficient
d	Diameter sphere
E	Energy state of a particle
$\vec{F}_{\mathrm{ab}}$	Force exerted by magnet a on magnet b
g	Gravitational acceleration
k	Boltzmann constant
$\vec{M}$	Magnetization
$\vec{m}_{\mathrm{a}}$	Magnetic dipole moment of magnet a
$\vec{r}$	Position vector from magnet a to magnet b
T	Temperature
V	Volume
v_{t}	Terminal velocity

Abbreviations

CAD	Computer-Aided Design
DLP	Digital Light Processing
FDM	Fused Deposition Molding
IDE	Integrated Development Environment
KIST	Korean Institute for Science and Technology
PCB	Printed Circuit Board
RFID	Radio-Frequency Identification
SA	Self-Assembly
SLS	Selective Laser Sintering
SMD	Surface Mounted Device

Chapter 1

Introduction

Envision a future in which whatever can be made, whenever, wherever, not limited by scale or tooling. Where more complex devices can be made with all functional parts integrated. Complex systems like this are already present in nature, and they are built up from the bottom without external help. Humans build up the smallest structures layer by layer with photolithography and the largest structures top down by taking away material, in both cases limiting the complexity of the shape; the usable materials and the possible structures. If devices could be made in a self-assembling fashion like in nature, this would mean a paradigm shift in technology. It would be possible to construct improved devices in one go, with all functionality integrated. This still seems a mere hypothesis, but the process of self-assembly is already being researched to harness its uses.

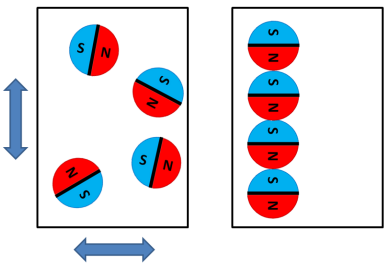

Figure 1.1: Self-assembly by shaking a box with magnetic spheres. The spheres are the structured particles, the magnetic force is the binding force, the box is the environment and the shaking is the driving force.

Self-assembly is the process were building blocks assemble in the desired system while external energy is applied. Or, according to the definition of Whitesides and Grzybowski: a process by which preexisting components autonomously organize into patterns or structures without human intervention [2]. This assembly process is governed by information "coded" in the components (e.g. specific shapes or other physical properties) [3]. In nature self-assembly can be found from the smallest level (e.g. DNA replication, crystal formation) to very large levels (weather systems) [4].

In self-assembly there are four key components: structured particles, binding forces, the environment and a driving force. All these components can be altered to control the self-assembly process [5]. As an example we shake a box with rolling round magnets. When one shakes the container the magnets will pull together and form a chain, as shown in figure 1.1. The structured particles are the magnets that do the actual assembling. The binding forces are the magnetic forces, holding the particles together. Most of the times this binding force is reversible, allowing the system to go from local to global energy equilibrium. The particles are embedded in an environment: the box, which is needed for the binding force to act. For self-assembly to occur the particles must have some stochastic interaction, which is the shaking in the example. This is the driving force, which is usually regarded as noise.

For self-assembly still the fundamental process is researched before it can be used for production. A major step in designing a self-assembly system is the control of the particle interaction. In this report a new measurement system for macro self-assembly experiments is researched.

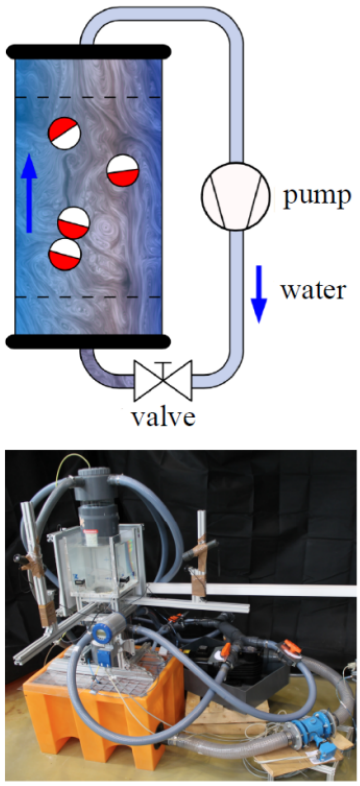

Figure 1.2: Schematic (top) and experimental (bottom) set-up of the macroscopic self-assembly reactor [1].

1.1 Problem Statement

Macro experiments in self-assembly are done at the Korean Institute of Science and Technology (KIST) in Saarbrücken [1]. In these experiments 3D-printed spheres containing a dipole magnet are placed in a water column with a turbulent flow (self-assembly reactor), as shown in figure 1.2. It has been shown that for short observation periods the particles show a random-like motion comparable to Brownian motion, making the SA reactor suited for self-assembly research (the found results can be scaled down to micro scale [6]) [1]. The size of the macroscopic set-up enables observation of the balls by using ordinary cameras. The movement of the balls is monitored using two perpendicularly placed cameras in combination with tracking software (used to detect how the spheres assemble). However this set-up does not fully scale for more than two spheres. In case the dynamics of SA is researched with many spheres it would not be possible to monitor any irregularities inside the emerging structures using the cameras, since the spheres are overlapping. To be able to do self-assembly experiments in the reactor when using more than two balls, another way of measuring connections of the spheres is needed.

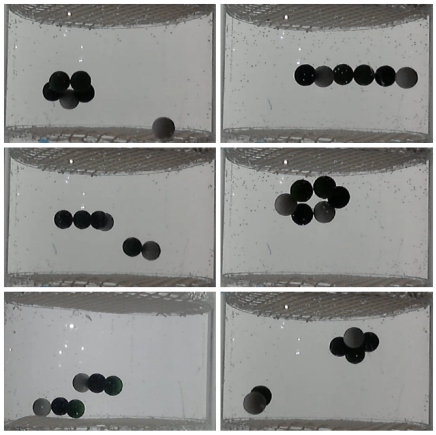

Figure 1.3: Self-assembly reactor containing spheres in local and global energy minima [1].

configuration		magnetostatic energy U/M^2 J$(Am^2)^{-2}$
3.a		−0.85
3.b		−0.75
4.a		−1.31
4.b		−1.34
4.c		−1.28
4.d		−1.00

Figure 1.4: Magnetic energy minima for dipole spheres found from numerical simulations [7]. The energy for a ring and a line of 4 spheres are almost the same, making it interesting to study.

1.2 Assignment

A potential solution for the problem of the non-scalability of measuring the connection events of balls is to integrate functionality within the balls by embedding functional parts with for example 3D printing. A single sphere should comprise two main functions whilst operating in the self-assembly reactor: a means of sensing connections with other spheres and a means of providing data on connections. Electrical, magnetic, mechanical or electromechanical effects will be needed (e.g. capacitance, strain, magnetization or inductance) to detect the connection events of spheres and this will be approached through integrating functionality and 3D printing. This gives rise to the goal of this BSc-assignment:

The goal is to design, manufacture and test spheres for macro self-assembly experiments in a turbulent water flow that can sense connections with other spheres and provide data on connections.

First the needed background theory and practice will be studied. Then the requirements on the spheres will be investigated and choices will be made on both a system and subsystem level. The subsystems and their relations will be studied to obtain a detailed final design. The total system will be manufactured. Tests on the total design will be performed in the self-assembly reactor at KIST. The findings of this thesis yield a prototype for the self-assembly experiments at KIST and recommendations are made on different subsystems of the design.

1.3 Previous Work

A considerable amount of work has already been done connected to the self-assembly experiments at KIST. In this section an overview is given.

In SA research two groups can be recognized, SA with externally and with internally driven parts [4]. The research at KIST falls under the first group, however the second group is also of interest for this assignment. At KIST the dynamics of SA have already been investigated with several particle shapes (tripods, spheres, ovals), the reactor and into the magnetic field of the used cylindrical magnets (posing important boundaries for this assignment) [6], [8]. Also numerical simulations for dipole spheres have been done, looking at the energy minima of configurations of spheres. This showed minima where only the poles of the spheres touched, but also where other points on the spheres touched as shown in figure 1.4[7]. Hence to measure all important energy minima or defects during SA, sensing functionality would be needed which does not only measure connections at the poles of the spheres but also cases were spheres are connected at other locations. Next to that it was found that the energy minima for a ring of four spheres and for a line of four spheres is almost the same (figure 1.4), making it interesting to study with spheres with an internal measurement system (especially since it is difficult to distinct between a line and a ring with video analysis).

Notable examples of projects on this topic can be found in floating magnetic tiles (looking at the aggregation for different tile shapes) [10], magnetic cubes in a turbulent fluid flow (looking at influence of the flow on the chain length in combination with theoretical predictions) [11] and excited monolayers of magnetic spheres (investigating micro and macro patterns of magnetic spheres) [12]. A macro scale example that uses 3D printing is shown in figure 1.5, where 3D printed parts with specific shapes are excited to build structures.

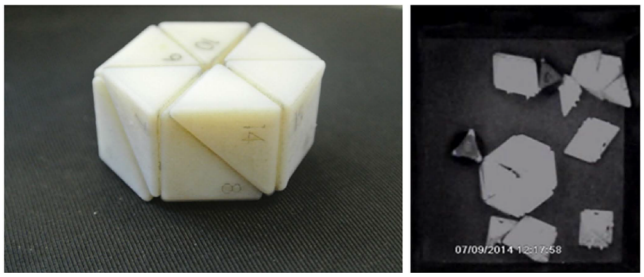

Figure 1.5: 3D-printed parts with specific shapes are excited to obtain self-assembled structures [9].

Next to that also examples of SA with electrical components is researched. Working electrical networks made by SA have already been demonstrated: making parallel and series circuits of LED's [14] and making logic gates through random connection of special electrical "unit cells" [15], [16].

All these examples on the one hand show the large interest and possibilities of macro SA experiments (whether or not in combination with 3D printing, electrical components and magnetic dipole spheres), helping to define the requirements of the to-be designed system. On the other hand these examples have in common that for all of them the measurements are solely done with a single camera (only allowing 2D measurements) or interfacing electrodes. For previous work with regards to sensing connections and communicating data on these connections, one has to look into literature of other fields.

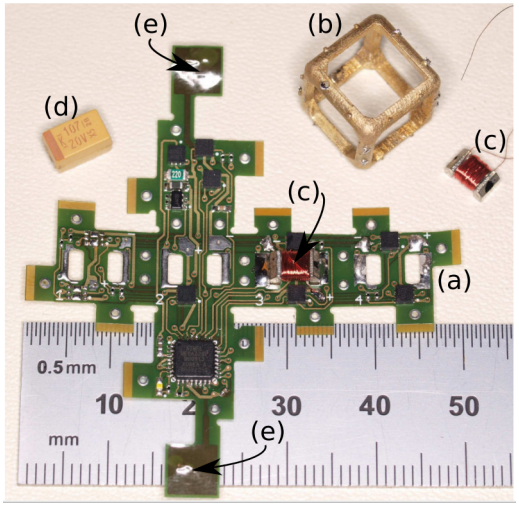

Figure 1.6: The robot pebble is composed of a flex circuit (a), a brass frame (b), four electropermanent magnets (c), and an energy storage capacitor (d) which mounts to the bottom of tabs labeled (e). [13].

Another field of interest for SA research is that of modular robotics. Several proofs of concept for self-assembling modular robots have been made and researched, yielding useful results. Especially when it comes to communication, sensing and power options one has to look into these results. There are two cases of modular robotics: the externally driven and internally driven systems. We will first look at the stochastically, externally driven case since it has close relation to the spheres at KIST. Numerous examples of this can be given, together with their communication, sensing and power features, as shown in table 1.1 [17], [18].

For all examples from table 1.1 functionality has to be fit in limited space. Some systems solve the problem of space by having external power being passed on, others use "seed modules" (modules with the sole function of carrying a power source). Powering happens exclusively with lithium polymer batteries (Lipo batteries) or via an external source. Remarkably almost no system has a way to sense what happens in the environment and

Table 1.1: Examples of stochastically, externally driven modular robots with their functional parts. All devices are used for research into self-reconfigurable robotic systems

Device	**Communication**	**Sensing**	**Power**	**Connecting**
Programmable Parts [19]	IR	-	Lipo battery	Movable magnets
Electromechanical Assembler [20]	Communication coils	-	Lipo battery	Latches
Stochastic 2D [21]	Contacts	-	External power	Electromagnets
Miche [22]	IR	-	Lipo battery	Rotating magnets
Robot pebble [13]	Electropermanent magnets	-	External power	Electropermanent magn
SMORES [23]	Xbee rf	-	Lipo battery	Movable magnets
EM-cube [24]	Zigbee rf	-	External power	Permanent magnets
Swalloable robot [25]	-	Hall sensor	External power	Permanent magnets

next to that only few systems exist that operate underwater. Almost all system connect via magnetic force. An important note is that the devices from table 1.1 are larger than the spheres at KIST (while having the functionality which is needed for this assignment). From these examples only the robot pebble is smaller than the size of the spheres at KIST (the pebbles are $1cmx1cmx1cm$) [13], as seen in figure 1.6. The pebble's size is so small since all functionality is combined in one part: electro-permanent magnets, the electropermanent magnets work as transformers to pass on power from an external source, they are also used as transformers to communicate data. These examples show that both power and sensing at this scale need compact solutions to make it work.

1.4 Structure of the report

Throughout the report a certain structure has been applied. Chapter 2 focuses on some theoretical background needed for this assignment. In the chapters 3 to 7 the method of this research is given in the form of the design, manufacturing and testing of the different components and the total system. The results of the testing are presented in chapter 8 and discussed in chapter 9. Chapter 10 finally presents the conclusion and recommendations for further research.

Chapter 2

Fundamentals

This chapter presents theory as needed for working with the self-assembly reactor at KIST. Next to that analytical equations for magnet calculations are presented.

2.1 Self-Assembly at KIST

At KIST research is done on small scale self-assembly for magnetic particles by means of a macroscopic reactor with a turbulent water flow. In particular the self-assembly process of magnetic micro-particles in a thermal bath is investigated, that connect and disconnect due to their magnetic attraction forces. In the macroscopic experiments water flowing upwards through a pipe (self-assembly reactor) is used to counteract gravity and introduce disturbing energy in the form of a turbulent flow to replace the thermal disturbance energy at small scales. It has been proven by trajectory analysis that the macro particles perform a confined random walk inside the reactor for small numbers of parts and for short observation periods (comparable to Brownian motion) [27].

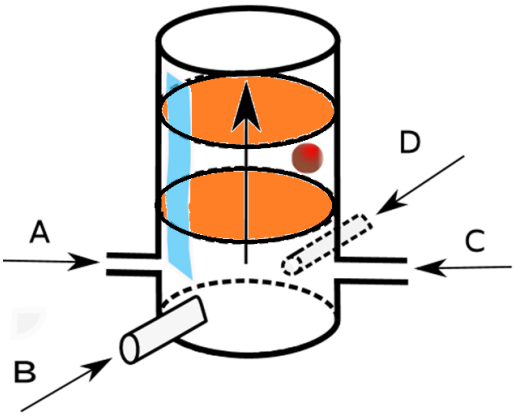

Figure 2.1: Schematic view of the reactor. The colored ellipses are nets that confine the spheres. The four inlets can be adjusted independently to both regulate the flow and the turbulence. [26]

For the set-up a large reactor is used with four inlets at the bottom to provide a flow of water, schematically shown in figure 2.1. Two nets are used to confine the particles to the measurement area. The four water inlets are controlled independently by valves (the so-called *turbulator*) to adjust the asymmetry in the flow and thereby the turbulence, as shown in figure 2.2. In this way the turbulence can be altered while keeping the flow velocity constant. The description as proposed for the turbulent flow is stated to be a 'Richardson cascade". It describes the turbulence as propagation of a vortex which breaks down in a cascade of smaller vortices. The turbulence is said to form due to the balance between the energy initially put in and the subsequent energy dissipation [26].

A picture of the total set-up can be seen in figure 1.2. The yellow basin is used as water reservoir, the grey pipes guide the water, the orange handles are the valves from the turbulator and finally the perspex square basin surrounds the reactor (a square basin is constructed around to reactor to prevent distorted recordings from the cameras by diffraction). Two cameras (Allied Vision Mako G131C) are positioned perpendicularly with regards to each other and to the reactor for recording. The information of the set-up can be used to design experiments.

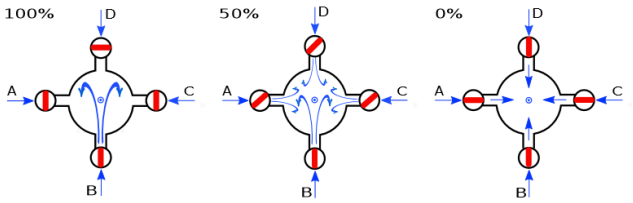

Figure 2.2: Top view of the four valves (turbulator) of the self-assembly reactor. The water flow is shown in blue and the red lines show the state of the valves. [26]

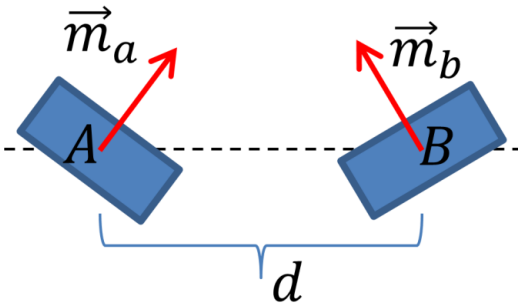

Figure 2.3: Magnet a and b with their orientation.

2.2 Magnets

In the spheres there are magnets to provide the means of connecting to other spheres. These magnets can be modeled by ideal dipoles. For two magnets, magnet a and magnet b as shown in figure 2.3, the B-field, forces and torques can be calculated with the following relations (equation 2.1 to 2.6). In case of multiple magnets, superposition can be applied. For close interaction (from distances of 5 millimeters and closer a significant difference arises between the dipole calculations and reality, appendix B) more precise calculations are needed. For this the finite element method (FEM) will be used. A comparison between the dipole calculations and FEM simulations as applied to this research is given in appendix B in section B.1.

The magnetic dipole moment $\vec{m}_\mathrm{a}$ of a magnet with magnetization $\vec{M}$ (magnetization is the vector field used to express the density of magnetic dipole moments inside a material) is found from:

$$\vec{m}_\mathrm{a} = \vec{M}V = \vec{B}_\mathrm{r}V/\mu_0 \tag{2.1}$$

where $\vec{B}_\mathrm{r}$ is the remanence (the residual magnetization, the field when there is no external field), $\vec{M}$ is the magnetic moment per unit volume, V is the volume of the magnet and μ_0 is the permeability of free space. The permeability of free space is used, since the relative permeability of both water and the shell material are approximately 1. The material of the magnets, neodymium, has a relative permeability of 1.05 which is accounted for in the FEM models. The influence of the batteries on the magnetic field is not taken into account in the calculations (the batteries will have a negative influence, however it is difficult to calculate this and it is expected to be small when the batteries are as far as possible from the magnets and switches). The magnetic field of a magnetic dipole is given by:

$$\vec{B}_\mathrm{ab} = \frac{\mu_0}{4\pi}\frac{1}{|\vec{r}|^3}(3\hat{r}(\vec{m}_\mathrm{a}\cdot\hat{r}) - \vec{m}_\mathrm{a}) \tag{2.2}$$

where $\vec{r}$ is the position vector from magnet a to magnet b. The force exerted by magnet a on magnet b (with B_ab the magnetic field of magnet a experienced by magnet b) can be calculated with:

$$\vec{F}_\mathrm{ab} = \nabla(\vec{B}_\mathrm{ab}\cdot\vec{m}_\mathrm{b}) \tag{2.3}$$

Substituting equation 2.2 and rewriting yields [28]:

$$\vec{F}_\mathrm{ab} = \frac{3\mu_0}{4\pi r^4}((\hat{r}\times\vec{m}_\mathrm{a})\times\vec{m}_\mathrm{b} + (\hat{r}\times\vec{m}_\mathrm{b})\times\vec{m}_\mathrm{a} - 2\hat{r}(\vec{m}_\mathrm{a}\cdot\vec{m}_\mathrm{b}) + 5\hat{r}((\hat{r}\times\vec{m}_\mathrm{a})\cdot(\hat{r}\times\vec{m}_\mathrm{b}))) \tag{2.4}$$

Finally the torque exerted by magnet a on magnet b can be found from [29]:

$$\vec{\tau}_\mathrm{ab} = \vec{m}_\mathrm{b}\times\vec{B}_\mathrm{ab} \tag{2.5}$$

Which can be rewritten to:

$$\vec{\tau}_\mathrm{ab} = \frac{\mu_0|\vec{m}_\mathrm{a}||\vec{m}_\mathrm{b}|}{4\pi|\vec{r}|^3}[3(\hat{m}_\mathrm{a}\cdot\hat{r})(\hat{m}_\mathrm{b}\times\hat{r}) + (\hat{m}_\mathrm{a}\times\hat{m}_\mathrm{b})] \tag{2.6}$$

In figure 4.3 equation 2.4 has been used to calculate the force over distance for the separation of magnet a and magnet b for different magnet sizes (every line represents the separation of two other equally sized magnets).

The equations as presented in this section will be used for determining the ideal layout and sizes for magnets.

Chapter 3

Systems Engineering

The spheres will be containing integrated functionality and they will operate in a harsh environment, making up a complex system. To design this complex system, a system engineering methodology will be applied. The requirements of the system will be analyzed together with the budgets and functions of the system. This can be used to define several subsystems. The different options for the subsystems will be investigated from which multiple scenarios of the total design can be derived. From the requirements low level criteria can be derived on which the scenarios can be judged, yielding a total design of the system.

3.1 Requirements

The spheres will only be used for specific self-assembly research. Among others the users (the stakeholders), the environment and the experimental set-up directly pose requirements for the design. The spheres should be designed with regards to the following set of requirements:

- Offer a way of connecting the spheres
  - Magnet(s)
- Be able to detect connections of spheres
  - Band width of 3 Hz
  - Only connections on the sides of the magnetic poles needs to be detected
- Communicate connections of spheres
  - Real-time or after the experiment
  - The data needs to be synchronized for all separate spheres
  - The data needs to be stored for all spheres (centralized (main hub) or decentralized (inside balls))
- Process experimental data
  - A file with time stamps of connections of the spheres needs to be the result after using the spheres
- Provide homogeneous, identical spheres
  - The center of mass needs to be in the hydrodynamic center (the middle of the spheres)
  - The spheres can have at most a diameter of 30 mm (posed by the size of the self-assembly reactor)
  - The spheres can have no protruding parts (smooth spheres)
  - Structural integrity is needed
  - The same effective density is needed for all spheres
- Provide a terminal velocity of the spheres within the flow velocity of the reactor
  - The spheres need a suited effective density
- Provide a watertight housing
  - The functionality inside the spheres needs to be protected from the turbulent flow
- The spheres need to be able to operate for 30 min
  - Have an acceptable energy consumption
  - Low energy leakage when not used
- House the parts needed for the experiments
  - House a magnet and other functional parts.
- Reasonable usability and safety
  - The device should be reasonably operable and safe to use

3.2 Budgets

System budgets are used to allocate parts of the system requirements to subsystems, assemblies, components and parts. A budget in the sense of systems engineering is an available quantity which is divided over the

subsystems in a certain way. Important budgets for this system are:

- Volume: spheres of at most 30 mm diameter need to comprise all parts
- Power: only a limited amount of power will be available to the total system (to ensure operation of 30 min)
- Costs: design costs are minimized
- Weight: the weight has to be in a certain range to yield a suited density for usage of the system since the volume is set (a density in the range of $1000\,\mathrm{kg\,m^{-3}}$ to $1300\,\mathrm{kg\,m^{-3}}$ requires a weight of 14.1 g to 18.4 g)

These budgets can be used as guideline in making design choices. With a realization of the budgets, the system can be validated and improved (section 9.2). In the requirements already some trade-offs are made with regards to the budgets. For example the current spheres have a diameter of 20 mm, whereas the requirement is set at 30 mm. Size is given up to maintain complexity of the system.

3.3 Functional Analysis and subsystems

As found from the requirements, the system has to perform several functions. The following functions need to be fulfilled:

- Connect spheres (required to be magnet(s) due to the experiments)
- Detect connections of spheres
- Communicate connections of spheres
- Process the experimental data
- House all parts (watertight) and offer structural integrity
- Deliver electric power

From these functions already a functional block diagram can be made, as seen in figure 3.1. With the needed functions a step can be made from the problem domain to the solution domain: the subsystem level, where several scenarios composed of different subsystems can be compared. The subsystems derived from the functions become (in the same order as they follow from the functions):

- Magnet(s)
- Sensor(s)
- Data communication
- Processor/electronics
- Shell
- Battery

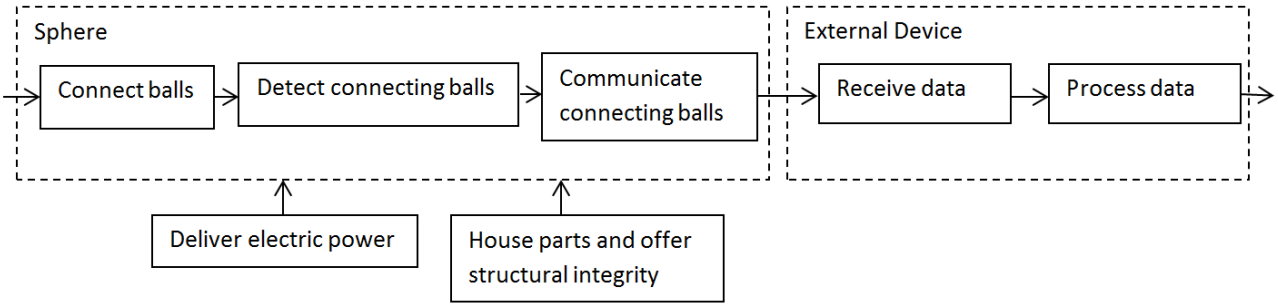

Figure 3.1: Functional block diagram of the system.

3.4 Design choices

Different options for the subsystems have been considered, yielding the design tables as shown in figure 3.2to 3.5. By evaluating the different options for subsystems with the budgets and low level requirements, several scenarios were chosen. In the following sections the trade-offs and choices are given. Information for sensing mechanisms was found from sources on tactile sensing [30], [31], for information on real-time underwater data communication sources on underwater drone communication were used [32], [33].

3.4.1 Sensor(s)

For the sensing mechanism 11 different options have been considered. Next to the budgets, sensing requirements (one can think of sensitivity, directionality, noise level) were used to evaluate the performance of each option.

For sensing mechanisms a distinction is made between methods that sense proximity and methods that sense contact. In the experiments proximity is preferred over contact sensing, since it gives additional statistical

information. None of the options significantly changes the environment (the shape of the shell needs to deform or piezoresistive measurements and the magnetic field slightly changes due to a reed switch, however this is all not significant). Several options directly drop out: capacitive sensing (if the capacitance between the spheres has to be measured, all the spheres need to have the same ground, which is difficult for water tight spheres), inductive sensing (expensive bulky sensors), optical link (optical sensing is difficult since the spheres need to be watertight and let through the light at the same time), ultrasonic sensing (the turbulence of the reactor causes a lot of noise), accelerometer (it will be difficult to distinguish shaking of the sphere from gentle connections with other spheres) and finally 3D printed transducers (despite the promises of 3D printing integrated transducers into the walls of the sphere, at the moment the technology is not advanced enough for making this complex system). Both piezoresistive and piezo electric sensing are questionable, since the wall of the spheres have to be flexible for large enough deformations. The hall sensor, switch, piezoresistive sensor and reed contact will be used for the scenarios.

Sensing (contact/proximity)	Volume	Power	Costs	Weight	Sensing requirements
Hall sensor (proximity)	++	0	+	++	++
Switch (contact)	++	++	++	++	0
Capacitance (proximity)	0		+	++	+
Piezoresistive (contact)	0	- -	+	++	+
Inductive (proximity)	-	0	--	+	++
Reed-contact (proximity)	++	++	++	++	+
Optical link (proximity)	+	-	+	++	0
Ultrasonic (proximity)	-	-	-	+	+
Accelerometer (contact)	0	-	+	++	--
Piezoelectric (contact)	0	+	+	++	+
3D printed transducer	+	+	+	+	-

Figure 3.2: The options of the sensor(s) subsystem valued with the budgets.

3.4.2 Data communication

For data communication the most important distinction can be made between real time measurements and offline processing. With the low level requirements for the real-time systems one can think of signal range, bandwidth, directionality, speed and for the storage options for example of storage space and the limit of write cycles. In the experiments real-time communication does not offer any benefits over data storage. Several options directly drop out: ultrasound (turbulence and the hard water flow will give a lot of noise), wired communication (having the spheres connected to the outside world would distort the results), optical link (just as with video analysis, an optical method does not scale for larger numbers of spheres), direct contact (making the spheres watertight with electrodes on the outside could pose large difficulties) and electropermanent magnets (a wonderful option, however too expensive). For the wireless communication platforms only two options fit within the size requirements: the esp8266 (a micro-controller with integrated wifi) and RFID tags. However to ensure their operation underwater (water has very high attenuation for electromagnetic waves in the wifi and RFID bandwidths [34]), small experiments have been performed (appendix A.1.2 and A.1.1). These experiments showed that the esp8266 can be used (but has a large signal attenuation and a huge power consumption) and RFID cannot be used with the available sources (it has been used underwater for identifying fish however [35]). For return current communication (transmitting a modulated signal with two exposed electrodes), only little research has been done, however it has been shown to work in fresh water [32]. Finally also several data storage options exist. For data storage and 3 Hz switching (hence 6 events per second, 3 times a connection and 3 times a disconnection) for 30 min of experiments while assuming 4 bytes per event are needed yields: $30\,\text{min} * 60\,\text{s} * 6 * 4\,\text{B} = 43\,200\,\text{B} = 337.5\,\text{kbit}$. As final solution flash memory is chosen (in section 3.4.3).

3.4.3 Processor/electronics

The choice of the electronics depends upon the sensing mechanism and data communication. In some cases no additional electronics are needed (with a passive RFID chip and an interconnected switch for example all

Data communication	Volume	Power	Costs	Weight	Data requirements
Arduino RF module	0	-	+	++	-
Zigbee (RF)	-	-	0	++	-
Xbee (RF)	-	-	0	++	-
RFID tag	+	++	0	++	-
Wifi (ESP8266)	-	-	+	++	-
Ultrasound	-	0	-	+	+
Wired communication	++	++	++	++	--
Optical link	+	+	+	++	-
Return current	+	+	+	++	-
Direct contact	+	0	++	++	-
Electropermanent magnets	+	-	--	+	++
SD card	-	-	-	++	+
Flash memory	+	0	+	++	+
Micro controller internal storage	++	+	++	++	+

Figure 3.3: The options of the data communication subsystem evalued with respect to the budgets.

powering and processing functionality could be placed outside of the reactor). One choice however can be made in the cases where a micro-controller is needed.

For micro-controllers currently two popular options exist in the field: the ATmega series and the esp8266 series. Both options have there own advantages and disadvantages. Scenarios have been designed to compare between the two, where a reed switch is used as sensing example and different data and powering options are used, as shown in figure 3.4. In the comparison the esp8266 shows the best specifications (small size, low power consumption, the size of the internal storage makes separate storage or communication functionality superfluous). In the end however scenario 1 is preferred over scenario 3 by the author. Due to time reasons it is easier to work with the ATmega328P because of the extensive documentation, libraries and community. Moreover the specifications of the ATmega328 are still within the requirements. The flash memory is chosen as data storage for its high reliability, simplicity and relatively low power consumption (it only draws power when in operation and consumes four times less power than an SD card).

For the electronics it was chosen to design a PCB, for the following reasons:

- **Easy stabilization**: With a PCB it is easier to stabilize the sphere due to the symmetry and control of the position of components
- **Robust design**: The robust design makes it easier to assemble and use the spheres in experiments, increasing its usability
- **Integration of components**: Functional components like magnets can be integrated into the PCB, helping to get a smaller and more compact system

3.4.4 Magnet(s)

Only two options exist for the use of the magnets (single centered and double separated magnets). Since the PCB has to be placed in the middle of the sphere for minimizing the size of the sphere (with micro-controller and flash memory in the middle of the PCB to make everything fit), two small magnets at the sides are chosen. Additional research is done on the effects of using two magnets in chapter 4.

3.4.5 Battery

The powering options are compared in figure 3.5. Several battery types are considered as well as a so-called seed particle. A seed particle would in this case be a particle with as single function powering the other spheres (hence having a connection to an outside power source or carrying a large battery). A seed particle will not be possible because of the experimental set-up and volume restrictions (an external seed particle has to be connected to the wall or to a wire, lowering the movement freedom of spheres. An internal seed particle carries a large battery. Furthermore for all types of seed particles additional infrastructure inside the spheres will be

Processing/Electronics	Scenario 1	Scenario 2	Scenario 3
Controller	ATmega328P TQFP	ATmega328P TQFP	ESP8266-09
Battery	2x LR 44 (series)	2x CR2032 (parallel)	2x LR 44 (series)
Crystal	16MHz crystal	16MHz crystal	Internal clock
Magnets	2 small magnets	2 small magnets	2 small magnets
Sensing	2 SMD reed switches	2 SMD reed switches	2 SMD reed switches
Memory	1Mbit external flash	2GB SD card	1MB internal memory
Write cycles	100k	100k	10k
Programming	6 I/O pins	TQFP package programming cable	6 I/O pins
On/off switch	no	no	no
VCC	3V	3V	3V
I/O pins	14 digital, 8 analog	14 digital, 8 analog	6 digital
PCB needed?	yes	yes	yes
Complexity use	+	++	-
Batteries capacity	220mAh	440mAh	220mAh
Power consumption controller	10mA	10mA	15mA
Power consumption memory	25mA	100mA	-
Power consumption switches	0.6mA	0.6mA	0.6mA
Total current at 3V	40mA	110mA	16mA
Operating time	5.5h	4h	13.7h

Figure 3.4: The scenarios for the processor/electronics subsystem.

Battery	Volume	Power	Costs	Weight	Battery requirements
Lithium polymer battery (rechargeble)	0	+	--	+	++
Button cell LR44	+	+	++	+	+
Button cell CR2032	0	+	+	+	+
Seed particle (externally powered)	++	++	++	++	--

Figure 3.5: The options of the battery subsystem valued with the budgets.

Table 3.1: Comparison of 3D printing technologies as adapted from Mathijs Schlepers [36]

Technologies	Cost	Resolution	Mechanical	Material range	Build speed
FDM	++	-	+	+	-
DLP	+	++	-	+	++
SLS	-	+	++	++	+
Polyjet	-	++	-	+	+

needed to transfer the power). Both button cell and lithium polymer (lipo) batteries are suited. Due to there size, price and the ease of use LR44 button cell batteries will be used.

3.4.6 Shell

The shells will be made by 3D printing. 3D printing offers free form design with customized performance, easy integration of all components (yielding a smaller volume and a better system architecture), small costs and a fast process. A comparison of the available printing technologies has been adapted from Mathijs Schlepers in table 3.1 [36] (at the University of Twente and through external services). Fused Deposition Molding (FDM) has a low resolution, limited supports are possible and it is known for its porous structures, however it is also cheap and simple to use. Polyjet technology has a very high resolution, but supports have to be removed manually and the method is costly. Digital Light Processing (DLP) also has a high resolution and is relatively cheap, but the support structure can pose difficulties. Selective Laser Sintering (SLS) does not need supports, high mechanical strength parts can be made and the material cost is low, however it has a low resolution when compared to for example polyjet technology.

Except for FDM all mentioned technologies can be used for water tight structures. From the comparison between the technologies in table 3.1 it was found that polyjet and DLP printing are the most suited for high resolution parts [36]. An Objet Eden 250 polyjet printer is available at RAM, hence this technology will be used.

3.5 Scenarios

All subsystems with their possible options have been discussed. Scenarios for the best options are put together and are shown in figure 3.6.

By comparing the four scenarios, scenario IV comes out as the most suited for this research. All wireless forms of data communications have shortcomings in the experiment. From the experiments in appendix A it has been shown that RFID and wifi are difficult to use due to the attenuation of the signal by the water. Furthermore proximity sensing technologies like hall sensors and read switches are easier to implement than contact sensing (needing a flexible wall or external components). Moreover reed switches have a very low energy consumption (they only need a pull-up resistor) and are easy to use.

Scenario IV allows for all top level requirements to be fulfilled. Reed switches have a large bandwidth (up to hundreds of Hz switching can be performed). With 1 megabit of data over 30000 events can be stored (4 bytes per event are needed if for every event a time stamp in milliseconds and the state of both reed switches needs to be recorded). The micro-controller can send the data over serial connection to a computer, where it can be analyzed (and put in a txt file). The PCB design allows for homogeneous, identical spheres where weights can be added for a proper terminal velocity. Finally with the system an acceptable energy consumption can be achieved while the system is easy to use.

3.6 Proposed system

An overview of the chosen options for subsystems is given in figure figure 3.6, scenario IV. For the implementation of the subsystems, some choices will be elaborated on in the coming chapters. For the behavior of the

Total system scenarios	Scenario I	Scenario II	Scenario III	Scenario IV
Data communication	Return current	Wifi (ESP8266)	RFID	Flash memory
Sensor(s)	Hall sensor	Piezo resistive	Switch	Reed switch
Power	Lipo battery	Lipo battery	-	Button cell battery
Magnet(s)	2 small permanent magnets	1 permanent magnet	2 small permanent magnets	2 small permanent magnets
Shell	Polyjet	Polyjet	Polyjet	Polyjet
Processor/Electronics	Amplifier circuit	ESP8266 and wheatstone bridge	External processor	ATmega328P with circuit
External equipment in experiment	Yes	Yes	Yes	No

Figure 3.6: Four scenarios with different implementations of the subsystems have been proposed for the final design.

system a state transition diagram has been made, figure 3.7. This diagram will be used for writing the code of the micro-controller.

The different subsystems will be embedded into the spheres for the optimal use of space. A PCB will be used to house the electronics, reed switches and magnets. Two batteries will sit on both sides of the PCB (for balance and the correct voltage). Finally the shells will be designed in such a way that the whole system will be a "plug and play" device. The batteries are connected into holders and the PCB with batteries can be slid into a shell. The edges of the shells will be covered with vaseline (to make it water tight) and the other shell will be put in place. An impression of this system is shown in figure 3.8.

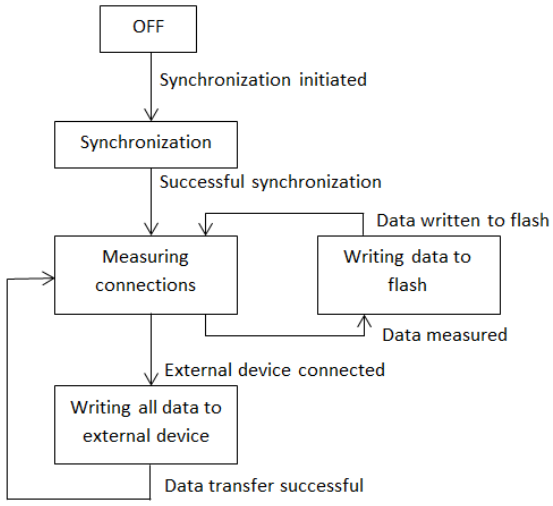

Figure 3.7: A state transition diagram of the systems behavior.

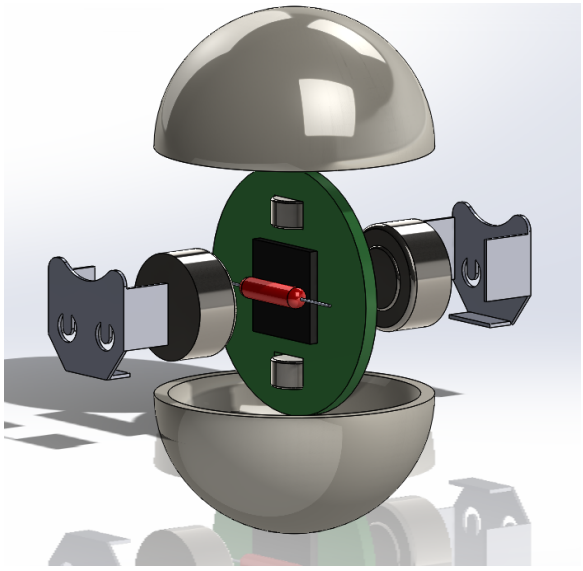

Figure 3.8: An impression with an exploded view of the proposed design and its components, with all components as adapted from scenario IV (figure 3.6).

Chapter 4

Magnets and sensing

In this chapter the final magnet configuration is calculated and a sensing mechanism with reed switches is designed.

4.1 Magnets

Magnets are used for connecting the spheres and the magnetic field of these magnets is used for sensing connections. For both functions the magnet size and position has to be determined.

4.1.1 Single and separated magnets

To determine whether smaller, separated magnets can be used instead of a single, large centered magnet, ideal dipole calculations (with the equations as shown in section 2.2) have been performed for the magnetic fields (equation 2.2), forces (equation 2.4) and torques (equation 2.6). For different orientations of the spheres and magnet sizes these calculations have been performed. The different orientations are shown in figure 4.1. Since the magnetic field for smaller magnets falls of at smaller distances than for larger magnets it is expected that below a certain magnet size, two separated magnets cannot be used.

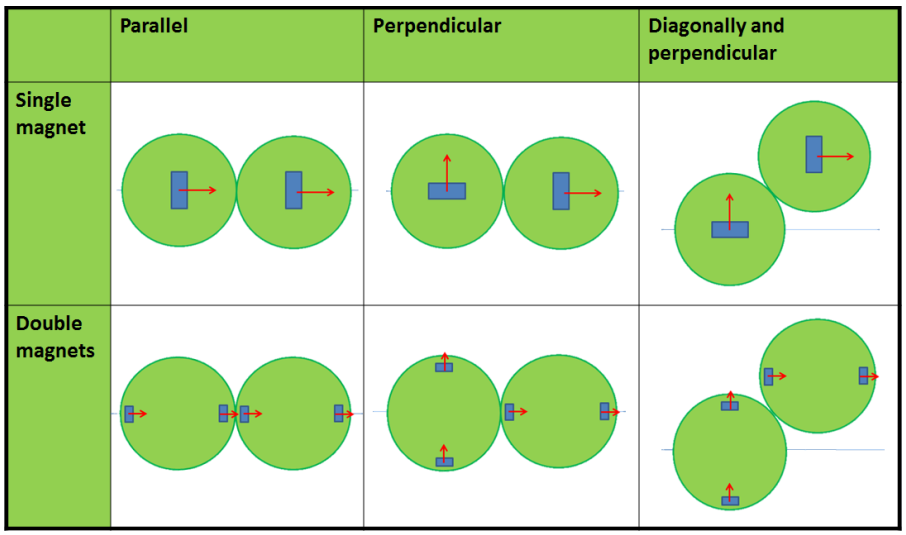

Figure 4.1: The orientations of the magnets and spheres as used for the energy calculations.

The magnets and orientations considered can be found in table 4.1. All magnets were taken as cylindrical N35 magnets (N35 magnets have a remanence of 1.2 T, hence at the surface of the magnet the field is 1.2 T if there is no external magnetic field).

The largest magnet (⌀ 12 mm×4 mm) is taken as reference for the calculations and is placed in the center of the sphere. In the calculations it was first assumed that the connection force of the spheres is approximately equal to 0.0138 N, the connection force of a sphere with a 30 mm diameter and the 12 mm diameter and 4 mm height magnet sitting exactly in the middle. From the force curves as shown in figure 4.3 the spacing needed for proper connection of the spheres can be calculated (a connection force of 0.0138 N), the distances are shown in table 4.1. By looking at the B-field for spheres with different magnets and the same connection force (the

Table 4.1: Magnet sizes and spacing as used in modeling the sphere interaction forces, torques and energies.

Colour	Diameter [mm]	Height [mm]	Spacing magnets [mm]
dark blue	1	1	1.3
dark green	2	1	2.5
red	2	2	3.5
light blue	4	2	7.1
purple	4	4	10.0
light green	12	4	30.0

same connection force hence a different offset), it can already be seen that for the separated magnets the field drops of a lot faster than for larger magnets, figure 4.2. The normalized field for both magnets drops off the same, however they have a different size and thus a different scaling factor. This makes that the magnetic field outside of a sphere for large and small magnets with different offsets with the same connection force, drops of quicker for the smaller magnets (as shown i figure 4.2). In figure 4.2 a sphere is shown for different cases of table 4.1, were in every case a different sized magnet is placed in such a way that the connection force with an equal sphere is 0.0138 N.

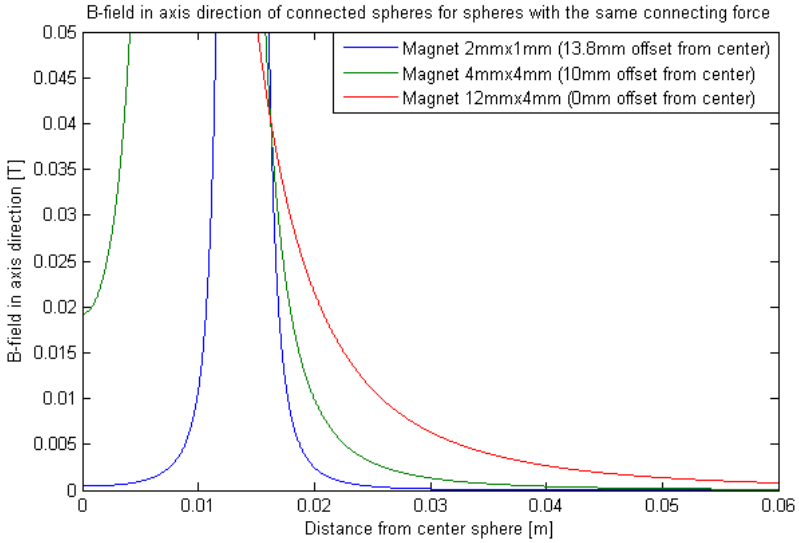

Figure 4.2: Comparing the B-field for spheres with a different magnet with the spacing from table 4.1and the same connection force. Spheres with smaller magnets with a large offset from the center of the sphere are shown to drop off over a shorter distance than large magnets with a smaller offset.

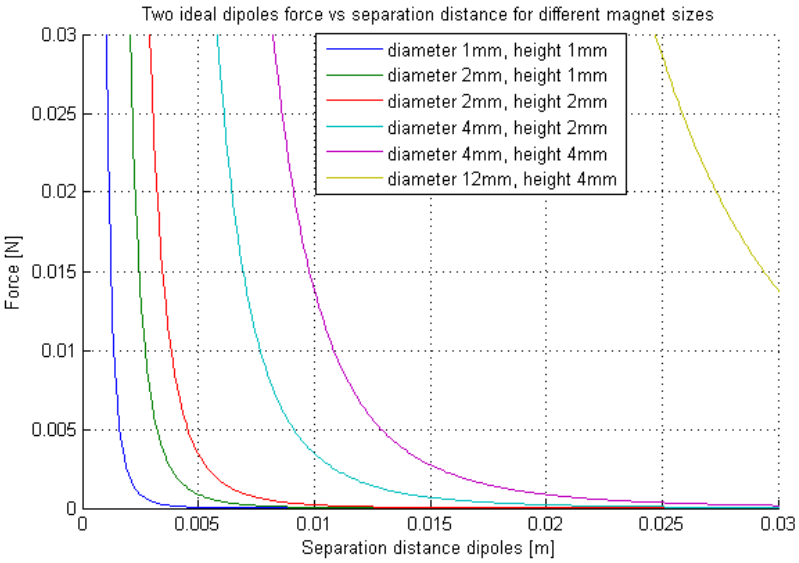

Figure 4.3: Force over distance for different different sizes of dipoles when they are parallel with each other (the force between two parallel single magnets).

Table 4.2: The energy needed for separating connected spheres with parallel magnets to 10 cm distance between the sphere edges.

Magnet	⊘ 1 mm×1 mm	⊘ 4 mm×4 mm	⊘ 12 mm×4 mm
Seperation energy	-1.01×10^{-8} J	-8.56×10^{-7} J	-5.89×10^{-6} J

Table 4.3: The forces and torques as calculated for the different sphere and magnet orientations as found in table 4.1

	F [N]	d [m]	τ [Nm]
Aligned			
⊘ 12 mm×4 mm	0.0138	0.030	0
⊘ 4 mm×4 mm	0.0138	0.010	0
⊘ 2 mm×1 mm	0.0138	0.0025	0
Perpendicular			
⊘ 12 mm×4 mm	6.9e-3	0.030	6.9e-5
⊘ 4 mm×4 mm	7.9e-4	0.020	4.7e-6
⊘ 2 mm×1 mm	4.2e-6	0.01625	2.1e-8
Diagonally			
⊘ 12 mm×4 mm	0.0104	0.030	7.0e-5
⊘ 4 mm×4 mm	1.8e-3	0.0159	7.5e-6
⊘ 2 mm×1 mm	3.2e-5	0.0106	8.0e-8

The energy of the connection is expected to be different for spheres with small magnets and for a sphere with a single large magnet. To show the difference in energy needed to separate spheres (which is relevant for the reactor experiments since the magnetic energy can best be based on the disturbing energy) with small and with large magnets, the energy to separate spheres has been calculated. With the magnets mentioned in table 4.1 and the parallel sphere orientation in figure 4.1 the energy to separate the spheres from connection to 100 mm separation distance between the sphere edges has been calculated. This can be done by performing the integral in equation 4.1 (moving one of the two spheres from location 1 to 2).

$$E_{12} = \int_{x1}^{x2} \vec{F} \cdot \vec{ds} \tag{4.1}$$

For the double magnets, all four magnet-magnet interactions have to be added to the integral. This has been done for several magnets, as shown in table 4.2. The forces as shown in figure 4.3 have been used for performing the integral. From the calculations can be seen that for spheres with separated smaller magnets, the separation energy is significantly lower than for spheres with one large magnet in the middle, table 4.2.

For all cases in table 4.1 also the force and torque when connected have been calculated for some magnets, this can be found in table 4.3.

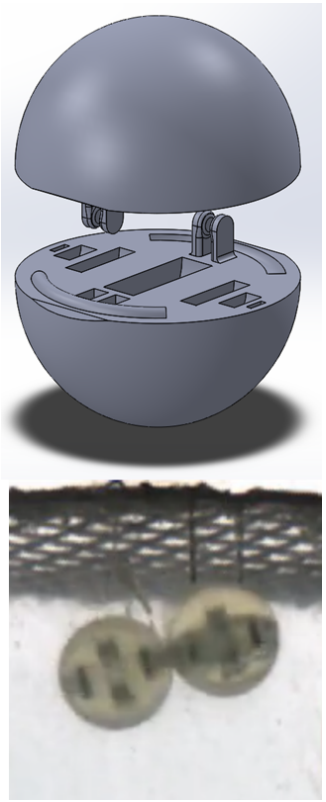

Figure 4.4: A sphere with different slots or experimenting with different magnets in the self-assembly reactor (top), the sphere during the experiment in the self-assembly reactor (bottom).

4.1.2 Magnet experiment self-assembly reactor

from both table 4.2 and 4.3 it may be clear that, although the connection force is the same for the different sizes of magnets, the forces and torques in different orientations and the energy to separate the spheres is completely different. From these calculations it can be concluded that single magnets can be used for higher turbulence in the reactor (since a flow with a higher turbulence has more disturbing energy). It can also be concluded that the smallest magnets will be in a range were already flows with only little turbulence have enough disturbing energy to separate the spheres.

4.1.3 Fluid forces and magnets

To determine the connection force needed, one has to consider the water flow in the reactor. The flow in the reactor is approximately equal to the terminal velocity of the spheres, to make them hover. The connection force of the spheres

Specifications	**Current spheres** [7]	**Design**
Radius r [m]	0.005	0.015
Density ρ [kg m^{-3}]	1300	$\approx$ 1100
Drag coefficient C_D	0.5	0.5
Estimated drag force [N]	0.0031	0.028
Connection force magnets [N]	0.0083	0.028
Calculated terminal velocity [m s^{-1}]	0.28	0.28

Table 4.4: Comparison of the specifications relevant for the fluidic forces for the currently used spheres and the design.

has to be overcome by turbulence to separate the spheres and simulate a random walk (dimers also perform a random walk). The terminal velocity in water can be calculated as follows [37]:

$$v_t = \sqrt{\frac{4gd}{3C_D}(\frac{\rho - \rho_w}{\rho_w})} \tag{4.2}$$

The data of the spheres already used at KIST is compared to the calculated specifications of the design in table 4.4 (the density is estimated from the size of the spheres and the weight of 3D printed parts, batteries and electronics). The drag force is calculated from $F_{drag} = \frac{1}{2}\rho A v_t^2 C_D$, were the drag coefficient $C_D = 0.5$ (for spheres $C_D \approx 0.5$ in a large range of turbulent flow).

To verify the connection force and to check whether separated magnets can still be used, an experiment has been performed in the self-assembly reactor at KIST. Spheres have been designed and made with slots for different magnet sizes at different positions, as seen in figure 4.4 and C.7. The spheres have been tested with one ⌀ 12 mm×4 mm magnet in the middle, two ⌀ 8 mm×2 mm magnets 8 mm from the center and two ⌀ 4 mm×1.5 mm magnets 11.5 mm from the center. In the experiment the flow speed was slowly increased and the turbulence was increased in stages. It was found that the smallest magnets (two ⌀ 4 mm×1.5 mm magnets) could not keep the spheres together, making them already separate during laminar flow (when all valves are opened equally). The single large magnet spheres were found to generate too strong forces, and only the highest flow with a lot of turbulence could separate the spheres. In the case in between, the connection force was found to be good, with a lot of events as a result. The connection force was found to be around 16 mN in this case (taken from figure 4.3). This is significantly lower than the rough estimate of the fluid forces (28 mN), this finding has been used for the further design. The choice of magnets was made ⌀ 4 mm×4 mm (small and a high field) with its center at 6.5 mm from the spheres edge (figure C.2).

4.1.4 Magnetic fields

The B-field has to be determined for a proper location and orientation of the sensing mechanism (reed switches). The reed switches need around 2 mT for switching (measured with a helmholtz coil). To determine the B-field ideal dipole calculations, with the equations from section 2.2, and FEM simulations with the COMSOL Multiphysics software have been performed (see appendix B). In these calculations the magnet lay-out as proposed in the previous section has been used. The dipole models have been used to show the validity of the FEM calculations (see section B.1). The B-field in z-direction has been considered for three different axes, as shown in figure 4.5 (the main axis through the magnets, an axis parallel to the main axis at 3 mm distance and an axis perpendicular to the main axis through the center of the sphere). These calculations have been done for both attracting and repelling polarity of the spheres.

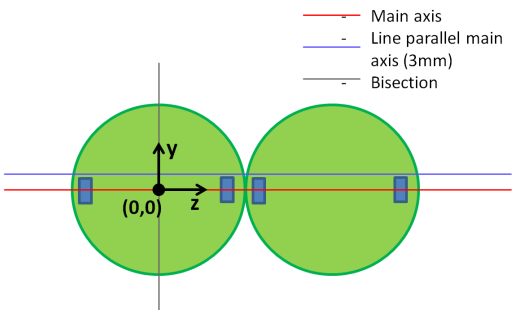

Figure 4.5: The three axes considered for the B-field calculations with the proposed magnet lay-out (for attracting and repelling polarity).

In figure 4.6, 4.7, 4.8 and 4.9 the results can be seen. From the calculations it could be found that the only location of interest for the reed switches is in between the spheres' edge and the magnets, since only at this location the B-field changes considerably upon attracting or repelling another sphere. Next to that the reed switches already switch at many places due to the magnetic field of the own sphere. More information on reed switches is needed for a proper placement of the switches.

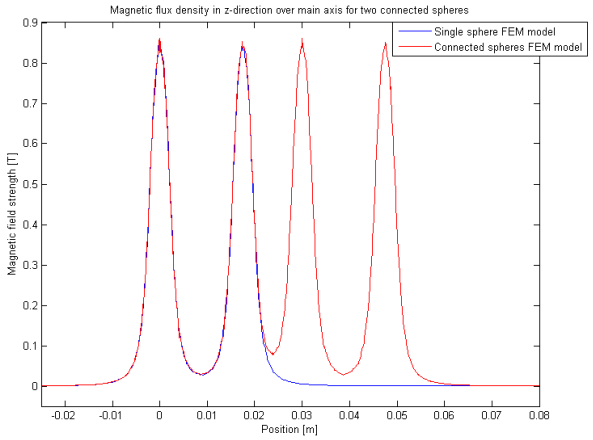

Figure 4.6: A comparison for the B-field in z-direction over the main axis for a single sphere and two attracting spheres.

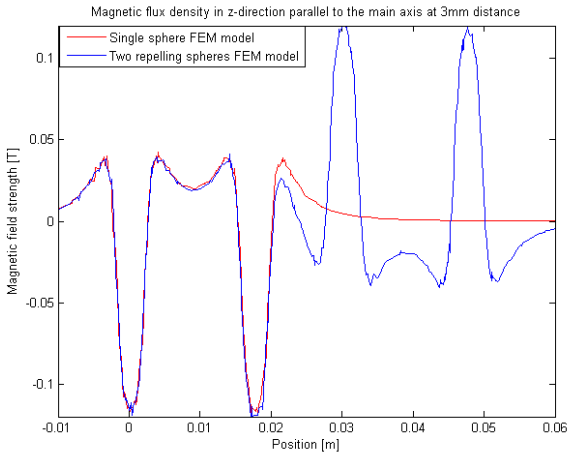

Figure 4.7: A comparison for the B-field in z-direction parallel to the main axis at 3 mm distance for a single sphere and two repelling spheres.

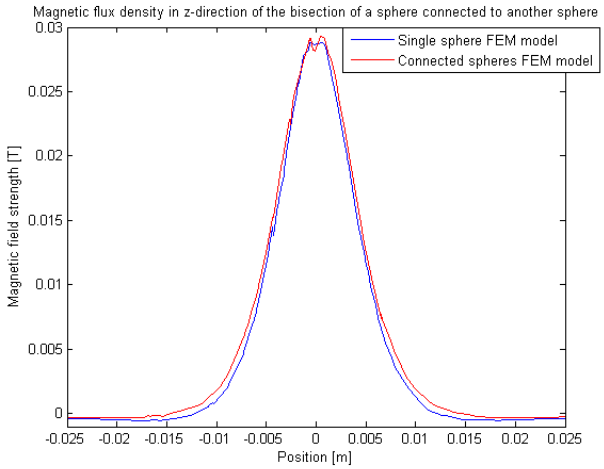

Figure 4.8: A comparison for the B-field in the z-direction of the bisection for a single sphere and two attracting spheres.

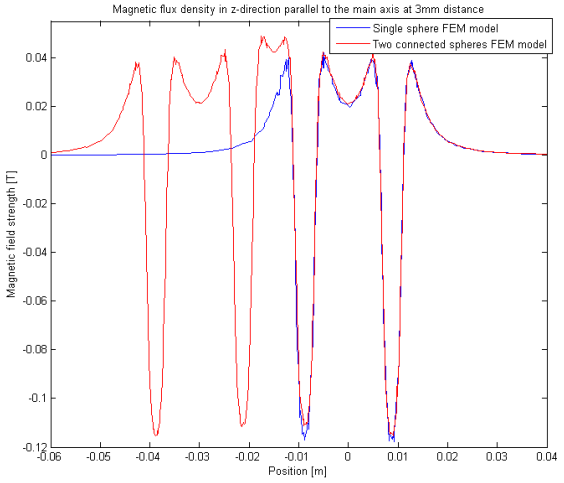

Figure 4.9: A comparison for the B-field in z-direction parallel to the main axis at 3 mm distance for a single sphere and two attracting spheres.

4.2 Reed switch

For the sensing mechanism reed switches were chosen. Reed switches are closed from a certain strength of the magnetic field onward (the switches used in this research close at approximately 2 mT) without significantly disturbing the magnetic field (there will be a change of the magnetic field, but this is very small). A reed switch consists of two ferromagnetic leads (e.g. nickel-iron alloy 52 with the same thermal expansion as the used glass seals) in a sealed glass cylinder. The two reeds are separated internally, forming a gap. When there is a magnetic field parallel to the switch, the reeds will serve as field guide. They will move towards each other by the torque exerted upon them, minimizing the energy in the gap (this has been checked with an optical microscope, the reeds move towards each other and not towards the magnet, hence a torque is exerted and not a force. Another way to think about it is that the magnet induces opposite magnetic poles on the ends of the reeds, resulting in attraction).

Sensitivity to closure of a switch is measured in mT (or A T, ampere turns, since standard coils are used to characterize switches). When a magnet is brought into contact the switch closes (pull-in) and when it moves away far enough again it opens (drop-out). In the operation of a reed switch there is some hysteresis, caused by the different pull-in and drop-out field limits. Bouncing also occurs in reed switches, however this only takes several milliseconds [38].

In figure 4.10 and 4.11 the sensitivity plots of a reed switch can be seen [39]. The solid lobes in the plot

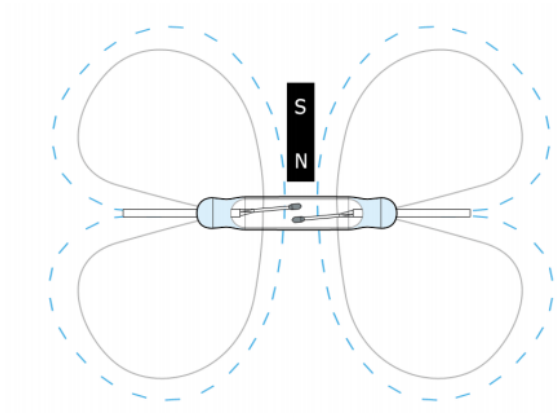

Figure 4.10: Sensitivity lobes for a magnet perpendicular to the reed switch [39].

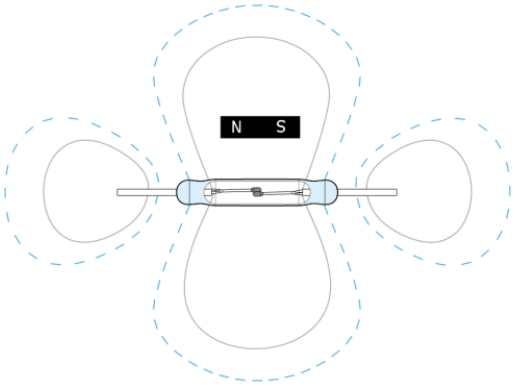

Figure 4.11: Sensitivity lobes for a magnet parallel to the reed switch [39].

Table 4.5: Characterizing the reed switches with a Helmholtz coil

	pull-in [mA]	drop-out [mA]	pull-in [mT]	drop-out [mT]
Reed switch (SMD)	88.5	66.3	2.15	1.61
Reed switch (through hole)	18.5	12.4	0.45	0.30

display the pull-in distance and the drop-out distance is shown with dotted lines (the piece in between is the region were hysteresis takes place). It can be seen that a switch only works in case of a magnetic field parallel to the switch. Hence when the reed switch is perpendicular to the field (no net parallel field component), it does not switch! For a perpendicular magnet this happens on both axes through the center of the switch (figure 4.10), for a parallel magnet this happens on two curved lines perpendicular to the switch (figure 4.11). The reed switches have to be positioned in such a way that the sensitivity lobes are only influenced by the magnet field of a near sphere. The magnetic fields as described in section 4.1.4 already show the difficulty of the reed switch positioning. Additional experiments will be done to verify the specifications of the switches.

4.2.1 Reed switch experiments

Experiments are done with an SMD reed switch (STANDEXMEDER MK23-35-B-2, figure A.5) and a through hole reed switch (STANDEXMEDER GP560-1015, figure A.4). First the switches have been characterized by placing them in a helmholtz coil, the results can be found in table 4.5 (the field of the coil was given as $H = 243.50\,\mathrm{Oe\,A^{-1}}$). It has to be noted that the legs of the through hole switch were not shortened yet (54.0 mm), making it a lot more sensitive than the SMD reed switch (with a length of 15.8 mm).

To measure the switching behavior in combination with magnets and the spheres, the schematic set-up as shown in figure 4.12 has been designed. The set-up consists of three 3D-printed parts: a slider to place the mock-up spheres on, a sliding and rotating mock-up sphere holding magnets and a rotating mock-up sphere holding a reed switch and magnets (⊘ 8 mm×2 mm N35 magnets). An LED is turned on upon pull-in, the distance between the spheres is measured with a calliper and the spheres contain a protractor for the angles.

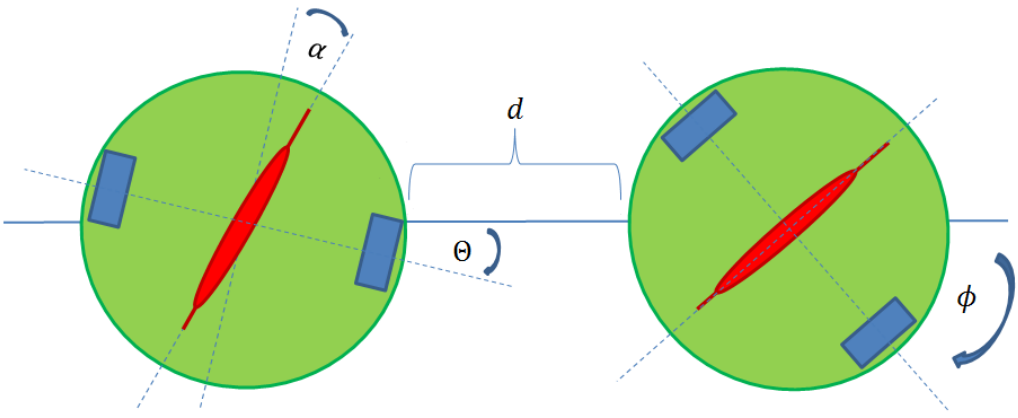

Figure 4.12: A schematic for the reed switch position experiment indicating the variables.

In the experiment both the SMD and the through hole switch have been tested. For both the following steps were performed:

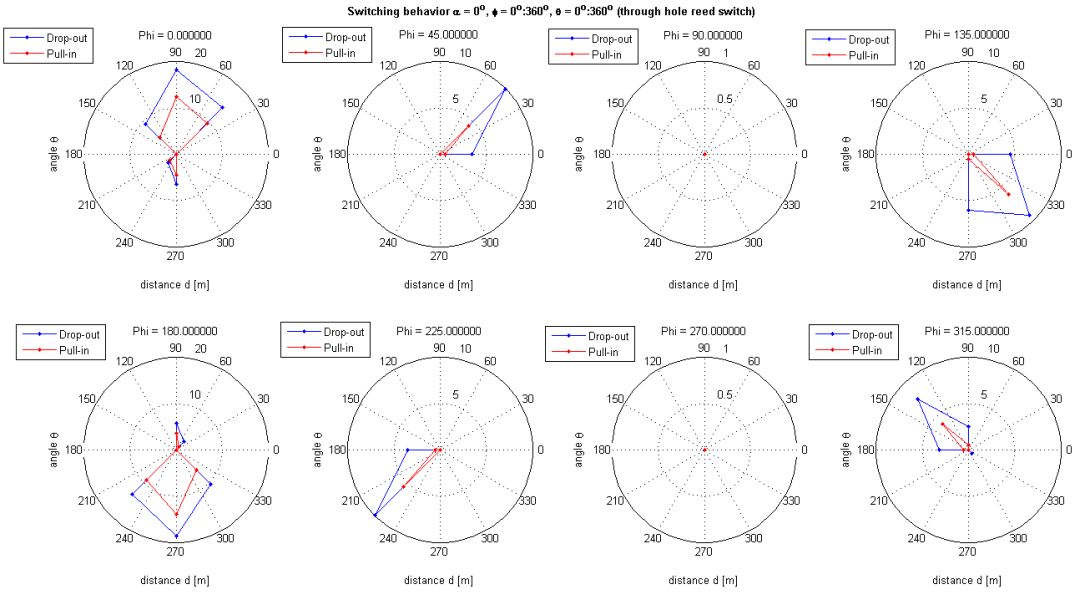

Figure 4.13: Plots for a measurement with the set-up from figure 4.12 and 4.14. Every graph represents a measurement for rotating θ for 360° for a set angle ϕ.

- Switch to a new angle ϕ
- Switch to a new angle θ
- Lower distance d until pull-in, then measure d
- Enlarge distance d until drop-out occurs and measure d
- Repeat this while changing θ with 45°
- After finishing a round of θ, shift ϕ with 45°

In the experiments the reed switch was always placed in the middle of the sphere, perpendicular to the main axis (α was never changed). From these experiments both the pull-in and drop-out distances could be found. Both 180° symmetry and hysteresis effects were recognized in the outcomes. In figure 4.13 the outcomes can be seen for the through hole reed switch. The asymmetry in the sensitivity lobes is assumed to be due to misalignment of both the magnets and the reed switch. The highest sensitivity in this lay-out was found for a sphere touching at the bisection of the rotating sphere (hence for the main axes of the two sphere being perpendicular). In the measurements for *phi* is 45°, 135°, 225°, 315° the lobes from a perpendicular magnet can be recognized and in the graphs for ϕ is 0° and 180° the lobes for a parallel magnet can be recognized. All measurements show a large lobe on the one side and a small lobe on the opposite side. Since reed switches are symmetrical and not sensitive to polarity, it is expected that the difference in lobe size is caused by misalignment of the magnets and the switch. Additional graphs are shown in appendix A.1.3. From the measurements can be seen that the middle is not a suited location for the reed switch if connections have to be measured. However at other locations the reed switch is already switched by the magnets of the own sphere. Another position is needed.

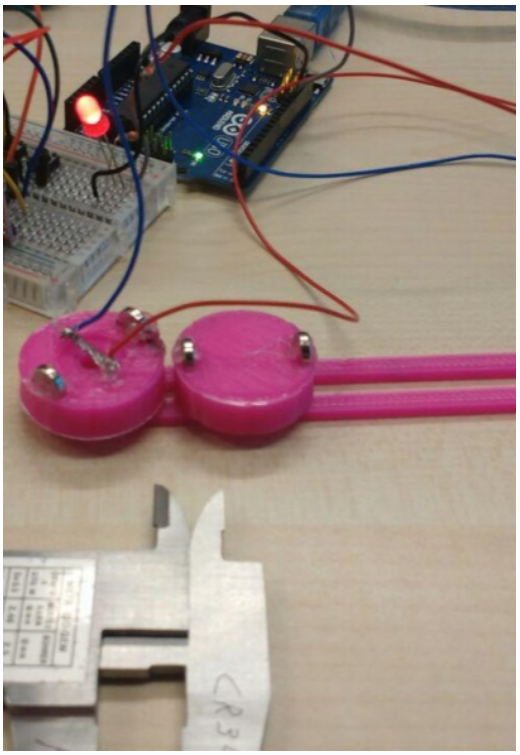

Figure 4.14: The reed experiment set-up containing: two mock-up spheres, a reed switch, a slider, a calliper and an LED.

4.2.2 Reed switch positioning

To prevent switching of reed switches by magnets from the own sphere, the switches have to be placed perpendicular to the magnetic field inside the sphere. This is done by placing the reed

switches next to the magnet with its low sensitivity lobe, as shown in figure 4.15. In this way the reed switches both experience the large field change during interaction with other spheres as found in section 4.1.4 while they are not influenced by their own magnets. In practice the reed switches can be placed closer to the edge of the sphere when they are tilted a bit with respect to the magnet (as can be seen in figure 5.1 were the magnets will be in the holes). The final location of the reed switch was determined by moving the SMD reed switch with respect to the edge and the magnets from the mock-up. The location of the reed switches has been show to work with a mock-up sphere and circuit, containing a reed switch in series with an LED, a resistor and a coin cell battery placed in a 3D printed board shaped like the PCB, figure 4.16.

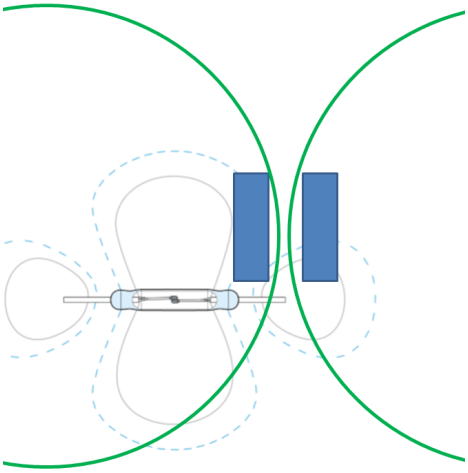

Figure 4.15: The reed switches are positioned next to the own magnets with its insensitive region.

Figure 4.16: The printed PCB mock-up used to test the sensing principle with a battery in series with a reed switch, LED and resistor (two reed switches etc.).

4.3 Conclusion

From this chapter several conclusions can be drawn. First of all it has been shown two small, separated magnets can be used for the system instead of a single large magnet. Since there is still sufficient interaction between the spheres with separated magnets. With smaller separated magnets the energy keeping the spheres together is lower, hence less turbulence is needed to take spheres apart. This implies a lower limit below which magnets are too small to be used for the system.

Based on the drag force for spheres in a flow and the connection force of the currently used spheres a suited connection force could be determined. ⌀ 4 mm×4 mm N35 magnets have been chosen with their centers 6.5 mm from the edge of the sphere.

The magnetic fields inside the sphere has been determined for the optimal positioning of the reed switches. The only suited position for a reed switch is in between a magnet and the spheres edge. Additional research into reed switches showed a suited sensing mechanism can be made by having the reed switches perpendicular to the magnet with the insensitive gap between the sensitivity lobes right next to a magnet.

Chapter 5

Electronics and programming

For the full operation of the system electronics are needed (a micro-controller and flash memory). The electronics provide the "infrastructure" for the sensing and data communication functionality. An electrical circuit, a PCB, and a program for the micro-controller have been designed. The electronics are based on scenario 1 from figure 3.4 and hence will contain a micro-controller and flash memory on a PCB. In the end the system has to perform the steps as shown in figure 3.7, this figure is used for the design of the programming code. The coming section gives an overview of the electronics design and of the code for the micro-controller.

5.1 PCB design

For the electronics several components are of importance. A micro-controller is needed for controlling everything, flash memory is needed for the data logging, reed switches are chosen as sensing mechanism, pins are needed for programming and communicating data, batteries are needed for powering the system and several components are needed to connect the electronics and to make it all work. The spheres can be at most 30 mm in diameter, hence the PCB is taken to be 27 mm in diameter. A two layer PCB with the default 1.55 mm thickness was taken. In the design the centers of the magnets are placed 5 mm from the edge of the PCB. The reed switches are placed as close to the edge as possible while still not triggered by the own magnets (in a skew orientation, because then they are still perpendicular to the magnetic field while closer to the edge of the PCB). The ATmega micro-controller and flash memory are placed on the middle of the PCB on opposite sides to leave enough space for the wiring in all directions. All other elements are positioned around this set-up.

With the software Eagle the schematics for an electrical circuit, figure C.1, and a PCB, figure C.2, have been designed. The following components are used for the circuit:

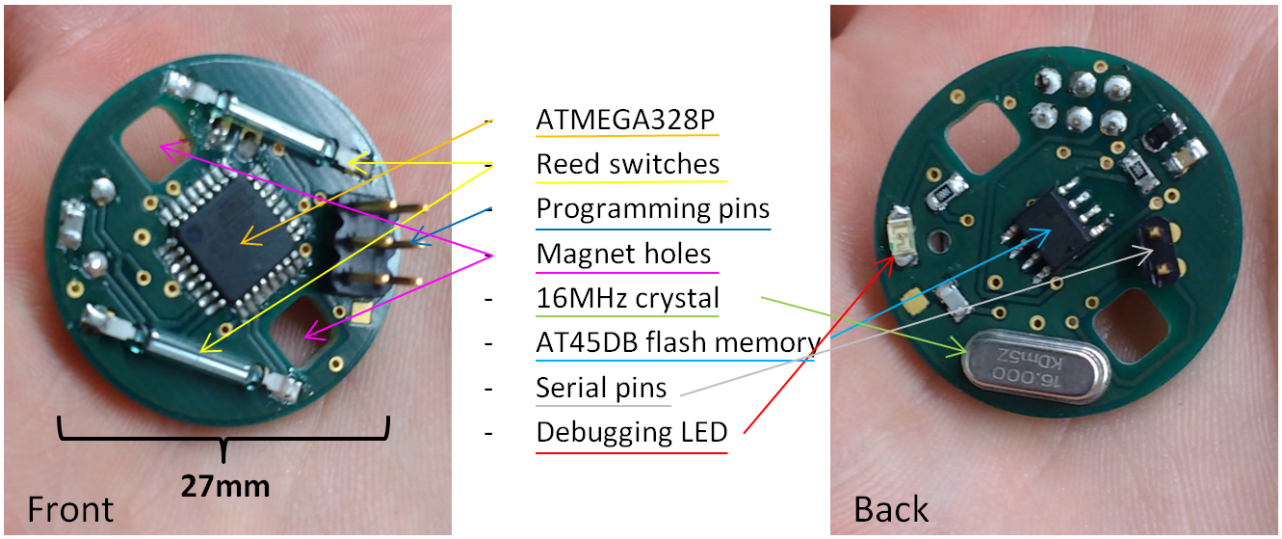

Figure 5.1: The manufactured PCB with its components.

- ATmega328P TQFP micro-controller
- AT45DB011D-SSH-B Flash memory
- 16 MHz crystal oscillator
- 2 Reed switches (MK23-35-B-2)

- 2 Capacitors 18 pF (for crystal oscillator)
- Capacitor 220 µF (decoupling capacitor)
- Capacitor 0.1 µF (decoupling capacitor)
- LED (for debugging)
- Resistor 10 kΩ (Pull-up of chip enable from the Flash memory)
- Resistor 100 Ω (Resistor for LED)
- 6-pin male dual row header (for programming)
- 2-pin male header (TX-RX connection)
- 2 Pads for connecting the batteries
- 2 Batteries (LR44)
- 2 Coin cell battery holders (11.6 mm)

The realization of the PCB with an indication for the most important components can be found in figure 5.1. Small tests have been described in chapter 8. In the design the size was a driving requirement. That is why for example the reed switches and RX were connected to the internal pull-up of the micro-controller (for usage as software interrupts). The design has been tested with a breadboard version. Some problems were not discovered in these tests. After manufacturing and testing several points of improvements were found. First of all the hole for a wire to connect the batteries in series was located below a reed switch, and had to be drilled somewhere else. Furthermore a pull-up resistor was soldered to the RESET, because it was forgotten in the design (during testing the reset wire of the programmer was still connected). It was also discovered that the micro-controller can be run on its own internal clock (8 MHz instead of the external 16 MHz crystal), making it possible to leave out a crystal and two capacitors. Combined with smaller headers for programming and the serial connection, it should be possible to shrink the size of the PCB significantly (down to 22 mm or lower).

5.2 Micro-controller program

The micro-controller is programmed with the arduino IDE. A code is written and written to the micro-controller with an external programmer (USBtiny programmer). The data is send to the pc over a serial connection with a usb to serial converter module (FTDI FT232RL USB to TTL Serial Converter Adapter Module). The actual code can be found in appendix D. The program has been based upon the state transition diagram in figure 3.7 (with some additional functionality in the improved versions of the code). In the program several main functions can be found:

- To synchronize the timer for time stamps and go into sleep mode
- To test if the circuit works in case a magnet is hold close

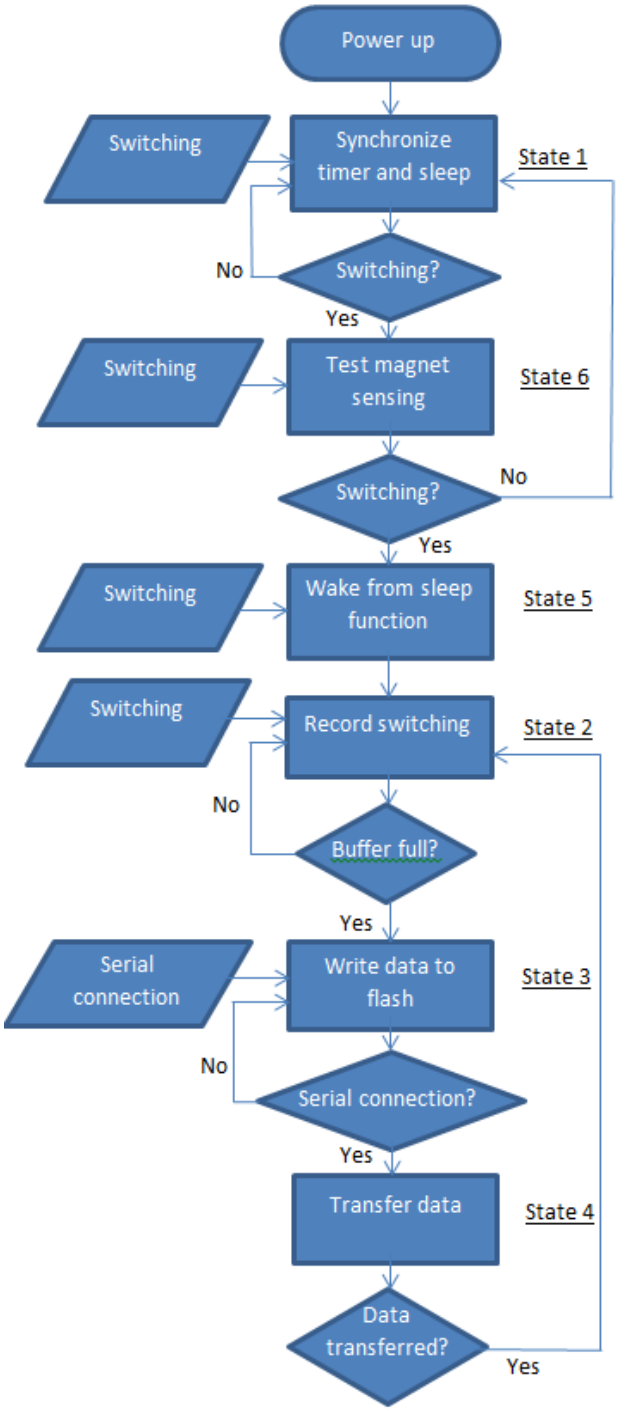

Figure 5.2: Flow diagram of the micro-controller code.

- To wake up from the sleep mode
- To detect switching of the reed switches and save time stamps in the flash buffer
- To write the flash buffer to a page in the flash memory
- To communicate the data from the flash memory over serial connection

These functions are realized with a state machine, in which every function is given its own state. The program flow of the code is shown in figure 5.2. After being powered the code starts in the first state, where it is in its sleep mode. The first moment a reed switch is triggered, the time is recorded and used as an offset for the timer. State 6 is then initiated, where a blinking LED shows there was a magnet connection. In case there is still a connection, the program moves on to state 5, where the micro-controller gets out of the sleep mode. Then the system switches to the second state, where asynchronous data communication is used every time a reed switch triggers an interrupt. Reed switches have a very short bouncing period, therefore a debouncing period of 5 milliseconds is used for sampling. Rising and falling of the reed switch signals are recorded with their time stamps and the switch positions. This is converted into one large variable (for every event an unsigned long, 4 bytes, holds both the time stamp and the switching positions). The variables are written to a buffer on the flash. In case the buffer is full, state 3 is triggered. In state 3 the whole buffer is written to a page in the flash memory (this particular flash chip has 512 pages with 256 bytes of memory ordered in several sectors with overall 64 blocks of memory which can be erased separately). After performing stage 3, the system can move back to stage 2. In case a connection is made via the serial port, stage 4 is initiated. In stage 4 all data is transferred via serial connection to another device.

Since the device will be working on batteries, at a later stage several features have been included in the code to save power. A sleep function has been implemented to have a very low power consumption before the experiment start (triggering a Pin change interrupt from a reed switch gets the device out of sleep mode again). Next to that the chip enable pin is pulled low when the flash memory is not in use (the library pulls chip enable high, which stops the flash memory from going into stand-by mode. This caused a lot of problems with powering the device at the start). An elaborate explanation on the problems with powering the device is given in section 8.2.

Chapter 6

Total Design

The total design displays the result of all decisions and modeling from all previous sections, as shown in figure 6.1 (technical drawings can be found in appendix C). The system has been build and where necessary adapted to obtain a working prototype, as one can see in figure 6.1. This chapter gives an overview of the realized design and some details are discussed.

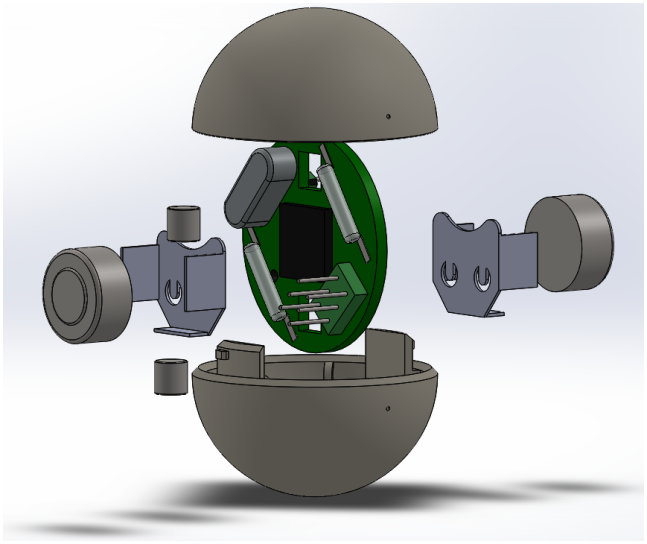

Figure 6.1: A CAD drawing of the total design.

Figure 6.2: The realization of the total design ready for testing.

6.1 Overview final system

The total design comprises a sphere of 30 mm diameter and a weight of 15.5 g (yielding a suited density of $1.1 \times 10^3\,\mathrm{kg\,m^{-3}}$). A strong nylon shell made by Selective Laser Sintering is used (the Objet Eden 250 printer of RAM broke down), details on the shell design are given in appendix C.2.1. A PCB comprises all functional parts, among other the magnets (⌀ 4 mm×4 mm N35 magnets) and reed switches next to the magnets. The reed switches can be read separately, for example making it possible to distinct whether spheres are connected in a line or in a ring.

Data can be stored on the 1 Mbit (131072 bytes) flash memory and an ATmega328P micro-controller is used for all processes. The micro-controller communicates with the flash memory over SPI (Serial Peripheral Interface). One event needs 4 bytes of data (the time stamp gives the milliseconds after synchronization and the state of the reed switches), hence $131072/4 = 32768$ events can be recorded. The recording of data is an asynchronous process: every time the reed state changes the controller saves a time stamp and the states of the reed switch (hence on

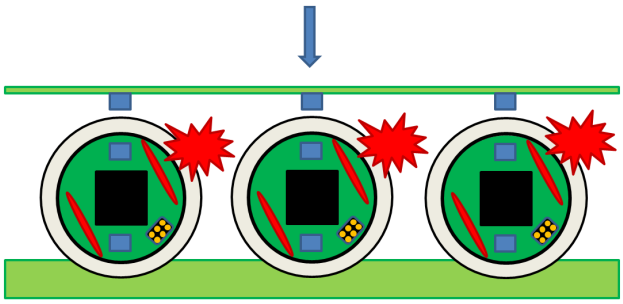

Figure 6.3: Multiple spheres can be synchronized at the same time by putting them in a holder and touching them simultaneously with a bar with magnets.

connections and disconnections data is saved). This
reduces the power and memory space needed.

Synchronization of a sphere happens by holding a magnet close at the start of the program. The sphere will wake up from its sleep mode and start measuring connections. Multiple spheres can be synchronized at the same time, by putting them in a holder and touching them simultaneously with a bar with magnets, as shown in figure 6.3. In this way all spheres start at the same time (this is not scalable for large numbers of spheres, for more than a dozen of spheres another solution has to be sought. Ideas could be to use an electromagnetic pulse or by connecting to an ntp server via wifi when the spheres are not in the water yet).

6.2 Differences realization and design

From figure 6.1 and figure 6.2 already one can see that some practical changes have been made during fabrication. The most important changes are listed:

- **Battery retainers**: The original battery holders from the design were not suitable for usage in the spheres. Several alternatives were tried The batteries now have soldered wires and are covered in shrink tube.
- **Batteries**: Three LR44 batteries were used instead of two due to problems with the power consumption. More information on the power consumption is given in section 8.2. The additional battery shifts the center of mass out of the center.
- **PCB hole**: The hole for wiring the batteries (since they are in series) was placed below a reed switch. A new hole was drilled close to the edge of the PCB to solve this.
- Reset pull-up resistor: A pull-up resistor was connected to the reset pin, since it had been forgotten in the design. This had slipped through with the breadboard test.
- **Oscillator crystal**: The oscillator crystal and capacitors were left out, since the micro-controller could run on its 8 MHz internal clock.
- **Magnets**: The magnets were glued to the PCB before the batteries were connected, to prevent waking the system from sleep mode (the magnets would stick to the batteries, triggering the switches).
- **Shell**: The structures inside the shell for supporting the magnets and batteries were removed to make extra space for the batteries.
- **Header pins**: The header pins were shortened on one side to make the PCB fit inside the shell.

Testing of the final system is necessary to check its performance.

6.3 Conclusions

The final design has been realized. Several changes were made with regards to the design for the optimal performance of the system. The most important changes are using three batteries instead of two and using the internal clock of the micro-controller instead of an external crystal. Tests have to be done to research the performance of the system.

Chapter 7

Experiments and preparation

This chapter gives steps that will be taken to test some of the subsystems as well as the total system. Both the methods and set-ups for the experiments are given.

7.1 Sub-systems Tests

Several subsystems will be tested before they will be implemented in the total system. Experiments have been designed for the magnet size, the water tightness of the spheres and for the electronics.

7.1.1 Magnets reactor test

Before usage in the final experiments, there has to be tested whether the $\oslash$ 4 mm×4 mm N35 magnets are suited as means of connecting element for the spheres. This will be checked qualitatively in a simple experiment. The magnets will be placed inside printed holders with the same size as the PCB. Weights will be added to the holders and the whole can be fitted inside two sphere. This will be placed inside the self-assembly reactor. The number of connections made by the particles will then be observed at different flow rates and turbulence settings. The magnets are suited as means for attracting spheres in case a reasonable number of connections (connecting at a rate slow enough to observe it with the cameras but high enough to obtain a significant amount of data after 30 minutes, hence dozens of connections in 30 minutes) will occur with a flow rate and turbulence settings which are within the working range of the set-up.

7.1.2 Water tightness tests

Since the spheres have to be water tight for the electronics to be usable, this will be tested extensively. Tests will be done for the water tightness of the shell and of the seal separately. Two types of shells are used: nylon shells made with selective laser sintering and ABS shells made with fused deposition molding. Next to that different types of sealing material will be tested (vaseline, plastic glue, silicone sealant).

- Water tightness shells: The tests on the water tightness of the shell are done by floating the shells in water. This does not account for the higher pressure inside the reactor, however to compensate for this the test will be performed over night for longer leaking times.
- Water tightness seals: For the tests with the different seal materials, weights are added to the shells and the material of choice is used to seal the sphere. Before the spheres are placed inside the reactor, they are weighted. They will be put in the reactor for 30 minutes, for which a couple of minutes on the highest flow and turbulence settings (which are not used for the self-assembly experiments). Afterwards the spheres are weighted again and then opened to check for any water that might have gotten in.

7.2 Total System Tests

For testing the total system two experiments have been designed: a controlled 2D experiment and an experiment inside the reactor. All tests are done with two spheres for simplicity reasons. Important for both experiments is to look at false negatives and positives: switching of the reed switches while there is no event and no switching while there is an event.

7.2.1 2D Controlled Experiment

The 2D experiment purely tries to test the performance of a single sphere while taking away the harsh environment. The test is performed by letting two spheres (a sphere with the total system and a sphere of the same weight with just magnets) roll on a 2D platform while filming the events (with a 13 megapixel camera). The platform is agitated by shaking and tilting by hand in a semi-random way. The disturbing energy is delivered by the spheres colliding with the walls of the platform as well as by the random motions and tilting of the 2D platform. A camera is placed over the platform, allowing to record events from above. A schematic drawing of the set-up is shown in figure 7.1.

For the analysis the video data will be analyzed by hand, noting the times of the events and the sides of the sphere touching the magnet sphere. The data as found from the video analysis can then be compared to the data recorded by the sphere itself.

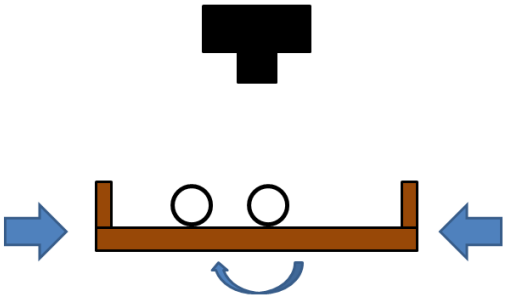

Figure 7.1: A schematic view of the 2D controlled performance experiment of the spheres. The spheres are placed on a shaking, tilting platform and the events are recorded by camera from above.

7.2.2 Self-Assembly Reactor Experiment

A full test will be done in the self-assembly reactor at KIST. For this test a sphere with the full system and an equally heavy sphere just containing the same magnets will be placed inside the reactor. The flow and the turbulence (amount of asymmetry of the flow) will be adjusted in such a way that the spheres move around the reactor in all direction with sufficient events (by using flow settings such that the spheres are not pressing against the nets confining them inside the reactor). The full tests will show the performance of the designed system in the harsh environment it has been designed for. The total performance of electronics, water tightness, sensing and data recording will be tested at the same time, to show the viability of this system.

The turbulent flow will serve as the disturbing energy, making the spheres perform a confined random walk. Two cameras are located at the sides of the reactor (perpendicular to each other) to record all events. Offline, the location of the spheres will automatically be detected using a custom written MATLAB script by people from KIST. The data from the video analysis will be compared to the data recorded by the sphere. A schematic side view of the set-up is shown in figure 7.2.

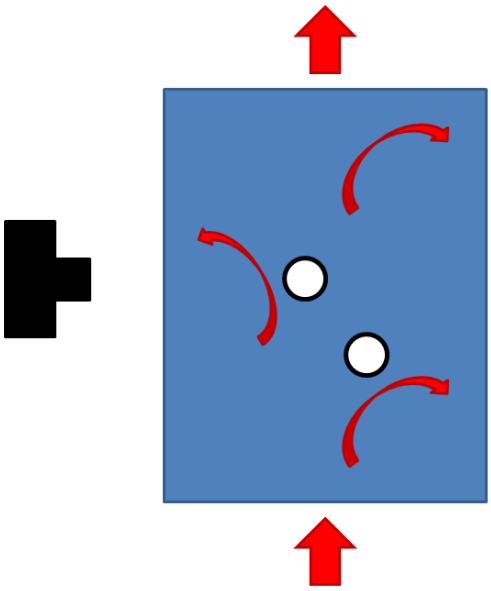

Figure 7.2: A schematic side view of the self-assembly reactor experiment of the spheres. The spheres are placed inside the reactor agitated in three dimensions by the turbulent water (red arrows) and the events are recorded by camera from two sides.

Chapter 8

Results

This chapter presents the results for test performed on the subsystem level as well as for the total system.

8.1 Subsystems Test Results

On the subsystem level tests have been done on the connecting performance of the spheres with the chosen magnets, on the water tightness of the spheres and on the batteries and power consumption.

8.1.1 Results magnets reactor test

The connecting performance of ⌀ 4 mm×4 mm magnets as chosen for the design has been tested in the self-assembly reactor. Magnets were placed in shells with a 3D printed magnet holder (like is done in figure 4.16 only without the electronics) and weights have been added to the spheres. Upon testing the spheres showed good connectivity (dozens of events) at an intermediate flow rate and turbulence level (with the pump and valve settings a higher flow rate and turbulence were still possible). This showed that the chosen magnet size was suited for the system. At the end of the test, one of the spheres opened up, releasing the magnet holder (figure 8.1). This showed that the bayonet fitting on its own is insufficient to withstand the turbulence inside the reactor.

8.1.2 Results water tightness tests

Figure 8.1: A sphere used for testing the magnets has opened up inside the reactor due to the disturbing flow.

Tests on the water tightness have been performed for both the shells as for the sealing of the shells. For the tests the shells were marked with dots to distinguish between them. To test how much water would get through the printed material, the shells were made to float in water. In this case a weight increase of 2% was measured for the ABS shells (which can be explained from the fact that they were made with Fused Deposition Molding, a printing technology known for porous end products. No water was found inside the shell, so the sealing did not show leakage) whereas there was no weight increase for the nylon shells (both the sealing and shell did not show leakage). Therefore the ABS shells were not used for further testing. For testing the sealing of spheres in the reactor, it was found that vaseline would only work if the edges of the sphere were nicely overlapping, any gaps would cause leakage. However the spheres were made with selective laser sintering technology whereas the design was meant for polyjet technology (the Objet Eden 250 from RAM broke down two weeks before the prints were needed). When a larger overlapping edge is used in combination with polyjet printing technology, vaseline is expected to work as sealant (the nylon spheres with nice edges could be made water tight with just vaseline). Different glues for plastics were also tested as sealing material for the shells, however these sealants leaked a lot. Silicone sealant was found to work if, besides the edges of the gap, also a large part of the outer sphere around the gap was covered (a sphere covered with silicone can be seen in figure 8.2). The spheres had a rough structure due to the SLS technology, and it was found that a large surface area was needed to prevent the sealing from coming off. Furthermore the edges of the shells were sanded and cleaned for better bonding of the sealant. Soap was used to smooth the silicone, for an even surface layer. In this way spheres could be made water tight with silicone sealant.

8.2 Battery testing and power consumption

During operation of the system with two batteries it was found that the voltage over the batteries slowly dropped to 2.8 V after which the device would be booting continuously. Furthermore sending of data over a serial connection sometimes only yielded corrupted or partial data. These problems did not occur when the device was connected to the programmer or to a voltage source. The differences between batteries and a voltage source can be found in the grounding, deliverable current and fluctuations in the voltage. Two batteries together have a capacity of 220 mA h. The current draw by the system was measured with a multimeter and an oscilloscope (with the oscilloscope the voltage drop over a small resistor in series with the batteries was measured). In cases where the system was hooked up to a voltage source, currents of 25 mA-30 mA were measured. In all cases the highest measured current when powering the system on batteries was 3 mA, whereas 25 mA-30 mA was expected during writing to the flash memory. Hence the batteries could not deliver a high enough current.

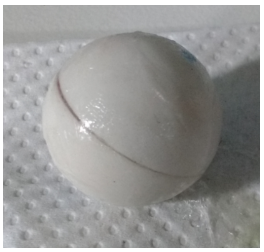

Figure 8.2: A sphere covered in silicone sealant put to dry.

To solve this three LR44 batteries were used, to be able to deliver more current. Next to that a bug was found in the flash library, causing the flash memory to be in active mode all the time (consuming a significant amount of power). In this way the system could be used throughout experiments without power issues.

8.3 Total System Test Results

For testing the total system two experiments have been performed: a 2D experiment in a controlled environment and an experiment inside the self-assembly reactor at KIST.

8.3.1 Results 2D Controlled Experiment

For the 2D Controlled Experiment both video data and data from the spheres was obtained. The video data was analyzed by hand. During the experiment plenty events could be observed by means of the blinking LED (the code makes the LED blink upon an event). The video could be analyzed by keeping track of the dots on the sphere and the fact that reed switch 2 is positioned the closest to the LED. Before testing it was observed that the $\oslash$ 4 mm×4 mm magnets inside the spheres were too weak to always trigger the reed switches and were therefore replaced by rectangular magnets of $6 \times 4 \times 4$ mm.

For the performance of the system it is helpful to look at the false positives (recording an event (blinking the LED) while there is no event) and false negatives (not recording an event while an event occurs) by observing the video data. The most common case for both situations is shown in figure 8.4. When the spheres rotate during connection, and the reed switches are on the opposite side of the main axis with regards to the connected sphere, an event is recorded (false positive), while in the case where the spheres connect (and afterwards disconnect) in the rotated orientation the event is not recorded. An example of a false positive in this case can be seen in figure 8.5. For few other cases with proper connections and disconnections there was also no LED blinking. The cause of these false negatives is not known (too weak magnets could still be possible).

The data from the video can also be compared to the data as obtained from the sphere, as seen in figure 8.3. Interesting to see is that for reed switch 1 the switching in the video data and the reed switch data is the opposite. This can be explained by the fact that during synchronization reed switch 1 was accidentally kept next to a magnet (setting the state to open while the switch was closed). Next to that there seems to be a scaling difference between the data from the video and the sphere (especially for reed switch 2). However tests have been done with the micro-controller under the same circumstances yielding correct results for the timing of the micro-controller (see appendix A.1.4 for these experiments), hence the micro-controller can be properly used without a crystal oscillator for these experiments. In the range of 20-25s and 35-40s a large difference for the amount of events can be seen for reed switch 1. In this region the spheres were found to bounce against each other quickly, which was not put into the data from the video analysis (at these high connection frequencies the LED does not blink because an interrupt is already called by the next event, making the video analysis more difficult). A final interesting effect is switching of both switches at the same time (so in this case reed switch 1 being low and reed switch 2 being high), which in testing conditions sometimes happened. A possible explanation of this could be the battery casing acting as field guide (it was observed multiple times that when a battery touched a magnet and was close to a reed switch with its other side, an event was recorded by the system). When a battery was very close to a reed switch this could switch the other switch. Overall a large error source in the video data was the precision with which the video analysis was done, this also has a large influence on deviations of the data (causing an error of around 200ms in the video data as well as some quick moments of contact which were not noted).

r

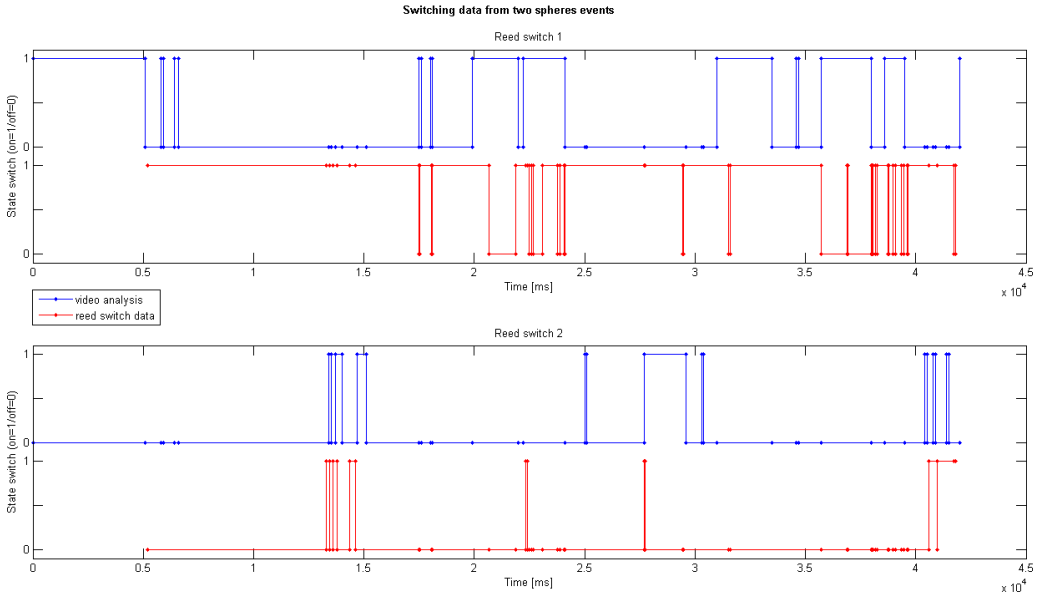

Figure 8.3: A comparison of the data of the 2D controlled experiment, showing the recorded events for both switches as found from the video analysis and as obtained from the sphere.

8.3.2 Results Self-Assembly Reactor Experiments

Two tests have been performed with the total system inside the reactor, in both cases with a complete sphere and a sphere just containing magnets and weights. The weights of the spheres were matched by adding weight to the sphere with just magnets.

In the first experiment plenty of connections were observed. During the most proper connections (connections in which the spheres are neatly aligned) the LED could also be observed blinking (indicating the event was measured and recorded), in figure 8.6 this is shown for both a connection and disconnection event. At the moment of the experiment the problems with the batteries were not solved yet. To prevent the battery power from dropping below 2.8 V before the experiment was finished, the batteries were only connected at the start of the reactor experiment. This was done by letting the two connection wires stick out of the shell separately and only solder them together at the start of the experiment (and after sealing the sphere with silicone). Unfortunately after 15 minutes water entered the sphere and caused a shortening of the system. The batteries had to be removed and upon booting the system, the buffer with the data was erased before it got to the memory. Next to that a flaw was found in the micro-controller code which overwrote the first page of data after powering up.

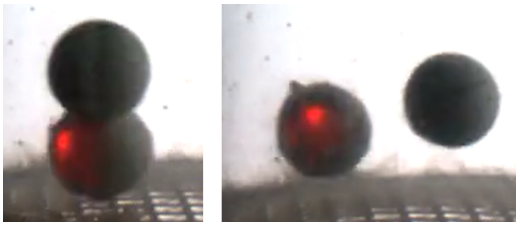

Figure 8.6: A situation in which the spheres measured a connection (left) and disconnection (right) inside the reactor.

A second experiment was done after implementing a sleep function (to have the micro-controller in sleep mode while the silicone is drying) and after finding a bug in the flash library (which caused the flash chip to continuously drain battery power) which greatly improved the power consumption. Furthermore the code was altered such that the data would not be overwritten. The spheres were placed in the reactor for 15 minutes and tested. While connecting it via serial connection the reset pin was triggered again (the pull-up of the reset had come off on removing of the silicon sealing, making the reset pin float), again no data could be retrieved. Unfortunately no quantitative video analysis has been performed on the videos, since the MATLAB processing script at KIST was not working. Since there has not been a proper experiment with analysis of the full system in the reactor, additional testing in the reactor is needed.

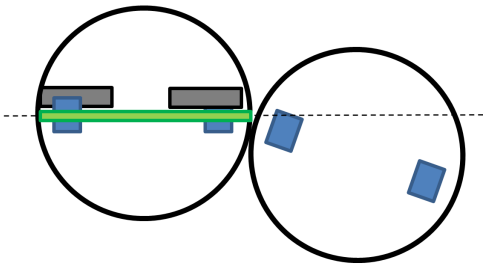

Figure 8.4: In cases where spheres were rotated with respect to each other with the reed switches on the other side of the main axis of the measuring sphere, switching was observed (false positives). No switching was observed when spheres connected with the main axes rotated with respect to each other (false negatives).

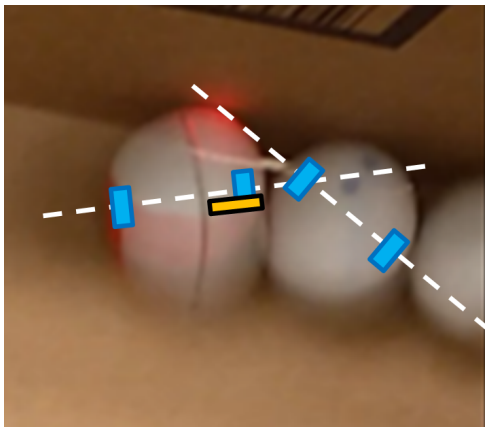

Figure 8.5: A false positive were the situation from figure 8.4 occurs. The white lines are the main axes through the magnets, the blue rectangles are the magnets and the orange rectangle is the reed switch (on the opposite side of the LED on the PCB)

8.4 Conclusions

All in all the experiments have shown the viability of the subsystems and of the total system. The magnet test demonstrated the suited operation of the chosen magnets, the water tightness tests showed it is possible to get a water tight sphere, the battery tests showed the possibility of running the full system on LR44 batteries, the dry testing showed that data could be recorded and retrieved and the reactor tests showed that operation inside the reactor is possible (everything in the reactor succeeded except for the data retrieval part). A redesign is needed for the edges of the spheres for a more reliable water tightness as well as for the reset pin on the PCB. Next to that a more sensible reed switch, stronger magnets or another way of sensing have to be used to have less false negatives and positives. Besides that it is advised to use other batteries, to always be able to supply the required power and have a balanced sphere. Finally in the future additional experiments have to be done in the reactor (with an analysis of the videos data) before the design further implemented.

Chapter 9

Discussion

With this research spheres that can sense connections with other spheres and provide data on connections for macro self-assembly experiments in a turbulent water flow have been designed, manufactured and tested. This chapter discusses the outcomes of the research. The realization of the design is verified by its requirements and budgets. Moreover the tests results are discussed.

9.1 System Requirements

The system is validated per requirement.
The magnets offer a good way of connecting the spheres. At the moment the magnet size and location is calculated via the forces, however due to the nature of the experiments (turbulence cannot be expressed properly in a force) it will be better to determine the magnet size for future designs by looking at the energy of the flow.

The sensing method has also been shown to work. From timer experiments (A.1.4) it could be seen that measurements over $2Hz$ do not give problems. On the other hand the videos from the reactor experiments showed there were only few events were high frequency measurement were needed. The sensing of connections only happens at the poles of the spheres. Though during the experiments the sensing did not register all connections. More sensitive reed switches or a different sensing principle are needed to record more accurate data (larger magnets are not an option, because the magnet size and position is good at the moment). Additional testing for characterizing the sensing is desirable (features like directionality have not been researched) before making changes to the design.

The data communication showed issues in the reactor experiments due to problems with water and the electronics. In dry settings all data could be retrieved and processed afterwards without issues. Synchronization of the spheres has never been tested, since not more than one sphere has been used at the same time.

After manufacturing the spheres were not identical, homogeneous entities. The silicone gave a uneven texture to the spheres and the three batteries moved the center of mass from the center of pressure. From the video footage it can be seen that the spheres are oriented predominantly with the two batteries facing down (by the wire sticking out in reactor test 1). For testing purposes this helped the experiment, since the probability of connections became higher (there were less degrees of freedom). The reactor could be operated at a mean velocity well within range, leaving head space for an increase in density with shrinking of the system.

The water tight housing proved to be a major difficulty. Silicone sealing was used to solve the problem, but this is not user friendly and it did not always give reliable results. Hence a redesign of the shell is needed for future designs, comprising larger overlapping edges combined with vaseline sealing. This should make for easier and more reliable sealing (the use of an o-ring could also be considered).

The time of operation is limited by the data storage and the battery lifetime, however a lifespan well beyond 30 minutes seems to be possible. With a more energy efficient micro-controller and code this could even be further improved.

With the safety no problems arise, however the user friendliness needs great improvements. The silicone sealing of the spheres does not fit the "plug-and-play" design. Furthermore the code has to be improved to prevent erasing data after resetting of the system.

9.2 Budgets

The realized budgets of the system have been determined (volume budget figure 9.2, power budget figure 9.3, costs budget figure 9.4 and weight budget figure 9.5). On the basis of these budgets, several remarks can be made.

In the volume budget there is still a significant amount of empty space which can be taken out. Next to that a thinner shell wall would help (thick walls are not needed). In combination with the size reduction of the PCB (no crystal needed, smaller and better micro-controller, no flash memory needed, possibly small hall sensors for sensing) and different batteries, shrinking the device significantly will be possible. It should be possible to go down to 25 mm as diameter with improvements of the current design.

The power budget has already been improved during the project (a sleep mode was included and flash memory energy consumption was improved). In the current budget the flash is estimated to be a tenth of the time in active mode. From this estimate the micro-controller is the biggest energy user. With the choice of a new micro-controller and more efficient programs a more energy efficient system can also be designed. In combination with better batteries (lithium polymer batteries are adviced since they can deliver high peak currents and have a high energy density) it should be possible to do measurements for several hours straight.

The main costs of the project comes from the PCB board and its components. In future versions the costs are expected to be lower, since more expensive PCBs had to be ordered due to time constraints.

When the volume and density are within the specifications, the weight does not have to be optimized. However for scaling down the system it has to be noted that the weight might not scale linearly with smaller components.

With the mentioned improvements, the stated requirements are well within reach. With the insights gained, a new set of requirements can be derived for future projects.

9.3 Test Results

Unfortunately only little data was collected on the system. For a proper validation of its performance more tests are needed. The obtained videos and measurement data did give (mainly qualitative) useful insights in the behavior of the spheres.

Several things affected the test results. The three batteries resulted in imbalance, causing the magnets to be positioned in the horizontal plane most of the time. This only has influence for the actual self-assembly research, however in testing the system it proved to be helpful by giving a higher probability for connections. The debug LED proved a beneficial addition for the experiments, helping in the analysis of the video data. The video analysis was done by hand for all experiments, yielding errors of up to 0 ms. For future experiments it is advised to use video recognition software in the reactor experiments, since analyzing 3D video data by hand is very difficult.

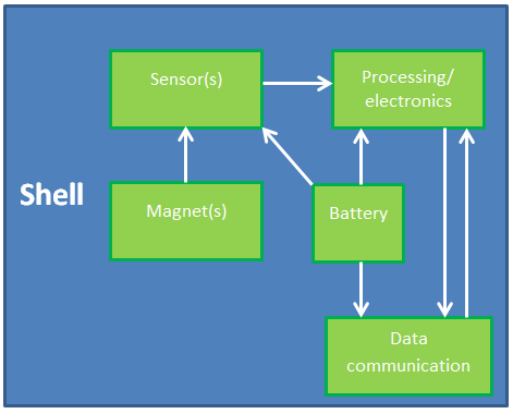

Figure 9.1: An interfaces diagram of the system.

The quantitative test results show many connections that have not been measured. This is attributed to a too low sensitivity of the reed switches or too weak magnets. Also cases with false positives and false negatives have been identified. The main causes of false switching are expected to be relative rotation of the spheres (causing misalignment of the switches and hence switching) and batteries acting as field guides (causing switching of both switches).

Separately all subsystems have done well on testing, although for the full system some changes are needed. In the design the subsystems have been approached as individual components, and additional attention could have been paid to dependencies of the different subsystems. In future designs a better study of the interfaces of the subsystem is needed, a useful tool for this is an interfaces diagram as shown in figure 9.1. From this diagram the important relation between the magnets and sensors could have been found.

It is difficult to give a conclusion for the whole system due to the problems with the reactor tests, since time limits and failure of several components obstructed a full reactor test of the working system. The combined operation of all subsystems has been shown in the 2D controlled tests. Next to that the most important subsystems have also been shown to work on their own (the magnets, the sensing, the water tight shells). Therefore it is concluded that the research has shown the viability of the design with the proposed improvements.

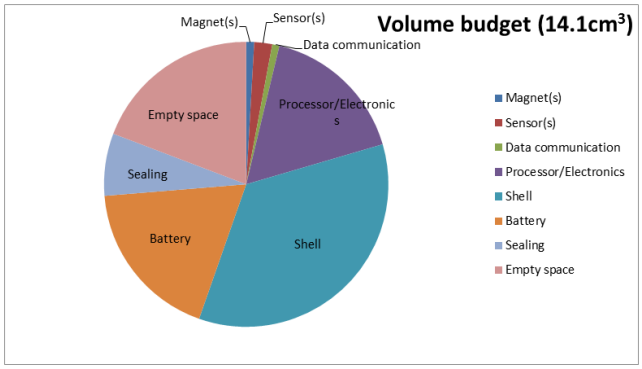

Figure 9.2: The realized volume budget of the system, showing how the volume is divided over the subsystems.

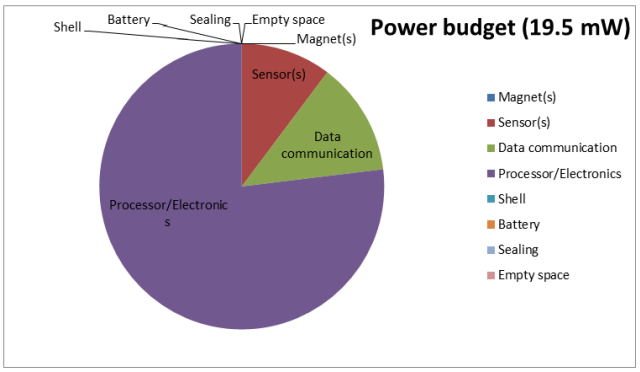

Figure 9.3: The realized power budget of the system, showing how the power is divided over the subsystems.

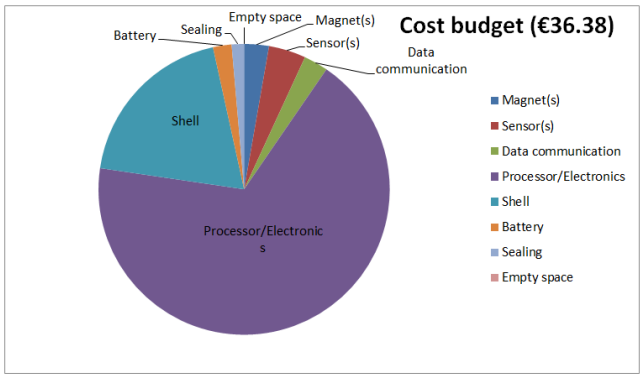

Figure 9.4: The realized costs budget of the system, showing how the costs are divided over the subsystems.

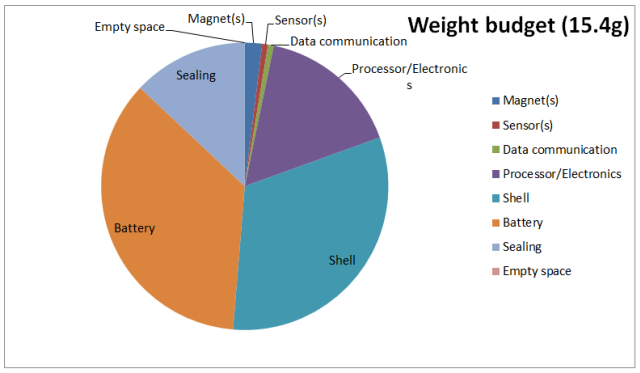

Figure 9.5: The realized weight budget of the system, showing how the weight is divided over the subsystems.

Chapter 10

Conclusions & Recommendations

10.1 Conclusions

The current measurement system of the self-assembly reactor at KIST does not work properly when experimenting with more than two spheres. Therefore research has been done on spheres that can sense connections with other spheres and provide data on these connections for usage in macro self-assembly experiments in a turbulent water flow. From the performed research, several conclusions can be drawn:

- **Magnets:** Two smaller magnets can be used for the experiments instead of a single large magnet without affecting the qualitative particle dynamics
  - When using separated magnets still sufficient interaction between the particles takes place
  - With smaller separated magnets, the spheres have less energy to stay together
- **Sensing:** Reed switches are suited as sensing mechanism with the proposed lay-out
  - Connections are measured while the magnets of the sphere itself do not distort the measurements
  - More sensitive reed switches are needed when using the current magnets
- **Total System:** The viability of the design has been shown, however improvements and different design choices are needed for seamless usage of the spheres in the experiments
  - A redesign of the shell is needed due to the high pressure in the water column to achieve a watertight and user friendly device
  - Different batteries should be used for the optimal performance.
  - The flaws in the electronics have to be taken out in next versions
  - Additional testing is needed for further implementation of the system

10.2 Recommendations

On basis of the discussion and the conclusion, several recommendations can be made for further research. From the discussion it may be clear that downsizing the system is very well possible (it is expected to be able to go down to ⌀ 25 mm). For follow up research on the system several things are needed. A redesign of the edges of the shells would improve the water tightness of the system. Lithium polymer batteries are recommended as replacement for the button cell batteries, due to their high energy density and their ability to deliver high peak currents. For more precise measurements one could look into smaller reed switches or hall sensors to be placed in between the magnets and the edge of the sphere. Furthermore a higher performance micro-controller like the esp8266 can be used, making the external memory obsolete yielding small, low power spheres. For further research one can also look at extending the functionality of the system. With additional magnets one could for example make tetrahedral devices to study self-assembly of specific crystals, enabling studies on the dynamics of crystal growth (an impression is given in figure 10.1). It has to be noted that the reactor might not work for large numbers of spheres. Clusters of spheres obstruct the flow, yielding a wake above the cluster (if a sphere would get in this wake it would just fall on top of the cluster).

By adding accelerometers to the design it could be possible to record the location of each sphere. The drift due to integration errors of the accelerometer could be compensated by using a camera system to calibrate the positions. With smaller spheres experiments could be done with large numbers of spheres, using the full potential of the design (for experiments with a couple of spheres video analysis is still sufficient). For future designs the sensing mechanism could also be used to make the system interactive. By for example adding electro-permanent

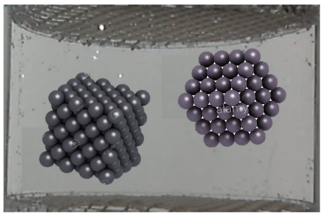

Figure 10.1: An impression of studying the dynamics of crystal growth inside the reactor.

magnets, selective attracting and repelling could be applied, which can be used for research into a wide variety of topics ranging from swarming applications and building of preprogrammed structures to research into the dynamics of bacteria.

Chapter 11

Bibliography

[1] T. Hageman, P. Lothman, T. Janson, A. Manz, and L. Abelmann, "Characterization of a macroscopic self-assembly reactor.".

[2] G. Whitesides and B. Grzybowski, "Self-assembly at all scales," *Science*, vol. 295, no. 5564, pp. 2418–2421, 2002.

[3] R. Gross and M. Dorigo, "Self-assembly at the macroscopic scale," *Proceedings of the IEEE*, vol. 96, no. 9, pp. 1490–1508, 2008.

[4] J. Esch, "Self-assembly at the macroscopic scale," *Proceedings of the IEEE*, vol. 96, no. 9, pp. 1487–1489, 2008.

[5] J. A. Pelesko, *Self Assembly The Science of Things That Put Themselves Together*. Chapman and Hall, 2007.

[6] P. Kamp, "Magnetic self-assembly in 3 dimensions at the macro scale.," Master's thesis, University of Twente, September 2012. Thesis BSc Assignment Advanced Technology.

[7] L. Alink, G. M. Marsman, L. A. Woldering, and L. Abelmann, "Simulating three dimensional self-assembly of shape modified particles using magnetic dipolar forces," in *Proceedings of the 22nd Micromechanics and Microsystems Technology Europe Workshop*, (Tonsberg, Norway), pp. 254–257, Vestfold University College, Department of Micro and Nano Systems Technology, 2011. `http://doc.utwente.nl/79399/`.

[8] M. Marsman, "Exploring magnetic self-assembly by studying the influence of shape on interactions of centimeter size particles," Master's thesis, University of Twente, March 2013. Thesis MSc Assignment Electrical Engineering.

[9] A. Hacohen, I. Hanniel, Y. Nikulshin, S. Wolfus, A. Abu-Horowitz, and I. Bachelet, "Meshing complex macro-scale objects into self-assembling bricks," *Scientific Reports*, vol. 5, 2015.

[10] S. Miyashita, Z. Nagy, B. Nelson, and R. Pfeifer, "The influence of shape on parallel self-assembly," *Entropy*, vol. 11, no. 4, pp. 643–666, 2009.

[11] F. Ilievski, M. Mani, G. Whitesides, and M. Brenner, "Self-assembly of magnetically interacting cubes by a turbulent fluid flow," *Physical Review E - Statistical, Nonlinear, and Soft Matter Physics*, vol. 83, no. 1, 2011.

[12] J. Stambaugh, D. Lathrop, E. Ott, and W. Losert, "Pattern formation in a monolayer of magnetic spheres," *Physical Review E - Statistical, Nonlinear, and Soft Matter Physics*, vol. 68, no. 2 2, pp. 026207/1–026207/5, 2003.

[13] K. Gilpin, A. Knaian, and D. Rus, "Robot pebbles: One centimeter modules for programmable matter through self-disassembly," pp. 2485–2492, 2010.

[14] D. Gracias, J. Tien, T. Breen, C. Hsu, and G. Whitesides, "Forming electrical networks in three dimensions by self-assembly," *Science*, vol. 289, no. 5482, pp. 1170–1172, 2000.

[15] D. de Ruiter, "Bucket brain, creating a logic gate in a random network using mortal switching," Master's thesis, University of Twente, May 2013. Thesis BSc Assignment Advanced Technology.

[16] M. Welleweerd, "Bucket brain, creating a logic gate in a random network using mortal switching," Master's thesis, University of Twente, August 2013. Thesis BSc Assignment Electrical Engineering.

[17] M. Yim, W.-M. Shen, B. Salemi, D. Rus, M. Moll, H. Lipson, E. Klavins, and G. Chirikjian, "Modular self-reconfigurable robot systems [grand challenges of robotics]," *IEEE Robotics and Automation Magazine*, vol. 14, no. 1, pp. 43–52, 2007.

[18] K. Gilpin and D. Rus, "Modular robot systems," *IEEE Robotics and Automation Magazine*, vol. 17, no. 3, pp. 38–55, 2010.

[19] J. Bishop, S. Burden, E. Klavins, R. Kreisberg, W. Malone, N. Napp, and T. Nguyen, "Programmable parts: a demonstration of the grammatical approach to self-organization," in *2005 IEEE/RSJ International Conference on Intelligent Robots and Systems*, pp. 3684–3691, Aug 2005.

[20] S. Griffith, *Growing Machines*. PhD thesis, Massachusetts Institute of Technology, 2004.

[21] P. J. White, K. Kopanski, and H. Lipson, "Stochastic self-reconfigurable cellular robotics," in *Robotics and Automation, 2004. Proceedings. ICRA '04. 2004 IEEE International Conference on*, vol. 3, pp. 2888–2893 Vol.3, April 2004.

[22] K. Gilpin, K. Kotay, and D. Rus, "Miche: Modular shape formation by self-dissasembly," in *Proceedings 2007 IEEE International Conference on Robotics and Automation*, pp. 2241–2247, April 2007.

[23] J. Davey, N. Kwok, and M. Yim, "Emulating self-reconfigurable robots - design of the smores system," in *2012 IEEE/RSJ International Conference on Intelligent Robots and Systems*, pp. 4464–4469, Oct 2012.

[24] B. K. An, "Em-cube: cube-shaped, self-reconfigurable robots sliding on structure surfaces," in *Robotics and Automation, 2008. ICRA 2008. IEEE International Conference on*, pp. 3149–3155, May 2008.

[25] Z. Nagy, S. Miyashita, S. Muntwyler, A. K. Cherukuri, J. J. Abbott, R. Pfeifer, and B. J. Nelson, "Morphology detection for magnetically self-assembled modular robots," in *2009 IEEE/RSJ International Conference on Intelligent Robots and Systems*, pp. 5281–5286, Oct 2009.

[26] P. Lothman, T. Hageman, A. Manz, and L. Abelmann, "Turbulence as the disturbing force in macroscopic self-assembly.".

[27] T. Hageman, P. Lothman, A. Manz, and L. Abelmann, "Characterization of a macroscopic self-assembly reactor.".

[28] P. B. Landecker, D. D. Villani, and K. W. Yung, "An analytic solution for the force between two magnetic dipoles," *Magnetic and Electrical Separation*, vol. 9, pp. 39–52, 1998.

[29] P. B. Landecker, D. D. Villani, and K. W. Yung, "Analytic solution for the torque between two magnetic dipoles," *Magnetic and Electrical Separation*, vol. 10, no. 1, pp. 29–33, 1999.

[30] M. Tiwana, S. Redmond, and N. Lovell, "A review of tactile sensing technologies with applications in biomedical engineering," *Sensors and Actuators, A: Physical*, vol. 179, pp. 17–31, 2012.

[31] R. Dahiya and M. Valle, *Robotic Tactile Sensing, Technologies and System*. Springer, 2013.

[32] F. Schill, *Distributed Communication in Swarms of Autonomous Underwater Vehicles*. PhD thesis, Australian National University, 2007.

[33] I. Vasilescu, P. Varshavskaya, K. Kotay, and D. Rus, "Autonomous modular optical underwater robot (amour) design, prototype and feasibility study," in *Proceedings of the 2005 IEEE International Conference on Robotics and Automation*, pp. 1603–1609, April 2005.

[34] S. Jiang and S. Georgakopoulos, "Electromagnetic wave propagation into fresh water," *Journal of Electromagnetic Analysis and Applications*, vol. 3, pp. 261–266, 2011.

[35] C. Swedberg, "Rfid chips tell fish tales at aquarium." `http://www.rfidjournal.com/articles/view?8592`, July 2011.

[36] M. Schlepers, "Investigation of the mechanical properties of 3d printed structures of objet and dlp.." BSc-thesis, July.

[37] Wikipedia, "Terminal velocity." `https://en.wikipedia.org/wiki/Terminalvelocity`, June 2016.

[38] MEDER electronic, *Basic Electrical Parameters of Reed Switch Products*.

[39] S.-M. Electronics, "Reed switch and magnet interation: Product training." https://standexelectronics.com/resources/technical-library/product-training/reed-switch-magnet-interaction-2/, 2016.

[40] H.-E. Nilsson, T. Unander, J. Siden, H. Andersson, A. Manuilskiy, M. Hummelgard, and M. Gulliksson, "System integration of electronic functions in smart packaging applications," *IEEE Transactions on Components, Packaging and Manufacturing Technology*, vol. 2, no. 10, pp. 1723–1734, 2012.

Appendix A

Experimental Data

This appendix presents additional data for some experiments as well as some small other experiments that have been performed for subsystems.

A.1 Wireless communication experiments

A.1.1 RFID experiment

At the moment already multiple 2D printed RFID sensors exist [40]. With these sensors passive sensing modules can be made, where the power functionality is located in an external device (the RFID antenna picks up power from another antenna). In the past it has already been shown that RFID can be used underwater (for example to identify fish in a zoo [35], figure A.1). For the use of RFID tags in this research only passive tags are considered (active tags are bulky and expensive).

To research the option, the group for Computer Architecture for Embedded Systems (CAES) from the university has been approached. They have a set-up with long range RFID readers (from NEDAP) for location detection of UHF RFID tags (ultra high frequency tags, these tags have relatively small antennas which makes them suited for the spheres). With this set-up dozens to hundreds of tags can be read per second, fulfilling the frequency requirement. In the experiment the RFID tags were first read with the antenna from several meters distance under several angles. This showed the omnidirectionality and long range capabilities of the set-up. To test the underwater capabilities, the RFID tag was placed in between two bottles of water (layers of 5 cm of water), yielding total shielding of the signal. The experiment showed that with standard UHF RFID tags and long range antennas it is not possible to receive a signal through only small layers of water. Furthermore the readers are very expensive. Therefore the option was of RFID tags is not considered for use in the system. A side note is that with low frequency tags (125 kHz) the attenuation of the signal in water is already a lot less while for the experiment only UHF tags (860 to 960 MHz) were available. The author thanks Jordy Huiting from CAES for his help with the experiment.

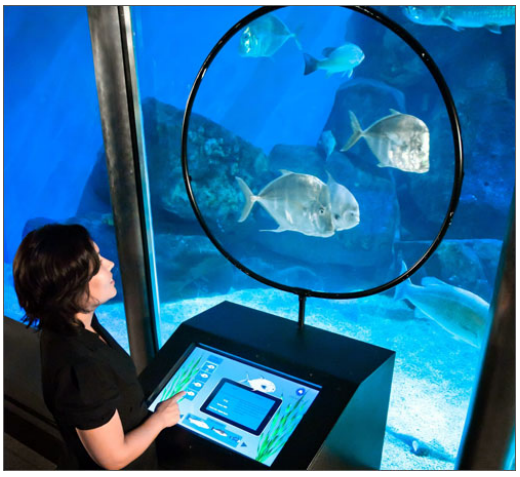

Figure A.1: The Virginia Aquarium & Marine Science Center uses RFID tags for identification of their fish [35].

A.1.2 ESP8266 Experiments

An esp8266-01 micro-controller has been used for wifi experiments. For the experiments, the micro-controller was connected to a USB to TTL converter to power the device, for programming and for communicating data over a serial connection (with buttons for resetting and programming), a schematic of this is shown in figure A.2. The arduino bootloader was burned on the micro-controller to program it with the arduino IDE (it can be programmed in arduino, however some functionality is missing). The standard "WiFiScan.ino" script as given as example script

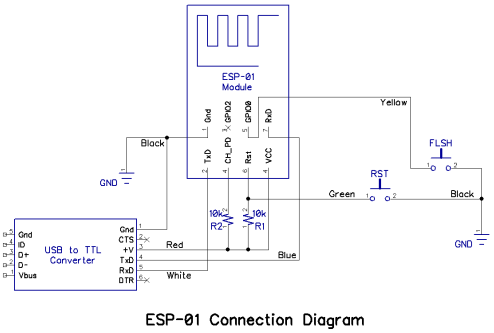

Figure A.2: Schematic diagram of the esp8266-01 connected to the USB to TTL converter.

Table A.1: My caption

Operation ESP8266	Current [mA]	Voltage [V]	Power [mW]
Uploading code	95-100	4.3	409
Scan for Wifi	75	4.8	360
LED webserver	77-85	4.8	370-408

has been used for scanning for wifi signals. With this code the esp8266 looks for wifi connections and communicates the RSSI (Received Signal Strength Indicator). This gives the relative received signal strength in arbitrary units.

For testing the signal strength underwater the esp8266 was placed in a plastic bag together with the USB to TTL converter and submerged in a basin of $20 \times 20 \times 20$ cm, as shown in figure A.3. A router with a local network was used to have a continuous signal strength. During the tests the esp8266 was rotated over all three axes to also take the directionality of the antenna into account (the micro-controller has a meandered, inverted f-antenna to match the impedance of the circuit and be reasonably omnidirectional). In normal operation the RSSI ranged from -19 dB to -27 dB, while submerged in water the RSSI dropped to -43 dB to even -77 dB depending on the orientation and the distance from the walls of the basin. For testing purposes the esp8266 was used to send data to a local webserver. In cases with a larger attenuation it was noticed that errors started to occur in the displayed data, showing the large attenuation of the signal by the water.

A second test was done on the power consumption of the device. During operation the current and voltage were measured through and over the USB to TTL converter. For several forms of operation the power consumption was determined: uploading code, scanning for wifi signals and for toggling an LED over a webserver. The measured values can be found in table A.1. It was shown that the esp8266 with wifi functionality consumes a lot of power compared to the micro-controllers as proposed in section 3.4.3.

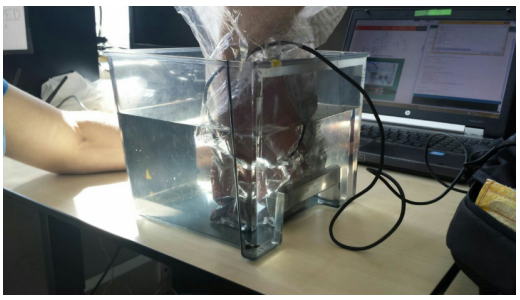

Figure A.3: The esp8266 and the USB to TTL converter submerged in water for measuring the wifi signal strength.

A.1.3 Polar measurements reed switches

In section 4.2.1 experiments as performed with the reed switches are described. This section gives extra data on these experiments. The reed switches used in the experiment are shown in figure A.4 and A.5.

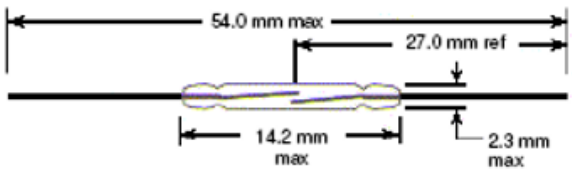

Figure A.4: The through hole reed switch as used in the experiments (STANDEXMEDER GP560-1015) [39].

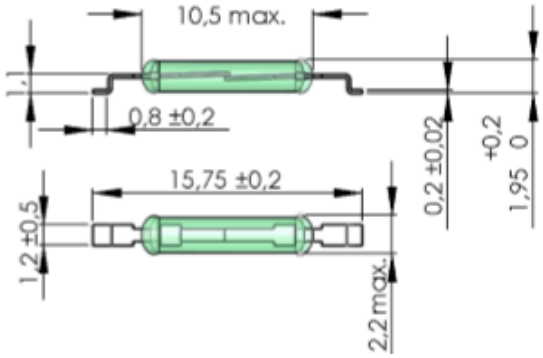

Figure A.5: The SMD reed switch as used in the experiments and in the final design (STANDEXMEDER MK23-35-B-2) [39].

The extra measurements done on the reed switches with the set-up from section 4.2.1 are shown in figure A.6 and A.7. It can immediately been seen that the SMD reed switch has the same sensitivity as the through hole switch (since the through hole switch was shortened for these measurements). Interesting to see is the large lobe on one side for both graphs and the small lobe on the opposite side. Since reed switches are symmetrical and not sensitive to polarity, it is expected that the difference in lobe size is caused by misalignment of the magnets and the switch.

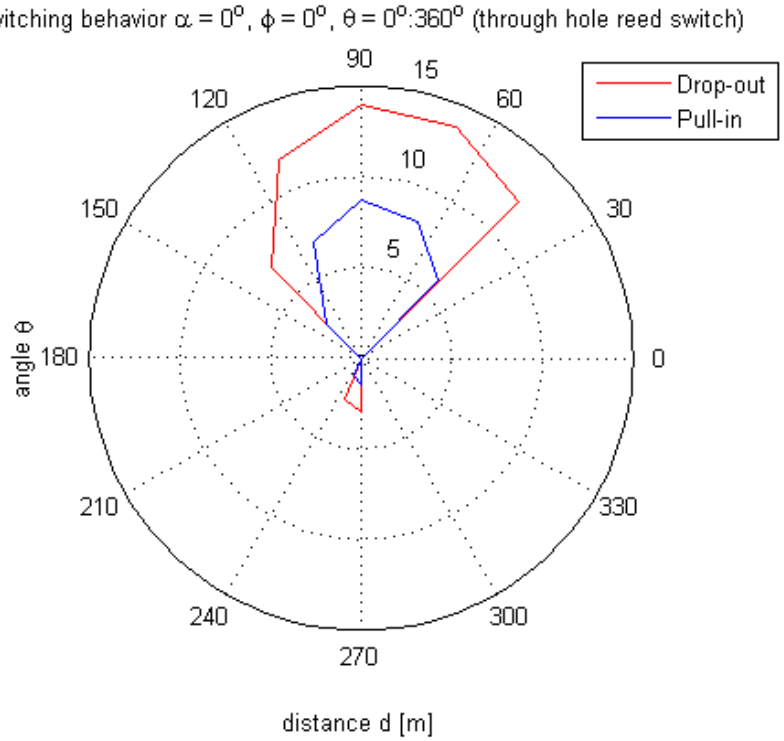

Figure A.6: Plot for a measurement with the set-up from figure 4.12 and 4.14. The measurement has been done for a through hole reed switch for the angles $\alpha = 0°$, $\phi = 0°$ and $\theta = 0° : 360°$

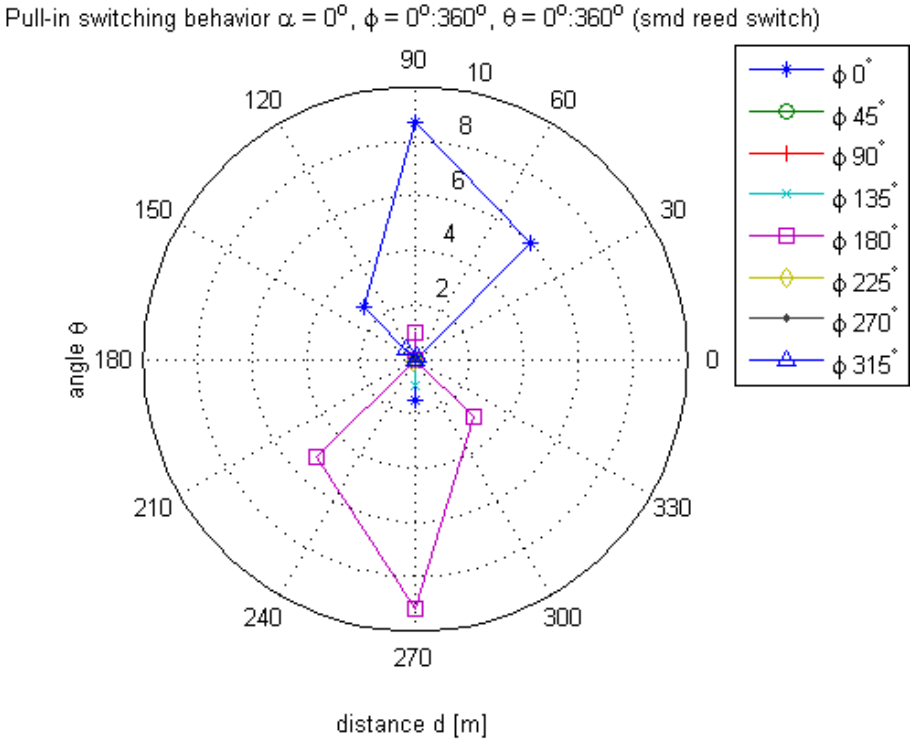

Figure A.7: Plot for a measurement with the set-up from figure 4.12 and 4.14. The measurement has been done for an SMD reed switch for the angles $\alpha = 0°$, $\phi = 0° : 360°$ and $\theta = 0° : 360°$

A.1.4 Micro-controller timer experiment

In the total tests of the system, section 8.3, there seemed to be a difference in time scale between the data from the video analysis and the data retrieved from the spheres. A possible explanation for this could be that the

Table A.2: Outcomes of the experiment to verify the timing of the micro-controllers internal clock

	time stopwatch [s]	time micro-controller [s]	number of events
Test 1	60	60.938	1 (at $t = 60\,\mathrm{s}$)
Test 2	300	301.740	1 (at $t = 300\,\mathrm{s}$)
Test 3	60	60.752	447
Test 4	60	60.654	58

internal timer of the micro-controller does not run steadily or runs at another frequency. An experiment has been done to verify whether the timing of the internal clock of the micro-controller (8 MHz) is correct.

For this the same PCB with the same batteries as used for the 2D controlled experiment were used. In the tests the timer would be synchronized by switching a reed switch by hand with a magnet. At the same instant, a stopwatch would be started. Then several events would be performed and the timer would be stopped. The data of the micro-controller would then be compared to the stopwatch time. For performing the events a reed switch would be switched by had with a magnet. This has been done for various times and number of events. The outcomes are shown in table A.2. The deviations of the final times from the micro-controller clock can be explained by the fact that the events were performed by hand, taking a reaction time into play. The outcomes from table A.2 show that the final times are very close to the times of the stopwatch. The offset caused by the reaction time of the author cannot be circumvented, however due to following a metronome with 60 beats per minute a set period was followed. Over the full 60 s it can be seen that the measurements did not shift significantly, this long time span is not really influenced by the reaction time. From this can be concluded that the timing can record a period of time accurate enough for the experiments (the offsets in 8.3 are larger than the precision of the micro-controller as shown in the timing experiment. Hence the offset is not caused by bad timing of the micro-controller).

However it could still be the case that the timer has a large fluctuation in the size of its timesteps (yielding the same final time however yielding wrong timestamps for particular events). For this in test 4 (table A.2) a reed switch was switched every second with a magnet by hand whilst following the pace of a metronome (60 beats per minute). The data from the sphere of this test can be seen in figure A.8. From the graph it can be seen that the timing is very accurate and only small fluctuations in timing occur (which can also be explained from the fact that the events were performed by hand). *Hence it is concluded that the internal clock of the ATmega328P is precise enough for usage in the self-assembly experiments.*

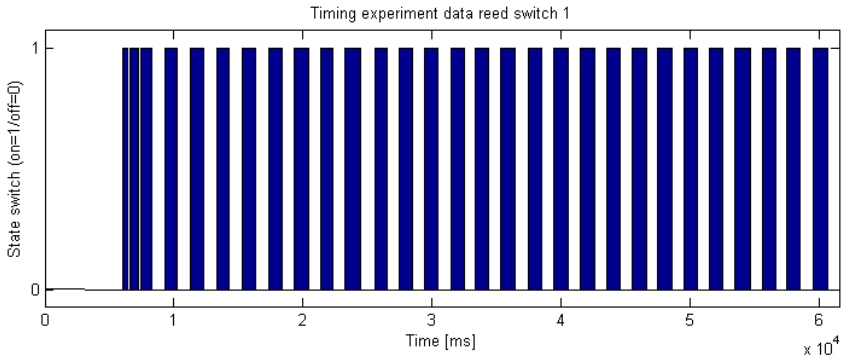

Figure A.8: The reed switch data for switching a reed switch with a magnet by hand with 60 beats per minute.

A.1.5 Total system experiments

In the experiments for the total system the following data analysis script was used. This script reads the event data (timestamp and total state of the switches) from a txt file. The states are then again split for both functions and separate graphs are generated. In this way the video data and sphere data can be plotted for the separate reed switches and can be compared. The MATLAB script used for this is shown below.

For the 2D controlled environment experiment also an experiment with one total sphere and two magnet spheres was performed. The data comparison from this can be seen in figure A.9. From 0 s to 15 s the synchronization and testing of the spheres is done. In the video data it can be seen that the author connects to spheres multiple times, however only 2 out of 8 connections was measured. This was most likely caused by too weak magnets and ppor alignment by the way the spheres were hold (remarkable is that these problems do only occur when the author connects two spheres, while rolling the proper connections are almost always measured). For reed witch 1 around 18 s and for reed switch 2 around 17 s also short connecting and disconnecting can be seen. In the video it was found to be false positives (figure 8.5 is a frame from the false positive for reed switch 1). It can also be seen that reed switch 1 is both barely connecting and has measured incorrect data. This can

r

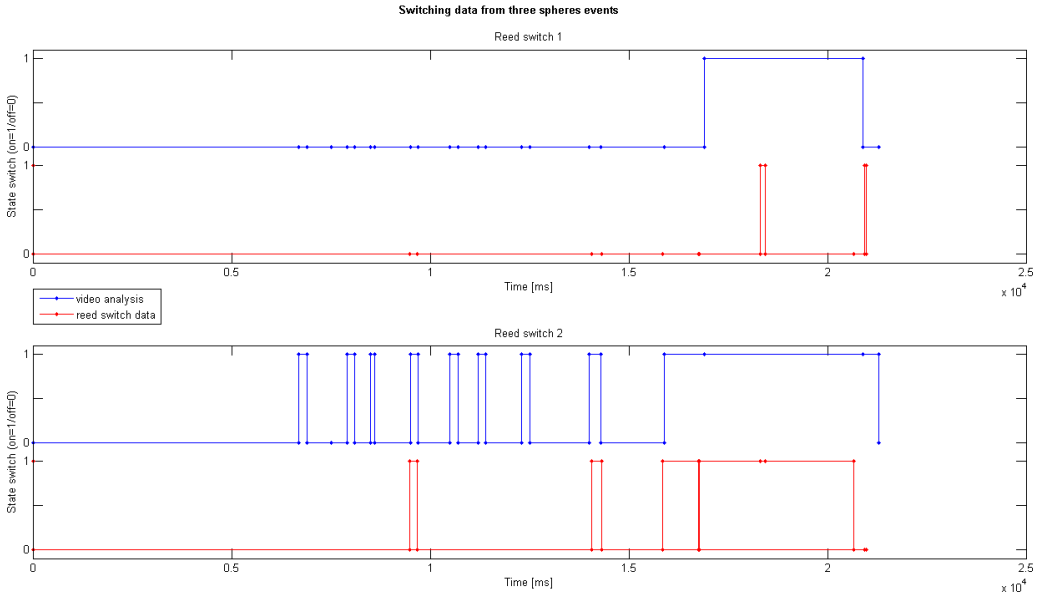

Figure A.9: A comparison of the data of the 2D controlled experiment with three spheres (one total system and two magnet spheres), showing the recorded events for both switches as found from the video analysis and as obtained from the sphere.

be explained by the fact that the second magnet sphere in this experiment used weaker magnets.

```
%%%%%%%%%%%%%%%%%%%%%%%%%%%%%%%%%%%%%%%%%%%%%%%%%%%%%%%%%%%%%%%%%%%%%%%%%%%%%%%%
%  Data analysis self-assembly experiments                                      %
%                                                                               %
%  Loads the test data and calculates the connection                            %
%  times for the different spheres.                                             %
%                                                                               %
% BSc-assignment (RAM EWI)                                                      %
% ALEXANDER DIJKSHOORN      S1479202                                            %
% 24 June 2016                                                                  %
%%%%%%%%%%%%%%%%%%%%%%%%%%%%%%%%%%%%%%%%%%%%%%%%%%%%%%%%%%%%%%%%%%%%%%%%%%%%%%%%

clear all
close all
clc

% Read data from a specific sphere from a textfile
txtname = {'data_3.txt'};

for i = 1:numel(txtname)
    fid{i} = fopen(txtname{i},'r');
    data{i} = textscan(fid{i}, '%u32 %u', 'CommentStyle','%');
    fclose(fid{i});
    data{i} = cell2mat(data{i});
end

temp_data = data{1,1};
timestamps = temp_data(1:length(temp_data(1:end,1)),1);
reed_states = temp_data(1:length(temp_data(1:end,1)),2);

% Determine occurence of the different states
n_0 = 0;
n_1 = 0;
n_2 = 0;
n_3 = 0;
temp_times = [0; 0];
temp_state = 3;
switches = zeros(2,length(temp_data(1:end,1)));

% Split states for both switches
for i = 1:length(temp_data(1:end,1))
    if reed_states(i)==0
        switches(1:end,i) = 1;
```

```
        n_0 = n_0+1;
    elseif reed_states(i)==1
        switches(1,i) = 1;
        n_1 = n_1+1;
    elseif reed_states(i)==2
        switches(2,i) = 1;
        n_2 = n_2+1;
    elseif reed_states(i)==3
        switches(1:end,i) = 0;
        n_3 = n_3+1;
    end
end

% Calculate the duration of the events
event_times1 = zeros(1,n_0+n_1);
event1_counter = 0;
event_times2 = zeros(1,n_0+n_2);
event2_counter = 0;
switches = cat(2,[0;0],switches);
for i = 2:(length(temp_data(1:end,1))+1)
    if (switches(1,i) == 1) && (switches(1,i-1)==0)
        temp_times(1) = timestamps(i-1);
        event1_counter = event1_counter+1;
    elseif (switches(1,i) == 0) && (switches(1,i-1)==1)
        event_times1(event1_counter) = timestamps(i-1) - temp_times(1);
    end

    if (switches(2,i) == 1) && (switches(2,i-1)==0)
        temp_times(2) = timestamps(i-1);
        event2_counter = event2_counter+1;
    elseif (switches(2,i) == 0) && (switches(2,i-1)==1)
        event_times2(event2_counter) = timestamps(i-1) - temp_times(2);
    end
end

event_times1 = event_times1(event_times1~=0);
event_times2 = event_times2(event_times2~=0);

% Plot separate graphs for both switches figure
subplot(2,1,1)
stairs(timestamps, switches(1,2:end))
ylim([0 1.1]);
title('Reed switch 1')
xlabel('Time [ms]')
ylabel('State switch (on/off)')
subplot(2,1,2)
stairs(timestamps, switches(2,2:end))
ylim([0 1.1]);
title('Reed switch 2')
xlabel('Time [ms]')
ylabel('State switch (on/off)')
```

graphics/data_analysis_report.m

Appendix B

Modelling and Simulations

B.1 Ideal dipole modeling compared to FEM simulations

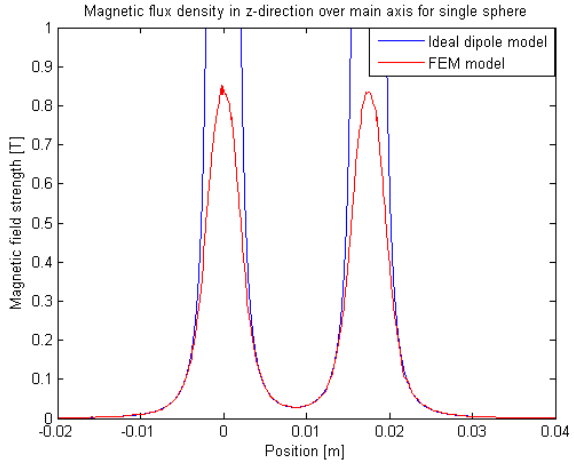

Figure B.1: The comparison of the B-field in the z-direction for dipole and FEM calculations for a single sphere over the main axis (figure 4.5).

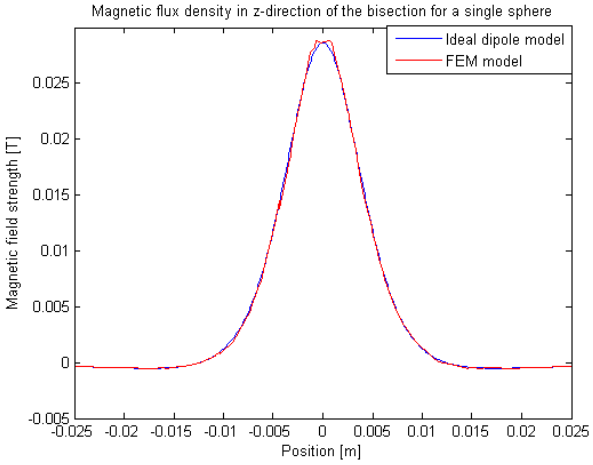

Figure B.2: The comparison of the B-field in the z-direction for dipole and FEM calculations for a single sphere over the bisection (figure 4.5).

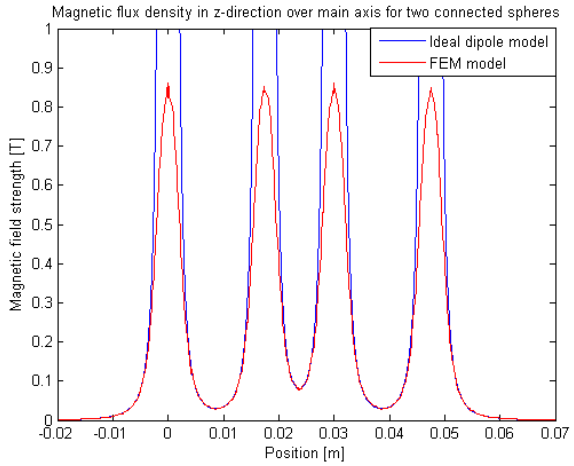

Figure B.3: The comparison of the B-field in the z-direction for dipole and FEM calculations for two attracting spheres over the main axis (figure 4.5).

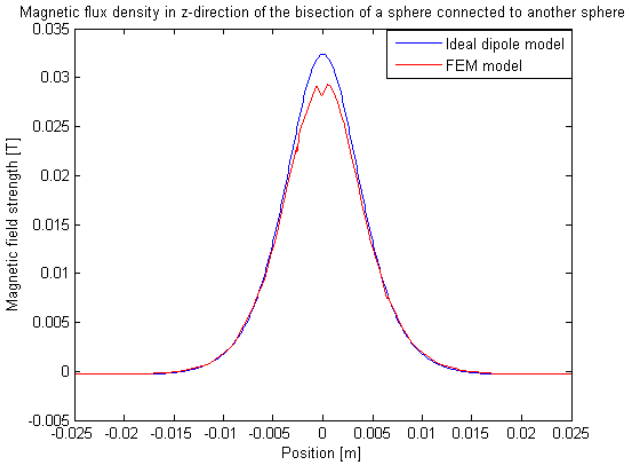

Figure B.4: The comparison of the B-field in the z-direction for dipole and FEM calculations for two attracting spheres over the bisection of the first sphere (figure 4.5).

Dipole calculations and FEM simulations have been done on the magnets and spheres from chapter 4. The

results can be seen in figure B.1, B.2, B.3 and B.4. From these results it can be seen that for distances from magnets larger than a couple of mm the results are the same. Only for close interaction the dipole models and FEM simulations deviate (from distances of around 5mm and closer to magnets). This can be seen from the calculations of the field for the main axis in particular (since this axis crosses the dipoles, causing to blow up to field very close to the dipoles). For the fields in the bisection there is almost no difference, since the magnets are at a large enough distance (in figure B.4 only in the middle of the bisection the B-field is significantly stronger). From these results it can be concluded that the FEM simulations in chapter 4 are valid and can be used for determining the B-fields in and around the spheres.

B.1.1 Ideal dipole script

The following code has been used for the dipole models of the magnets of the spheres, the equations of section 2.2 have been used for this. Plots are made combined with data exported from COMSOL. The parts were plots are generated have been left out of the code to limit the size of the report.

```
%% B-field spheres calculations

clear all
close all
clc

% Constants and parameters
mu_0 = 4*pi*10e-7;
Ms = 1.2;                       %[T]
diameter = 0.004;
height = 0.004;
offset = 0.0175;
Vm = 1/4*pi*diameter^2*height;     %[m^3]
M = Ms*Vm/mu_0;

% 1 Sphere ------------------------------------------------------------------
% y=0 B-field
x1 = -0.04:0.00001:0.05;
Bx = mu_0/(2*pi)*M./(abs(x1).^3) + mu_0/(2*pi)*M./(abs(x1-offset).^3);
plot(x1,Bx,'b')
hold on
axis([-0.02, 0.04, 0,1]);
title('Magnetic flux density in z-direction over main axis for single sphere')
xlabel('Position [m]')
ylabel('Magnetic field strength [T]')

% Comsol comparison
Comsol_data1 = importdata('Comsol_single_final.mat');
plot(Comsol_data1(:,1)+0.00875,Comsol_data1(:,2),'r')
legend('Ideal dipole model', 'FEM model') %'magnet1',


% x=middle B-field
a = 0.00875;        % offset x from sphere 1
y = -0.1:0.0001:0.1;
B_x = 2* mu_0/(4*pi).*1./(sqrt(a.^2+y.^2)).^3.*(3.*-a./(sqrt(a.^2+y.^2)).* (M.*-a./sqrt(a.^2+y
    .^2))-M); %2* since symmetric and two magnets

% 2 Spheres -----------------------------------------------------------------
% y=0 B-field
x1 = -0.04:0.00001:0.08;
Bx = mu_0/(2*pi)*M./(abs(x1).^3) + mu_0/(2*pi)*M./(abs(x1-offset).^3)+mu_0/(2*pi)*M./(abs((x1
    -0.03)).^3) + mu_0/(2*pi)*M./(abs(x1-(0.03+offset)).^3);

% x=middle B-field
a = 0.0085;
y = -0.1:0.0001:0.1;
B_x = mu_0/(4*pi).*1./(sqrt(a.^2+y.^2)).^3.*(3.*-a./(sqrt(a.^2+y.^2)).* (M.*-a./sqrt(a.^2+y
    .^2))-M)+      mu_0/(4*pi).*1./(sqrt(a.^2+y.^2)).^3.*(3.*a./(sqrt((-a).^2+y.^2)).* (M.*a./
    sqrt((-a).^2+y.^2))-M)+        mu_0/(4*pi).*1./(sqrt((-a+0.03).^2+y.^2)).^3.*(3.*-(-a+0.03)
    ./(sqrt((-a+0.03).^2+y.^2)).* (M.*-(-a+0.03)./sqrt((-a+0.03).^2+y.^2))-M)      + mu_0/(4*pi
    ).*1./(sqrt((a+0.03).^2+y.^2)).^3.*(3.*-(a+0.03)./(sqrt((a+0.03).^2+y.^2)).* (M.*-(a+0.03)
    ./sqrt((a+0.03).^2+y.^2))-M);
```

graphics/reed_plots_report.m

B.1.2 Dipole forces, torques and energies script

To calculate the forces, torques and energies of the magnets, the following script has been used. The results and plots have been used for section 4.1.1 and section 4.1.3. In the script also the drag force as function of sphere diameter for different possible densities of the sphere has been calculated, a plot is shown in figure B.5. Next to that the terminal velocities have been calculated as function of sphere diameter for different sphere densities, figure B.6. The terminal velocity is important for the flow speed at which the reactor will be operated (the flow speed of the reactor is set equal to the terminal velocity of the spheres to make them "weightless" in the flow) and the drag force is taken as guideline for determining the needed connection force of the magnets in the sphere. The drag force is calculated from $F_{drag} = \frac{1}{2}\rho A v_t^2 C_D$, were $C_D = 0.5$ (for spheres $C_D \approx 0.5$ in a large range of turbulent flow). The terminal velocity is determined by taking the drag force of the sphere equal to the weight and rewriting (equation 4.2).

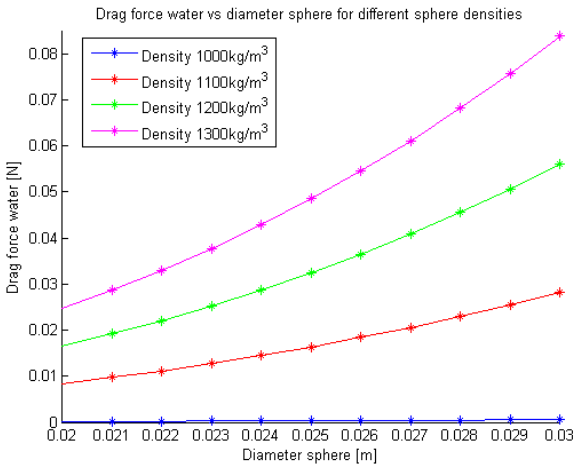

Figure B.5: The drag force on a sphere in the reactor as function of its diameter.

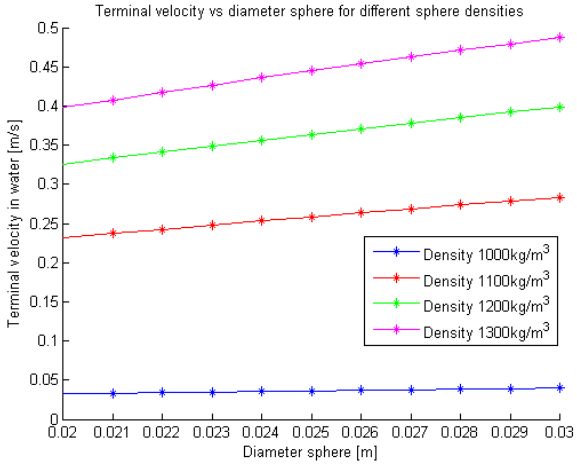

Figure B.6: The terminal velocity of a sphere in the reactor as function of the sphere diameter for different possible sphere densities.

```
clear all
close all
clc

%_Force plot separation distance_____________________________________________
d = 0.0005:0.0001:0.2;                          %[m] separation distance ideal dipoles
magnets = [0.001, 0.001; 0.001, 0.002; 0.002, 0.002; 0.002, 0.004; 0.004, 0.004; 0.002,
    0.008]; %[m] height and diameter respectively for different magnets
Bx = zeros(length(d), length(magnets));
Force = zeros(length(d), length(magnets));      %Initialize matrix for forces
Force_r = zeros(length(d), length(magnets));

for k = 1:size(magnets,1);                      % Loop through the different magnets

    for i = 1:length(d);                        % Loop through a range of separation distances
     of the dipoles
        %_Constants and parameters_____________________________________________
        h = magnets(k,1);                       %[m] height magnet
        d_m = magnets(k,2);                     %[m] diameter magnet
        mu_0 = 4*pi*10e-7;
        Ms = 1.2;                               %[T] remanence
        Vm = 1/4*pi*d_m^2*h;                    %[m^3] volume magnet
        M = Ms*Vm/mu_0;                         %[A/m] Magnitude magnetic moment

        %_Vectors______________________________________________________________
        % Different orientations of the magnets by changing the direction
        % of the magnetic dipole moment
        m_a = [M; 0; 0];
        m_b = [M; 0; 0];
%         m_a = [sqrt(2)*M; -sqrt(2)*M; 0];                 %[A/m] Magnetic moment
%         m_b = [sqrt(2)*M; sqrt(2)*M; 0];                  %[A/m] Magnetic moment
%         m_a = [sqrt(1/3)*M; -sqrt(1/3)*M; sqrt(1/3)*M];
%         m_b = [sqrt(1/3)*M; sqrt(1/3)*M; sqrt(1/3)*M];
%         m_a = [0; M; 0];
%         m_b = [M; 0; 0];
```

```
        x_a = [0; 0; 0];                                    %[m] position magnet a
%         x_b = [1.5*sqrt(2); 1.5*sqrt(2); 0];
        x_b = [d(i); 0; 0];                                 %[m] position magnet b
        r = x_b-x_a;                                        %[m] position vector from a pointing to b
        r_h = r./(norm(r));                                 %[m] unit vector a to b
        Bx(i,k) = mu_0/(2*pi)*M./(abs(x_b(1)).^3);

        %% Force_____________________________________________________________________
        % Calculate the force of magnet a on magnet b
        F = 3*mu_0./(4*pi*norm(r)^4)*( cross((cross(r_h,m_a)),m_b) + (cross((cross(r_h,m_b)),
    m_a)) - 2.*r_h.*(dot(m_a,m_b)) + 5.*r_h.*dot((cross(r_h,m_a)),(cross(r_h,m_b))) );
        FD(i,k) = dot(r,F);
        Force(i,k) = norm(F);
        Force_r(i,k) = round(Force(i,k).*10000)./10000;

        %% Torque____________________________________________________________________
        % Calculate the torque of magnet a on magnet b
        T_ab = mu_0*norm(m_a)*norm(m_b)/(4*pi*norm(r)^3)*(3*dot(m_a/M,r)*cross(m_b/M,r)+cross(
    m_a/M,m_b/M));
        Torque_ab(i,k) = norm(T_ab);
    end
end

%% Energy compared_____________________________________________________________
% Comparing energies for different magnets in spheres
% Forces and distances are looked up in matrices and used for integration

% Same force for 12x4mm magnet at center (30mm spacing) and 4x4mm magnet
% with 10mm spacing from the center during connection
FD_1 = FD(296:1296,6);

FD_21 = FD(96:1096,5);
FD_22 = FD(296:1296,5);
FD_23 = FD(496:1496,5);

FD_61 = FD(9:1009,1);
FD_62 = FD(296:1296,1);
FD_63 = FD(570:1570,1);
d_6 = d(9:1009);
d_63 = d(570:1570);

d_1 = d(296:1296);
d_2 = d(96:1096);
d_23 = d(496:1496);
q1 = trapz(d_1,FD_1);
q2 = trapz(d_2,FD_21)+2*trapz(d_1,FD_22)+trapz(d_23,FD_23);
q6 = trapz(d_6,FD_61)+2*trapz(d_1,FD_62)+trapz(d_63,FD_63);

%% Plot_______________________________________________________________________
% Generate graphs
figure
loglog(d,Bx)
axis([0.0005 0.2 0 1000])
legend('diameter 1mm, height 1mm', 'diameter 1mm, height 2mm', 'diameter 2mm, height 2mm', '
    diameter 2mm, height 4mm', 'diameter 4mm, height 4mm', 'diameter 4mm, height 12mm')
title('The B-field over distance modeled as ideal dipole')
xlabel('Separation distance dipoles [m]')
ylabel('B-field [T]')

figure
hold on
grid on
plot(d,Force)
axis([0 0.03 0 0.03])
% axis([0.006 0.015 0.01 0.03])
legend('diameter 1mm, height 1mm', 'diameter 2mm, height 1mm', 'diameter 2mm, height 2mm', '
    diameter 4mm, height 2mm', 'diameter 4mm, height 4mm', 'diameter 12mm, height 4mm')
title('Two ideal dipoles force vs separation distance for different magnet sizes')
xlabel('Separation distance dipoles [m]')
ylabel('Force [N]')

figure
plot(d,Torque_ab)
grid on
% grid minor
hold on
```

```
106 axis([0 0.03 0 0.001])
    % axis([0.006 0.015 0.01 0.03])
108 legend('diameter 1mm, height 1mm', 'diameter 1mm, height 2mm', 'diameter 2mm, height 2mm', '
        diameter 2mm, height 4mm', 'diameter 4mm, height 4mm', 'diameter 4mm, height 12mm')
    title('Torque ideal dipoles on A by B vs separation distance for different magnet sizes')
110 xlabel('Separation distance dipoles [m]')
    ylabel('Torque on A by B [Nm]')
112

114 %_Force in water with size sphere_____________________________________________________
    % Calculate the drag force on the spheres for different flow speeds and
116 % densities of the spheres
    diam = 0.005:0.001:0.03;          %[m] diameter of sphere
118 rho_c = 1000:100:1300;             %[kg/m^3] density current spheres
    g = 9.81;
120 C_d = 0.5;                      %Re for turbulent water
    rho_w = 998;
122 F_d = zeros(length(rho_c),length(diam));

124 figure
    title('Drag force water vs diameter sphere for different sphere densities')
126 xlabel('Diameter sphere [m]')
    ylabel('Drag force water [N]')
128 axis([0.02 0.03 0 0.085])
    C2 = {'b*-','r*-','g*-','m*-'};
130 hold on

132 %_Terminal velocity____________________________________________________________________
    % Calculate and plot the terminal velocity over sphere diameter for the spheres
134 % for different sphere densities
    for i = 1:length(rho_c);
136     for j = 1:length(diam);
            r_c = 0.5*diam(j);                  %[m] radius current spheres
138         A_c = 2*pi*r_c^2;               %[m^2] frontal surface current sphere
            v_c = 4/3*pi*r_c^3;             %[m^3] volume current spheres
140         m_c = rho_c*v_c;                % [kg] mass current spheres
            u_term = sqrt(4*g*2*r_c/(3*C_d)*((rho_c(i)-rho_w)/rho_w));
142         F_d(i,j) = 0.5*A_c*u_term^2*rho_w*C_d;
        end
144     plot(diam,F_d(i,:),C2{i});
    end
146 legend('Density 1000kg/m^3', 'Density 1100kg/m^3', 'Density 1200kg/m^3', 'Density 1300kg/m^3')

148 u_term = zeros(length(rho_c),length(diam));
    figure
150 hold on
    title('Terminal velocity vs diameter sphere for different sphere densities')
152 xlabel('Diameter sphere [m]')
    ylabel('Terminal velocity in water [m/s]')
154 xlim([0.02 0.03])
    for i = 1:length(rho_c);
156     for j = 1:length(diam);
            r_c = 0.5*diam(j);                  %[m] radius current spheres
158         A_c = 2*pi*r_c^2;               %[m^2] frontal surface current sphere
            v_c = 4/3*pi*r_c^3;             %[m^3] volume current spheres
160         m_c = rho_c*v_c;                % [kg] mass current spheres
            u_term(i,j) = sqrt(4*g*2*r_c/(3*C_d)*((rho_c(i)-rho_w)/rho_w));
162     end
        plot(diam,u_term(i,:),C2{i});
164 end
    legend('Density 1000kg/m^3', 'Density 1100kg/m^3', 'Density 1200kg/m^3', 'Density 1300kg/m^3')
```

graphics/magnetic_force_report.m

B.2 COMSOL Multiphysics

The software package Comsol Multiphysics has been used for FEM simulations of the B-field from the used magnets. It has already been shown by comparing the outcomes to analytical models that the FEM simulations are valid. For the FEM simulations several steps have been taken:

- Geometry: for the simulations magnets and the surrounding water have been modeled as cylinders. Electronics and batteries have not been taken into account in the model

- Materials: Water has been used as material for the water. For the magnets a material was made with a relative permeability of 1.05
- As physics package the *Magnetic Fields, No Currents* has been used. Magnetic flux conversation was used for all bodies and the boundaries of the water were given isolating boundary conditions. A magnetic flux conservation was given to the magnets themselves, with a remanent flux density of 1.2T (N35 neodymium magnets)
- Mesh: As mesh the *extra fine* setting was used (there was almost no convergence while switching to the *extremely fine* mesh settings)
- Study: The default settings of COMSOL Multiphysics (version 4.3) were used for performing the study
- Results: Both surface plots, slices, line plots and streamlines have been used for interpreting the results
- Export: the data has been exported to Matlab for comparison with the analytical models

In figure B.7 and B.8 steps in the simulation process can be found. In figure B.7 the bodies to be modeled are displayed, cylinders for both the magnets and the water. In figure B.8 outcomes can be seen, where the field is displayed in 2D planes by means of colour gradients. A large body of water compared to the magnets has been used to have minimal disturbance of the results by boundary effects.

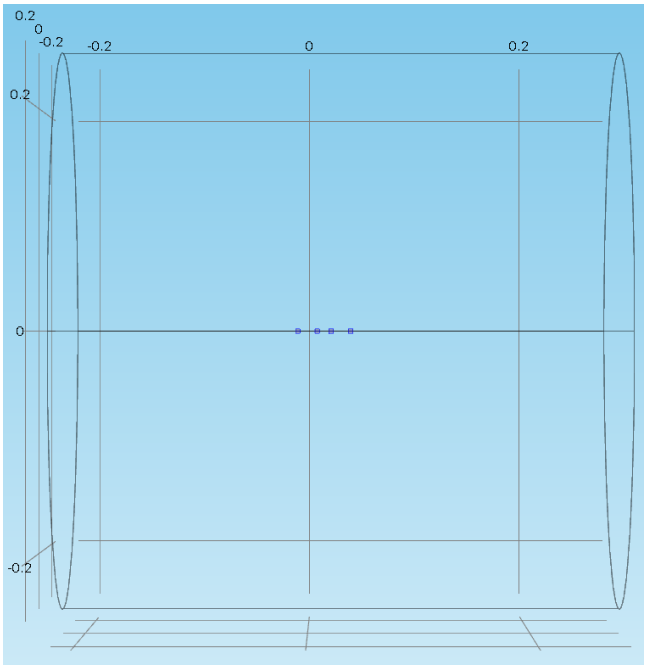

Figure B.7: Four cylindrical magnets inside a large cylinder of water simulate two connected spheres

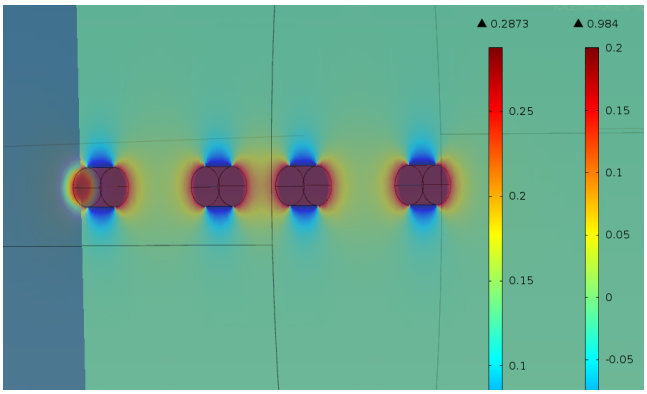

Figure B.8: Slices with colour gradients are used to represent the B-fields (mfnc.Bz is used for the magnetic flux gradient in the z-direction) in the 3D results.

Appendix C

Technical Drawings

This chapter presents the technical drawings of both the PCB and of the 3D printed parts.

C.1 Eagle drawings

The PCB design was done with the help of the CAD software Eagle. In this programme a schematic is made after which components can be oriented and routed in a PCB lay-out editor. Figure C.1 shows the schematics of the circuit. The components of the circuit can be found in section 5.1.

Figure C.1: The schematics of the circuit in Eagle.

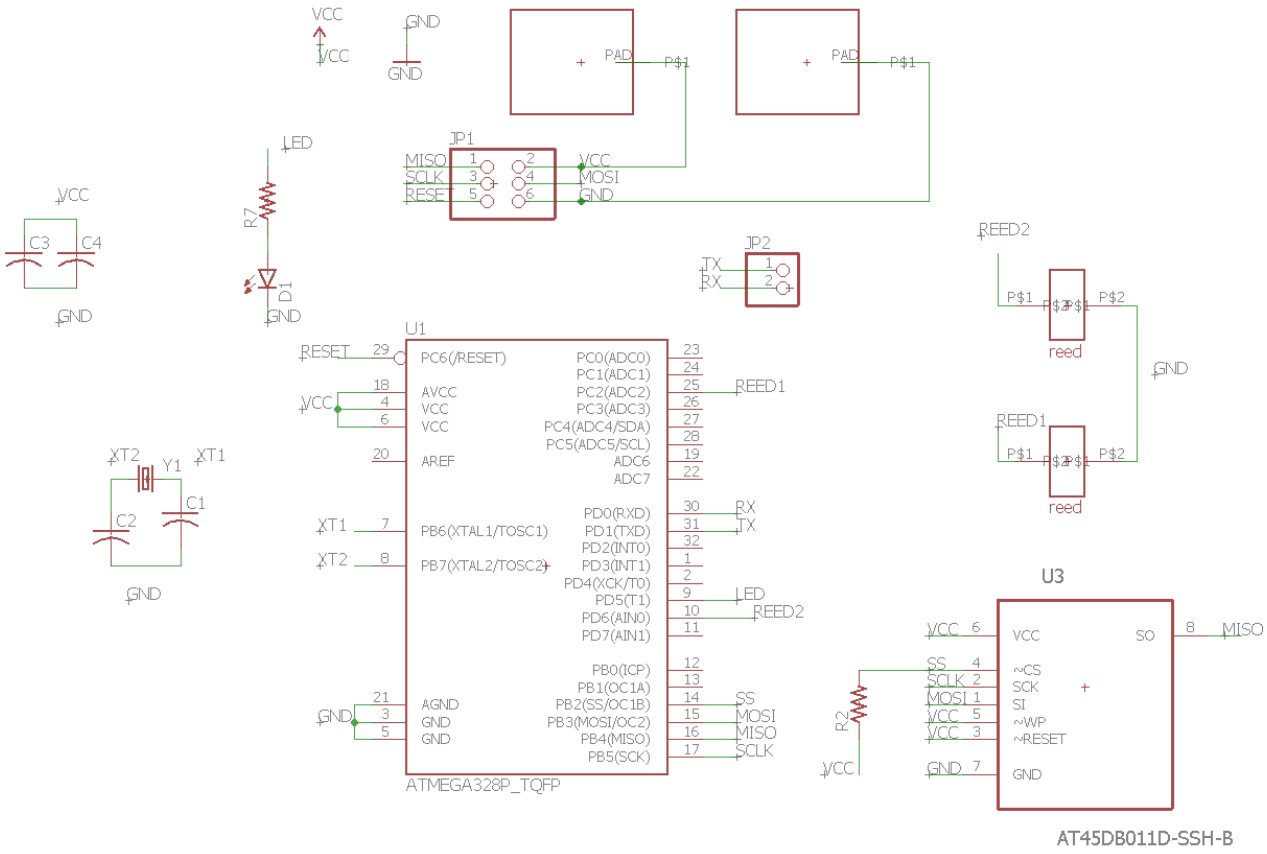

With these components a PCB layout has been made, as shown in figure C.2. This PCB is a round two layer PCB, with a diameter of 27mm. It has a thickness of 1.55mm and an outside copper layer thickness of 35μm. The bottom and top layer of the PCB can be seen in figure C.3. In future designs the crystal oscillator and it's capacitors can be taken out, since the internal clock of the micro-controller can be used. Furthermore a pull-up resistor for the reset pin should be included. The hole for wiring of the batteries was placed underneath a reed switch. This was solved by drilling a new hole at the edge of the PCB.

Figure C.2: The PCB board as designed in Eagle. It's diameter is 27mm.

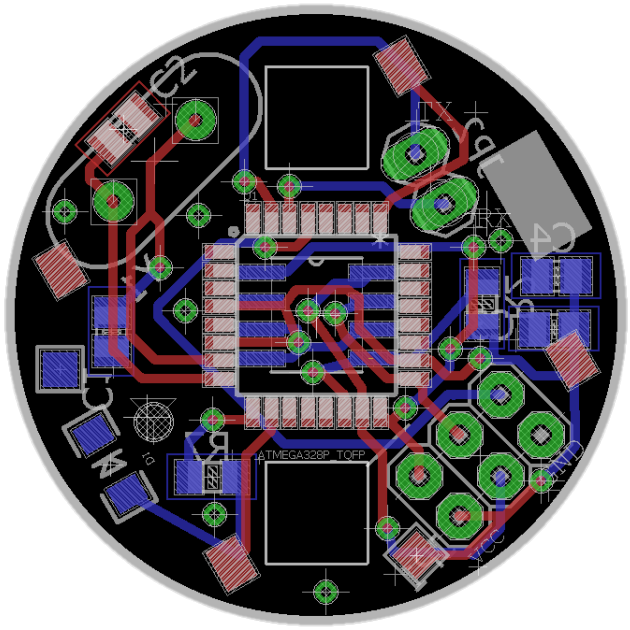

Figure C.3: The top layer of the PCB in red and the bottom layer in blue.

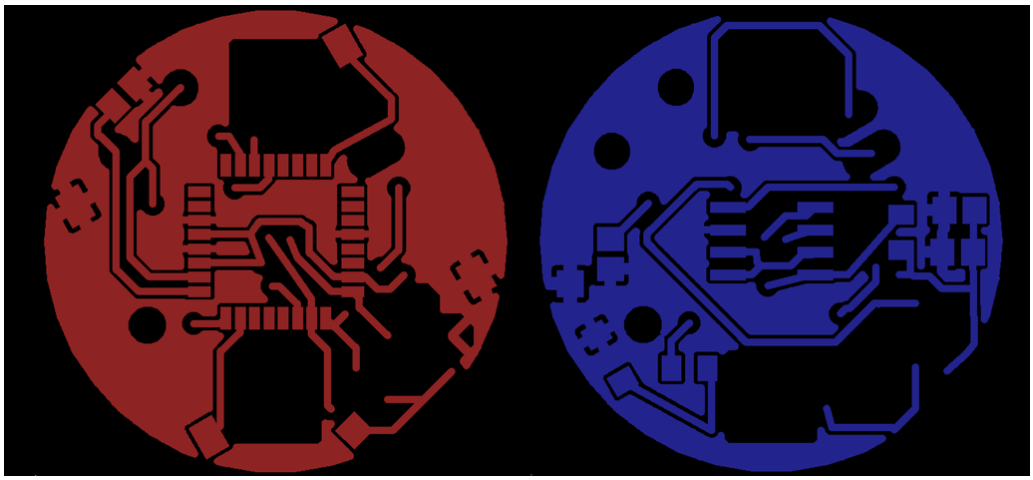

C.2 Solidworks drawings

All 3D printed parts have been designed with the CAD software Solidworks. The different parts have been printed with different 3D printers and different materials. The different printed parts are:

- The final upper and lower shell have been printed with the EOSINT P395 printer (Selective Laser Sintering technology) via 3DHubs in nylon(due to problems with the Objet Eden 250 of RAM). The drawings are shown in figure C.5 and C.6
- The PCB mock-up, figure C.9, as well as the reed experiment set-up, figures C.10; C.11 and C.12, have been printed with the RoVa3D with pla material (Fused Deposition Molding technology).
- The spheres for testing the magnets in the SA reactor, figure C.7, have been printed with the Objet Eden 250 with FullCure720 model material at RAM (polyjet technology).

A technical drawing with an exploded view and a top view is shown in figure C.4. From the top view it may be clear that there is plenty of space at the positions next to the batteries (for the realized case with three batteries this the side with two batteries does not have any space left).

Figure C.4: Technical drawing with exploded view and top view of the total system.

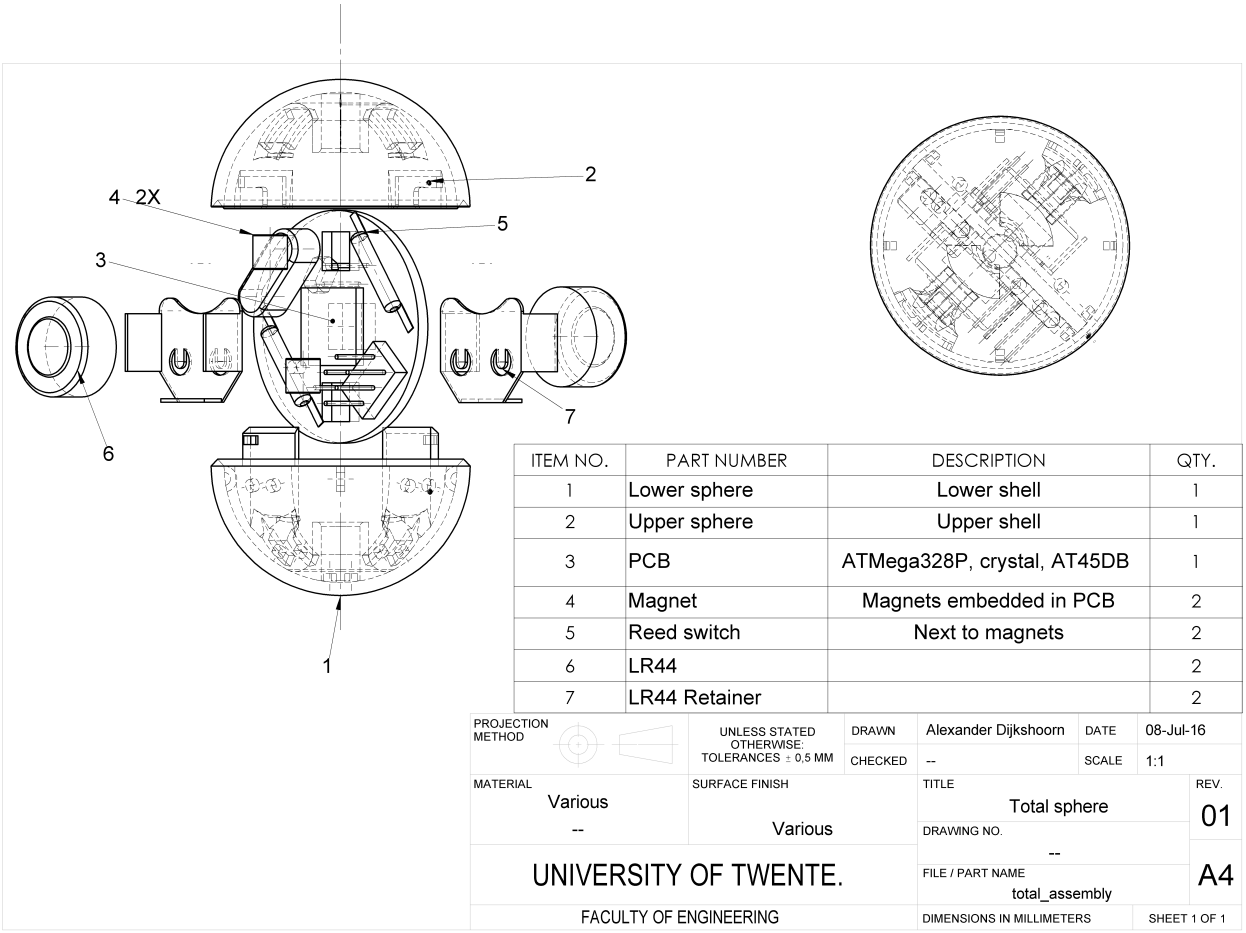

ITEM NO.	PART NUMBER	DESCRIPTION	QTY.
1	Lower sphere	Lower shell	1
2	Upper sphere	Upper shell	1
3	PCB	ATMega328P, crystal, AT45DB	1
4	Magnet	Magnets embedded in PCB	2
5	Reed switch	Next to magnets	2
6	LR44		2
7	LR44 Retainer		2

PROJECTION METHOD	UNLESS STATED OTHERWISE: TOLERANCES ± 0,5 MM	DRAWN	Alexander Dijkshoorn	DATE	08-Jul-16
		CHECKED	--	SCALE	1:1
MATERIAL: Various --	SURFACE FINISH: Various	TITLE: Total sphere			REV.: 01
		DRAWING NO.: --			
UNIVERSITY OF TWENTE.		FILE / PART NAME: total_assembly			A4
FACULTY OF ENGINEERING		DIMENSIONS IN MILLIMETERS		SHEET 1 OF 1	

C.2.1 Sphere shell drawings

The drawings of the final shell can be found in figure C.5 and C.6. The shell is designed for integration of all components. The hollow cylindrical parts in the middle are designed for keeping the magnets in place (the magnets slide in the PCB and the PCB is fitted in the slot in the cylinders). At the edges bayonet fittings are made for proper sealing of the spheres (the SLS printer could not cope with the thin edges, leaving gaps in between. This caused a lot of troubles with getting the spheres water tight). Support structures for batteries have been added at the sides (during the experiments they were removed to make space for three instead of two batteries. It was found that the batteries would stay in place by the tight fit). The hole design was made as robust as possible, with rounded edges and thick features, making 3D printing easier. After manufacturing it was found that the sealing edges of the spheres were to small for properly sealing the spheres of water. In future designs a redesign of the edges is needed with a thicker wall and a larger overlap.

C.2.2 Magnets sphere test

The spheres as used in the SA reactor experiment concerning different sizes of magnets at different locations in the spheres were printed with polyjet technology. The drawing of the spheres used for testing different sizes and locations of magnets can be found in figure C.7. In the design guiding edges are used to guide the halves to the correct place when put together. Snap fits are used for keeping the halves together. The FullCure720 model material however is a very brittle material. This resulted into broken snap fits after minor shocks. In the experiments the halves were kept together by sealing the touching sides with vaseline. For future designs only overlapping edges are needed and no fragile parts.

C.2.3 Plan B

For experimenting a mock-up of the PCB was printed, from which the technical drawing is shown in figure C.9. This mock-up contains holes for magnets (square holes) and LED's (round holes), as well as slots for the reed

Figure C.5: Technical drawing of the upper shell of the sphere.

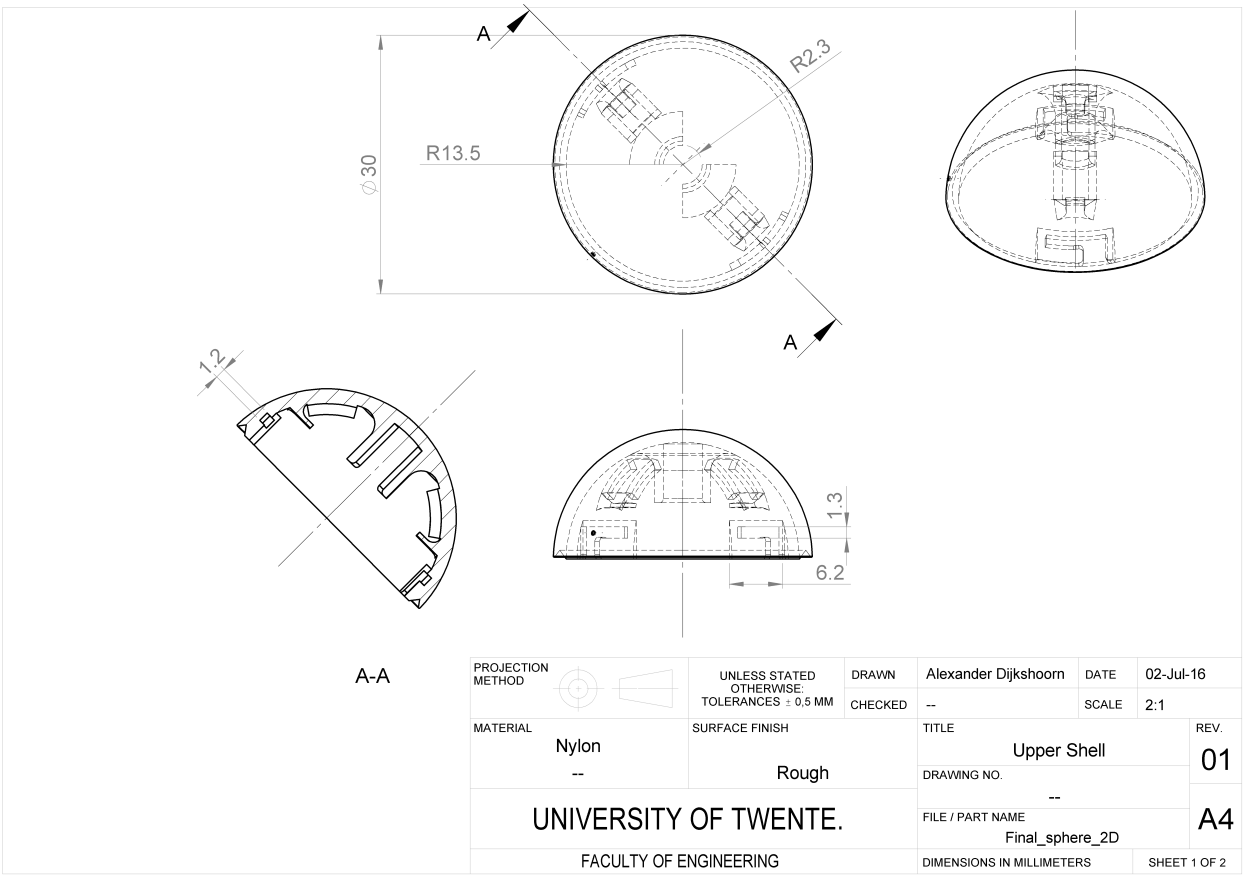

switches. The mock-ups have both been used for showing the sensing principle (with battery powered LED's switched by reed switches) and for reactor experiments with spheres containing magnets. A drawing of the mock-up circuit containing LED's is shown in figure

C.2.4 Reed switch experiments

For experiments with the reed switch orientation with respect to the magnets, a 3D printed set-up was designed and printed. The degrees of freedom of the set-up can be found in figure 4.12. The prints were made with a RoVa3D printer. Tolerances of 0.4mm were taken for the magnet holes was taken. The printed holes however were to small for the magnets (which was widened with a soldering iron). The set-up consists of three parts: a slider (figure C.12), a rotating holder with magnets and a reed switch (figure C.10) and finally a sliding holder with magnets (figure C.11).

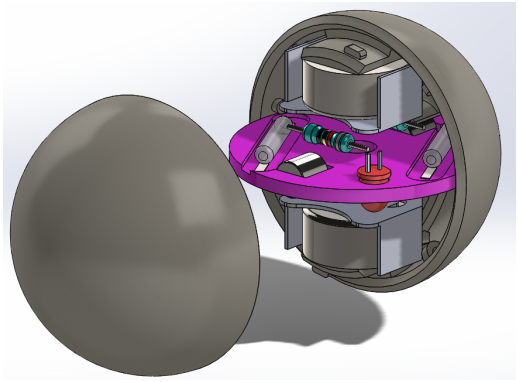

Figure C.8: CAD drawing of the PCB mock-up with electronics inside a sphere.

Figure C.6: Technical drawing of the lower shell of the final sphere.

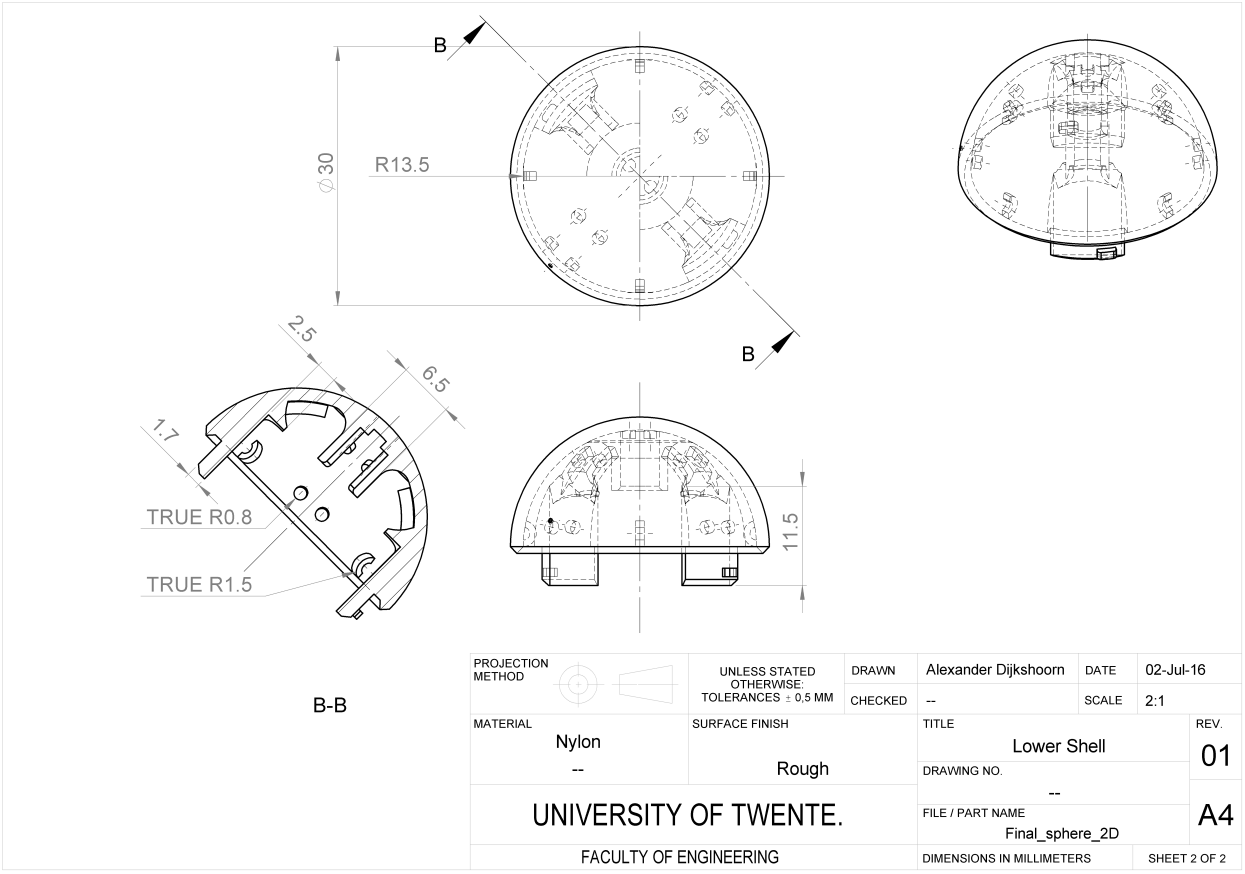

Figure C.7: Technical drawing of one of the identical halves of the sphere used for testing magnet size and position.

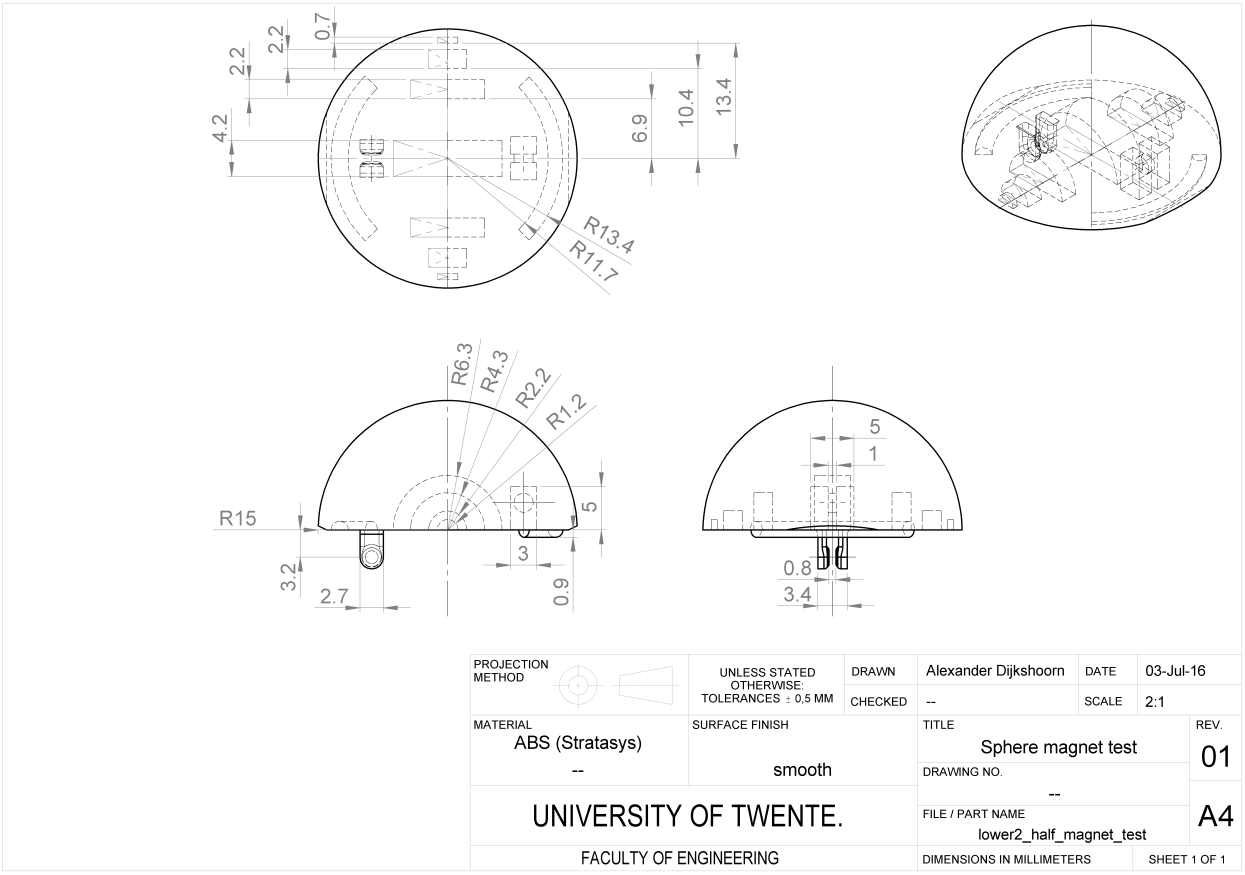

Figure C.9: Technical drawing of the PCB mock-up for the reactor experiments.

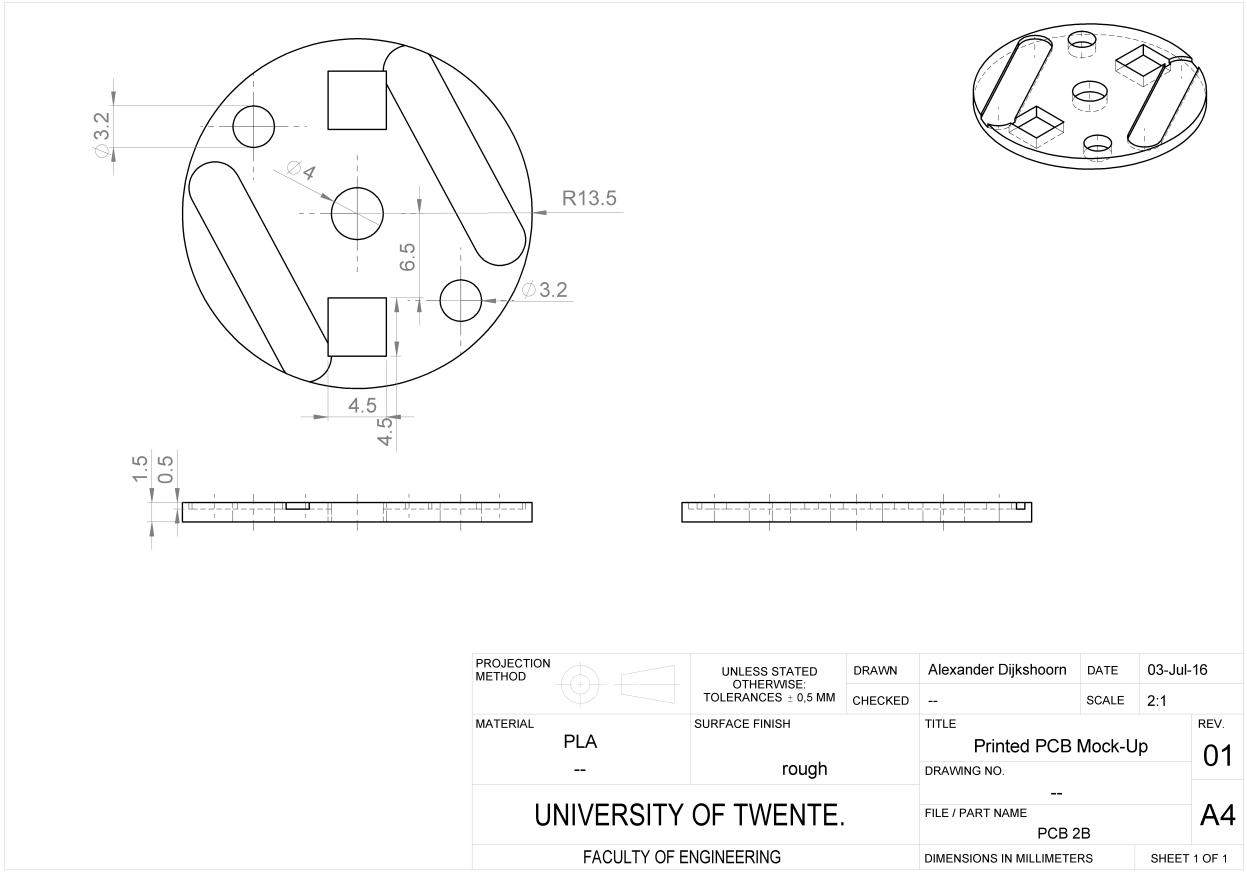

Figure C.10: Technical drawing of the rotating holder for the reed switch experiment.

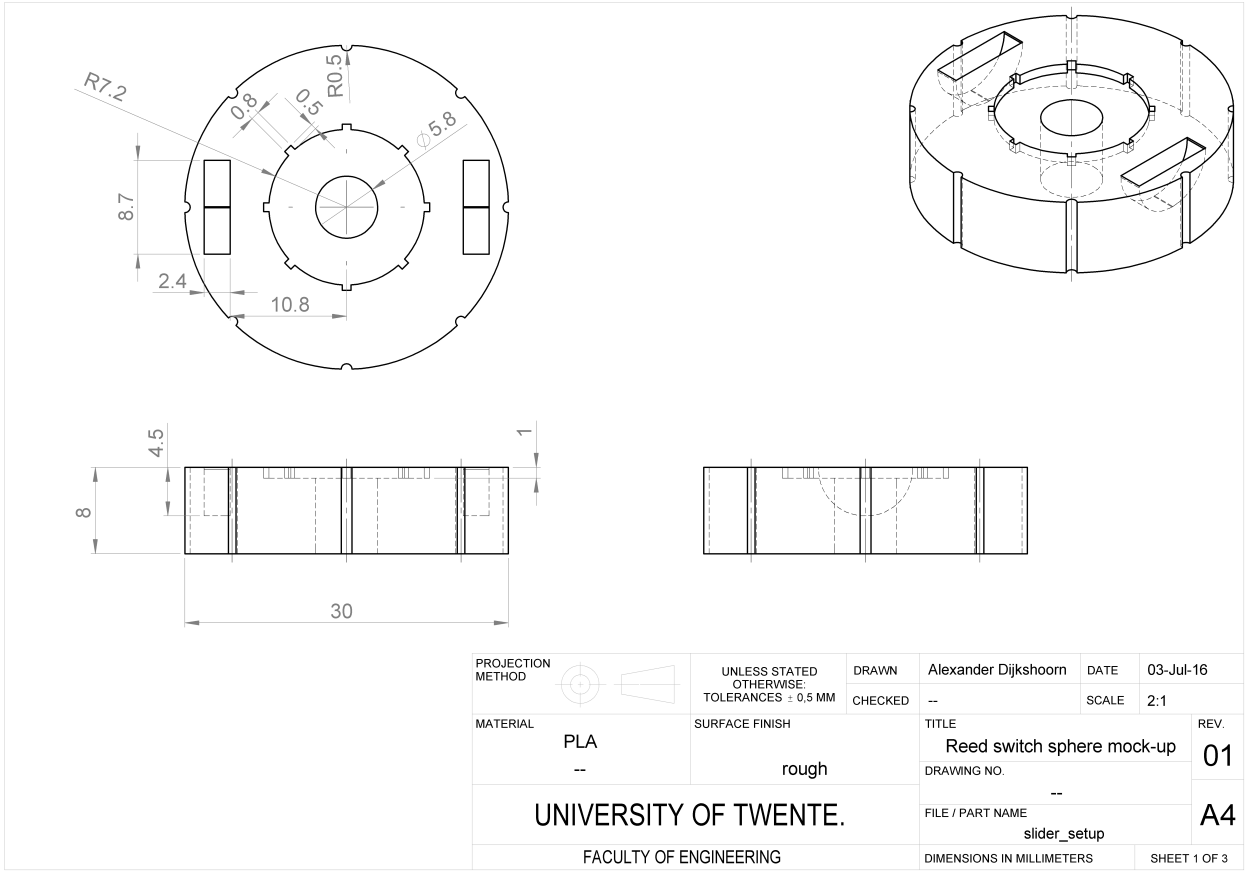

Figure C.11: Technical drawing of the sliding holder for the reed switch experiment.

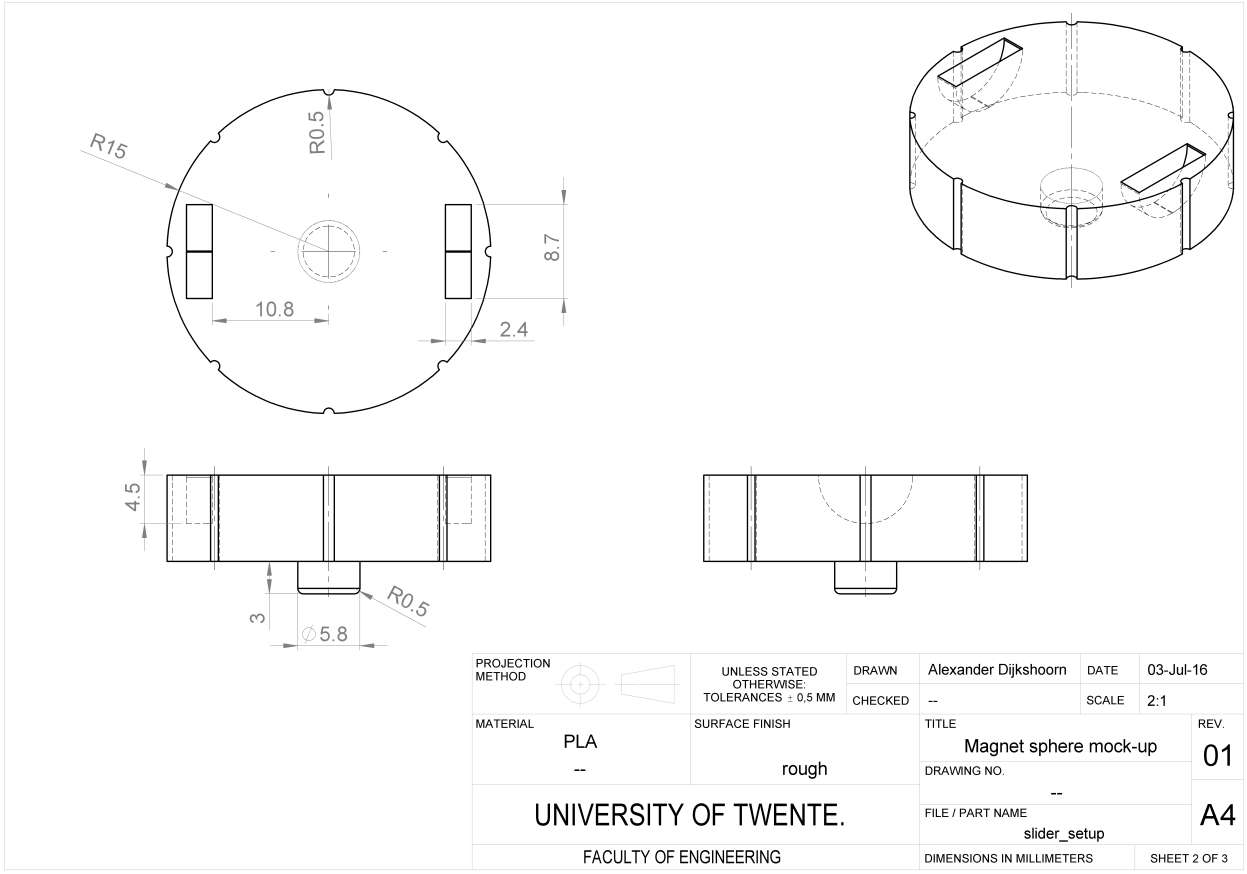

Figure C.12: Technical drawing of the slider for the reed switch experiment.

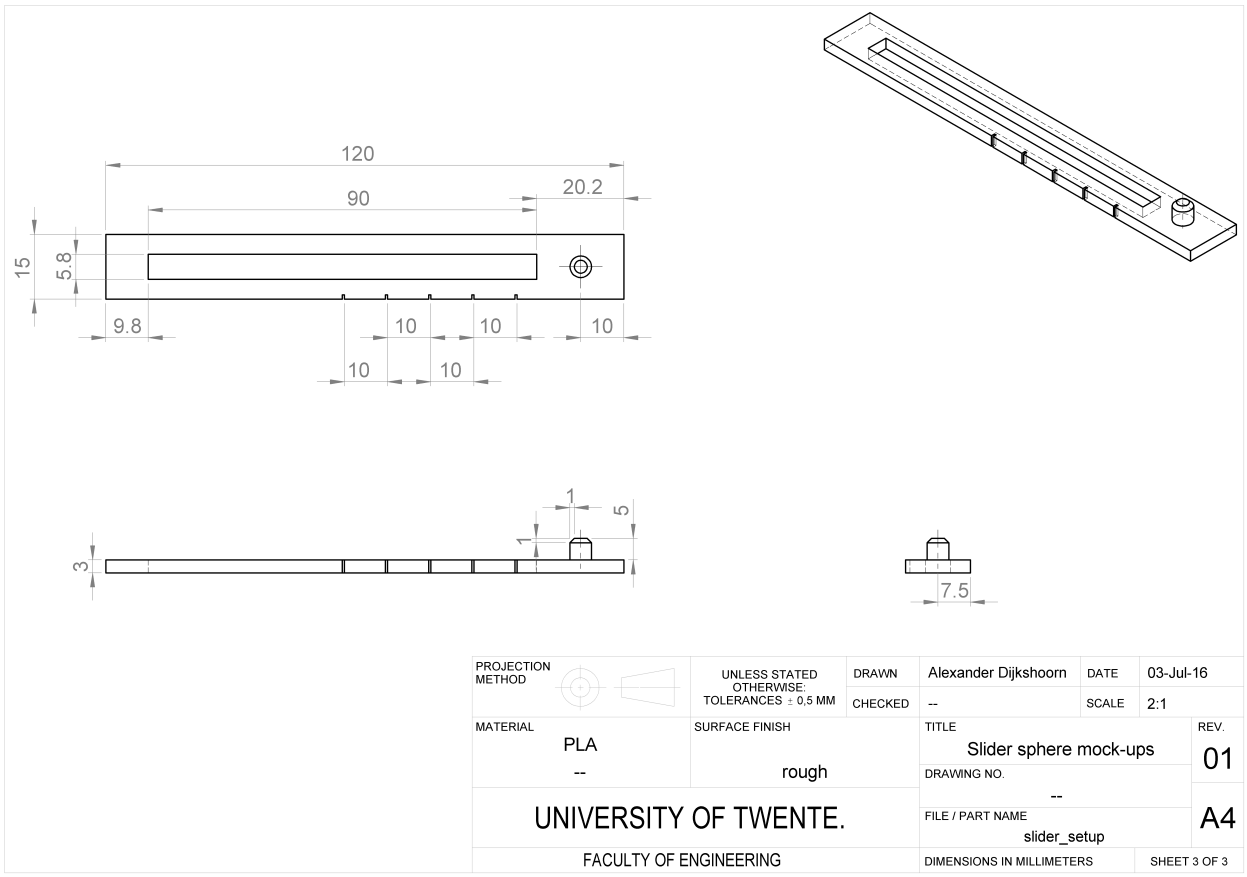

Appendix D

Micro-controller code

The ATmega micro-controller has been programmed with the arduino programming software. The used commented code can be found below. A program flow diagram of the code can be found in figure 5.2.

```
/*
  Self-Assembly spheres script
  Log data of macro self-assembly experiments.
  Connecting of spheres triggers reed switches. Time stamps from these events are logged onto
    a flash chip.
  In case a connection is made with a serial connection, all data is written to the serial
    port.
  The power should not be turnedd off, since the buffer of the flash chip will then be erased,
     losing data.

  A state machine that enables the several states of the experiment.
  State 1: Synchronization spheres and call sleep function
  State 2: Sensing switching and saving event data to buffer
  State 3: Writing buffer to flash page
  State 4: Sending data over serial connection
  State 5: Wake from sleep function
  State 6: Test if magnets can be sensed

  modified 02 Juli 2016
  by Alexander Dijkshoorn and Marcel Welleweerd
 */

#include <PinChangeInt.h>          // Interrupt library
#include <avr/sleep.h>             // Sleep library
#include <dataflash.h>             // Dataflash library
byte sensor_id = 5;                // Sphere 5

unsigned long start_time=0;        // time offset from synchronization
unsigned long temp_time0=0;
unsigned long temp_time1=0;
unsigned long temp_time2=0;
unsigned long temp_time3=0;

const int reed1Pin = A2;           // Reed switch 1 pin
const int reed2Pin = 6;            // reed switch 2 pin
const int LEDPin = 5;              // LED pin
int state = 1;                     // State from the state machine
int reed = 0;                      // ID of the triggering reed switch (1 or 2)
bool reedState1 = false;           // State reed switch 1
bool reedState2 = false;           // If there is a connection during syncrhonization, reed
    state is wrong
int reedState;                     // States 1 and 2 combined
int reed1_n = 0;                   // Number of events reed 1
int reed2_n = 0;                   // Number of events reed 2
bool flag = false;                 // Flag toggled to true in case of an event

// Variables flash
int buffer_counter = 0;            // Counts the number of taken spots in the buffer
int lastpage = 0;                  // Current page the buffer will be written to in flash
byte temp_write1 = 0;              // Used for writing timestamp to the flash buffer
byte temp_write2 = 0;
unsigned long bufbyte[4] = {0,0,0,0}; // array containing the four bytes of a timestamp
unsigned long test_t_r = 0;        // Event data reconstructed after reading from flash
unsigned long test_time = 0;       // Timestamp reconstructed after reading from flash
```

```
52 int test_state = 0;                // Reeds state reconstructed after reading from flash
   Dataflash dflash;
54
56
   void setup() {
58     pinMode(reed1Pin, INPUT_PULLUP);                        // Reed switches use the internal
       pull-up
       pinMode(reed2Pin, INPUT_PULLUP);
60     pinMode(LEDPin, OUTPUT);                                // Debugging LED
       pinMode(0, INPUT_PULLUP);                               // RX uses the internal pull-up
62     pinMode(10,OUTPUT);                                     // Chip enable of the flash

64     reedState_t();                                          // Intialize combined reedswitch
       state (0,1,2,3)
       dflash.init();                                          // Initialize the memory (pins are
       defined in dataflash.cpp)
66     digitalWrite(10,HIGH);                                  // Show the set-up takes place by
       blinking three times
       digitalWrite(LEDPin, HIGH);
68     delay(100);
       digitalWrite(LEDPin,LOW);
70     delay(100);
       digitalWrite(LEDPin, HIGH);
72     delay(100);
       digitalWrite(LEDPin,LOW);
74 }

76
   void loop() {
78   switch(state) {
    /*
       ================================================================================
       */
80     case 1:                                                 // Case 1: Synchronization timer at
       first connection
                                                               // Actions are performed in the
       interrupt reed1 or reed2
82        for(int v=0; v<256; v++){                            // Overwriting buffer to distinguish
        between data from previous experiments
          dflash.Buffer_Write_Byte(1,v,0);                     // Add zeros to the buffer were no
       new data was recorded
84        digitalWrite(10,HIGH);                               // Write chip enable high to
       minimize energy consumption
        }
86      sleepNow();                                            // Activate sleep mode, a pin change
        interrupt is needed to recover from sleep mode
        PCintPort::attachInterrupt(0, &serialData, FALLING);// Interrupt for incoming serial
       data at RX
88
          break;
90
    /*
       ================================================================================
       */
92     case 2:                                                 // Case 2: Detecting and logging
       switching
          if(flag == true){
94        reedState_t();                                       // Determine total state reed
       switches
          temp_time0 = millis();
96        digitalWrite(LEDPin, HIGH);                          // Show connection of spheres
          while(millis()-temp_time0<5){}
98        digitalWrite(LEDPin,LOW);
          if(reed == 1){                                       // Reed 1 started the connection
100         unsigned long timing1 = temp_time1-start_time;     // Timestamp time (total time -
       offset from synchronization)
            timing1 = timing1 << 2;                            // Bitshift two bits to make place
       for the reed state
102         timing1 = timing1 + reedState;                     // Timestamp combined with total
       reed state

104       reed1_n++;                                           // Counter reed switch 1

106           for(int k = 0; k<=3; k++){                       // Split data event into four
       separate bytes
```

```
            temp_write1 = (timing1 >> k*8) & 255;
108         dflash.Buffer_Write_Byte(1,4*buffer_counter+k,temp_write1); // Write to buffer
    1, 1 byte at a time
            digitalWrite(10,HIGH);
110       }
        buffer_counter++;                                   // Count bytes sent to buffer in
    flash
112
        if(buffer_counter==64){                             // Flash has 256 bytes, so 64 times
    4 bytes
114       buffer_counter = 0;                               // Buffer counter starts from 0
    again
          state = 3;                                        // Go to state 3 if buffer is full
116       break;
        }
118     }

120     else if(reed == 2){                                 // Reed 1 started the connection
        unsigned long timing2 = temp_time2-start_time;      // Timestamp time (total time -
    offset synchronization)
122       timing2 = timing2 << 2;
          timing2 = timing2 + reedState;                    // Timestamp combined with total
    reed state
124
          reed2_n++;                                        // Counter reed switch 1
126
          for(int l = 0; l<=3; l++){                        // Split data event into four
    separate bytes
128         temp_write2 = (timing2 >> l*8) & 255;
            dflash.Buffer_Write_Byte(1,4*buffer_counter+l,temp_write2); // Write to buffer
    1, 1 byte at a time
130         digitalWrite(10,HIGH);
          }
132       buffer_counter++;                                 // Count bytes sent to buffer in
    flash

134       if(buffer_counter==64){                           // Flash has 256 bytes, so 64 times
    4 bytes
            buffer_counter = 0;
136         state = 3;                                      // Go to state 3 if buffer is full
            break;
138       }
        }
140
        flag = false;                                       // Toggle flag after switching, with
     the next event state 2 is initiated
142     }
      break;
144
/*  ====================================================================================
    */
146 case 3:                                                 // Case 3: Write a full buffer to a
    page in the flash
      dflash.Buffer_To_Page(1, lastpage);                   // Write buffer 1 to the memory
148   digitalWrite(10,HIGH);
      lastpage++;
150   for(int w=0; w<256; w++){                             // Overwrite buffer (bad for flash)!
        dflash.Buffer_Write_Byte(1,w,0);                    // Add zeros to the buffer were no
    new data was recorded
152     digitalWrite(10,HIGH);
      }
154   state = 2;                                            // Go to state 2 again
      break;
156

158 /*  ====================================================================================
    */
    case 4:                                                 // Case 4: Write all event data over
     serial connection
160   PCintPort::detachInterrupt(0);                        // Detach RX interrupt before serial
     connection takes place

162   Serial.begin(115200);                                 // Start serial connection
      Serial.println("Sending data to computer");
```

```
164       Serial.print("Sensor ID: ");
          Serial.println(sensor_id);                          // Print sensor ID
166       dflash.Buffer_To_Page(1, lastpage);                 // Write buffer with data fully to
    the memory
          for(int p = 0; p<=lastpage; p++){
168         dflash.Page_To_Buffer(p, 1);                      // Copy pages to the buffer
            digitalWrite(10,HIGH);
170         for(int s=0;s<64;s++){                            // Reconstruct event data per 4
    bytes
              for(int t = 0; t<=3; t++){
172               bufbyte[t] = (dflash.Buffer_Read_Byte(1, 4*s+t));
                  bufbyte[t] = (bufbyte[t] << t*8);           // Bitshift the four bytes
174               digitalWrite(10,HIGH);
                  }
176           //Serial.println("3");
              test_t_r = bufbyte[0] + bufbyte[1] + bufbyte[2] + bufbyte[3]; // Combine the four
    butshifted bytes to the event data
178           test_time = test_t_r >> 2;                      // Reconstruct timestamp event
              test_state = test_t_r & 3;                      // Reconstruct reed state event
180           Serial.print(test_time);                        // Print timestamp event
              Serial.print(" ");
182           Serial.println(test_state);                     // Print reed states event
              Serial.print("\n");
184           }

186       }
          Serial.println("\n");
188       Serial.print("Reed switch 1 events: ");
          Serial. println(reed1_n);                           // Print number of events with reed
    1
190       Serial.print("Reed switch 2 events: ");
          Serial. println(reed2_n);                           // Print number of events with reed
    2
192       Serial.println("Finished sending data to computer");
          state = 2;                                          // Return to sensing state
194       pinMode(0,INPUT_PULLUP);
          PCintPort::attachInterrupt(0, &serialData, FALLING); // Attach interrupt again to RX
196       break;

198 /*  ================================================================================
    */
          case 5:                                             // Case 5: Wake up from sleep
    function
200         PCintPort::detachInterrupt(reed1Pin);             // Detach reed switch interrupt
    after synchronization
            PCintPort::detachInterrupt(reed2Pin);
202         for(int i=0;i<20;i++){                            // Show the micro-controller gets
    out of its sleep mode
              digitalWrite(LEDPin, HIGH);
204           temp_time0 = millis();
              while(millis()-temp_time0<50){}
206           digitalWrite(LEDPin,LOW);
              temp_time0 = millis();
208           while(millis()-temp_time0<50){}
            }
210         PCintPort::attachInterrupt(reed1Pin, &reed1, CHANGE);    // Interrupt connected to
    the reed switches
            PCintPort::attachInterrupt(reed2Pin, &reed2, CHANGE);    // Set to change after
    synchronization
212
            state=2;                                          // Start logging events
214         break;

216 /*  ================================================================================
    */
          case 6:                                             // Case 6: Test if magnets can be
    sensed
218         digitalWrite(LEDPin, HIGH);                       // Show connection with magnet
            temp_time0 = millis();
220         while(millis()-temp_time0<500){}
            digitalWrite(LEDPin,LOW);
222         temp_time0 = millis();
            while(millis()-temp_time0<500){}
224         digitalWrite(LEDPin, HIGH);
```

```
          temp_time0 = millis();
          while(millis()-temp_time0<500){}
          digitalWrite(LEDPin,LOW);
          temp_time0 = millis();
          while(millis()-temp_time0<500){}
          digitalWrite(LEDPin, HIGH);
          temp_time0 = millis();
          while(millis()-temp_time0<500){}
          digitalWrite(LEDPin,LOW);
          if(digitalRead(reed1Pin)==LOW || digitalRead(reed2Pin) == LOW){ // Check if the
    connection is still present
            if(reed==1){
              start_time = temp_time1;                    // Start the timer
            }
            if(reed==2){
              start_time = temp_time2;
            }
            state=5;                                      // Go to case 5 to wake up from
    sleep function
          }
          else{
            state = 1;                                    // Go to case 1 if there is no
    connection
          }

          break;
  }
}


/*
    ================================================================================
    */
// Determine total state reed switches

void reedState_t(){
  if(reedState1 == true && reedState2 == true){           // Both reed switches activated
    reedState = 0;
  }
  else if(reedState1 == true && reedState2 == false){     // Only switch 1 activated
    reedState = 1;
  }
  else if(reedState1 == false && reedState2 == true){     // Only switch 2 activated
    reedState = 2;
  }
  else if(reedState1 == false && reedState2 == false){    // No switch activated
    reedState = 3;
  }
}


/*
    ================================================================================
    */
//Handle interrupts on Trigger pins

void reed1(){                                             // Interrupt for reed switch 1
 if((millis()-temp_time1)>5){                             // Time for debouncing (5ms)
    temp_time1 = millis();

    if( state == 1){                                      // Record start time for
    synchronization time offset
      state = 6;                                          // If synchronizing, go to case 6
      reed = 1;                                           // Reed switch 1 is connected
    }
    else if( state == 2){                                 // Normal sensing operation
      reedState1 = !reedState1;                           // Switch from reed state
      flag = true;                                        // Set flag to true and select the
    correct reed to initiate state 2
      reed = 1;
    }
  }
}

void reed2(){                                             // Interrupt for reed switch 2
  if((millis()-temp_time2)>5){                            // Time for debouncing (5ms)
```

```
292     temp_time2 = millis();
\
294     if( state == 1){                                    // Record start time for
        synchornization time offset
          state = 6;                                        // If synchronizing, go to case 6
296       reed = 2;                                         // Reed switch 1 is connected
          reed = 2;
298     }
        else if( state == 2){                               // Normal sensing operation
300       reedState2 = !reedState2;                         // Switch from reed state
          flag = true;                                      // Set flag to true and select the
        correct reed to initiate state 2
302       reed = 2;
        }
304   }
    }
306


308
    void serialData() {                                     // Interrupt for RX connection
310   if((millis()-temp_time3)>500){                        // Time for debouncing
      temp_time3 = millis();
312   digitalWrite(LEDPin, HIGH);
      delay(100);
314   digitalWrite(LEDPin,LOW);
      state = 4;                                            // Go to case 4 for writing data
316   }
    }
318
    void sleepNow(){                                        // The micro-controller goes into
        sleep mode
320     set_sleep_mode(SLEEP_MODE_PWR_DOWN);//(SLEEP_MODE_IDLE);   // Sleep mode is set here
        sleep_enable();                                     // Enables the sleep bit in the
        mcucr register
322     PCintPort::attachInterrupt(reed1Pin, &reed1, FALLING);// Interrupt connected to the reed
        switches set to falling before synchronization
        PCintPort::attachInterrupt(reed2Pin, &reed2, FALLING);
324     PCintPort::attachInterrupt(0, &serialData, FALLING);  // Interrupt for incomping serial
        data at RX
        sleep_mode();                                       // The device goes into sleep mode
326     sleep_cpu();
        sleep_disable();                                    // First thing after waking from
        sleep mode
328 }
```